An approach to improving efficacy of cryosurgery: numerical and experimental (using gel phantoms) studies

Krishna Kumar Ramajayam

Department of Biotechnology and Medical Engineering
National Institute of Technology Rourkela

An approach to improving efficacy of cryosurgery: numerical and experimental (using gel phantoms) studies

Dissertation submitted in partial fulfillment

of the requirements of the degree of

Doctor of Philosophy

in

Biotechnology and Medical Engineering

by

Krishna Kumar Ramajayam

(Roll Number: 511BM101)

based on research carried out

under the supervision of

Prof. Arunachalam Thirugnanam

and

Prof. Sunil Kumar Sarangi

August, 2017

Department of Biotechnology and Medical Engineering

National Institute of Technology Rourkela

Department of Biotechnology and Medical Engineering
National Institute of Technology Rourkela

Prof. Arunachalam Thirugnanam
Assistant Professor

Prof. Sunil Kumar Sarangi
Professor, Mechanical Engineering

August 18^{th}, 2017

Supervisors' Certificate

This is to certify that the work presented in the dissertation entitled *An approach to improving efficacy of cryosurgery: numerical and experimental (using gel phantoms) studies* submitted by *Krishna Kumar Ramajayam*, Roll Number 511BM101, is a record of original research carried out by him under our supervision and guidance in partial fulfillment of the requirements of the degree of *Doctor of Philosophy* in *Biotechnology and Medical Engineering*. Neither this dissertation nor any part of it has been submitted earlier for any degree or diploma to any institute or university in India or abroad.

Sunil Kumar Sarangi
Professor, Mechanical Engineering

Arunachalam Thirugnanam
Assistant Professor

Dedication

This thesis is dedicated to everyone who supported me during the course of this degree. I would especially like to thank all my teachers till this day, parents and friends for supporting me and motivating me at crucial times and almighty for making this moment possible and supporting me throughout the difficulties.

Signature

Declaration of Originality

I, *Krishna Kumar Ramajayam*, Roll Number *511BM101* hereby declare that this dissertation entitled *An approach to improving efficacy of cryosurgery: numerical and experimental (using gel phantoms) studies* presents my original work carried out as a doctoral student of NIT Rourkela and, to the best of my knowledge, contains no material previously published or written by another person, nor any material presented by me for the award of any degree or diploma of NIT Rourkela or any other institution. Any contribution made to this research by others, with whom I have worked at NIT Rourkela or elsewhere, is explicitly acknowledged in the dissertation. Works of other authors cited in this dissertation have been duly acknowledged under the sections "Reference" or "Bibliography". I have also submitted my original research records to the scrutiny committee for evaluation of my dissertation.

I am fully aware that in case of any non-compliance detected in future, the Senate of NIT Rourkela may withdraw the degree awarded to me on the basis of the present dissertation.

August 18^{th}, 2017
NIT Rourkela

Krishna Kumar Ramajayam

Acknowledgment

I am deeply grateful to my supervisors, Prof. A. Thirugnanam and Prof. S.K. Sarangi whose insights and encouragements have helped me in shaping up this thesis. I would also like to thank Prof A. Kumar for the useful scientific discussions and critical review of the entire thesis work from time to time. Last five years were a fantastic amalgamation of scientific deliberations, discussions, doubts, agreements and disagreements which has helped me in developing my thoughts regarding various issues pertaining to research and life in general, especially planning research and its execution. The help provided by those people who created and made available Linux, LATEX, GnuPlot, Inkscape, Image J, LABVIEW and other software tools is also greatly appreciated.

NIT Rourkela

Krishna Kumar Ramajayam
Roll Number: 511BM101

Abstract

Freezing and ablating using cryosurgery is becoming a promising surgical tool for the treatment of tumours. For improving the efficiency of the cryosurgical procedure, different approaches have been implemented till now. Most of these techniques have focussed on the freezing process, without giving adequate attention to the damage to the surrounding healthy tissue. In this study, a novel concept is proposed which achieves the desired freezing while protecting the surrounding healthy tissue through the use of low thermal conductivity liquid layer (perfluorocarbons) around the interface of the tumour. Numerical modelling has been done to determine the location of the ice fronts in the presence of this perfluorocarbon layer around the boundary of the tumour. It is noticed that this method leads to a higher ablation rate substantially reducing the surgical time. Also, an optimal offset, i.e. the minimum distance between the tip of the cryoprobe and the boundary of the tumour, is identified for a given tumour radius and active length which gives maximum tumour necrosis in minimum time. It is also observed that for a 2 mm increase in the active length of the cryoprobe, the decrease in optimal offset is approximately 1 mm. Furthermore, for the tumour with different radii (between 10 mm and 15 mm), with same active length of the cryoprobe, the time taken for complete ablation of the larger tumour is nearly 2.7 times the time taken for the smaller one for every 2.5 mm increase in the tumour radius. The results also reveal that there exists an optimal thickness of the perfluorohexane layer around the tumour interface. It is also seen that among perfluorohexane, octafluoropropane and water, perfluorohexane acts as the best substitute for the formation of an insulating layer around the tumour interface.

Experiments have been performed to prepare pefluorocarbon (perfluorohexane and perfluorodecalin) emulsions in varied concentration (i.e. 30%, 50%, 70% and 90% (w/v)) through probe sonication. Further, this study reports the particle size, emulsion stability, functional group analysis, thermophysical properties of both perfluorodecalin and perfluorohexane emulsions. With regard to thermal conductivity, it is observed that perfluorodecalin emulsions possess a marginally lower thermal conductivity than perfluorohexane emulsions. It is interesting to note that during cryosurgery of gel phantom in the presence of low thermal conductivity perfluorodecalin emulsion (90% (w/v)), it is observed that the freezing front is not able to penetrate the gel while in its absence, there is a temperature of -4^oC at the same thermocouple location of 10 mm (in the axial direction).

Cryosurgery of glycine-containing gels is carried out in presence and absence of

perfluorohexane layer, and the thermal history is measured using K-type thermocouples connected to a data acquisition system. The presence of glycine causes rapid freezing during cryosurgery with an ice ball depth of 16 mm, while with a perfluorohexane layer at this gel interface, this depth is 13 mm, indicating the ability of this layer to limit freezing. In this study, alumina has also been utilised for the preparation of adjuvant containing gel phantoms. After cryosurgery, it is clearly evident that a temperature decrease is observed in the alumina consisiting gel phantoms when compared to the agarose gel phantoms. It is also noticed that with the increase in insertion depth of the cryoprobe (from 1 to 1.5 cm), there is a decrease in temperature at each thermocouple location in the gel phantoms. This study also demonstrates that in the presence of perfluorohexane layer, when the alumina consisting gel phantoms are cryosurgically cooled; even with the increase in insertion depth, the thermocouple placed axially at 10 mm which is inside the perfluorohexane solution layer indicates a temperature of 25^oC. However, in its absence, the temperature is found to be -5.47^oC at the same position, suggesting that the freezing is limited within the gel. Furthermore, this work also proposes a new approach that utilises glycine-alumina emulsions as an adjuvant. After cryosurgery of glycine-alumina containing gel, a substantial temperature decrease is observed at all thermocouples placed nearer to the probe, thus indicating an enhancement in freezing. In conclusion, this study proposes novel approaches to improve the cryosurgical procedure through numerical modelling and experiments in gel phantoms, thus, providing newer approaches to improve the cryosurgical outcome.

Keywords*: *Cryosurgery*; *temperature*; *perfluorocarbons*; *emulsions*; *low thermal conductivity*; *perfluorohexane*; *gel phantoms

Contents

List of Figures

List of Tables

Chapter 1

Introduction

Cryosurgery, commonly referred as cryoablation, is a surgical technique which uses very low temperature for the destruction of undesirable tissues or tumour [1]. Modern cryosurgery has come into existence in the early 1960s and grown tremendously in the last two decades. It is widely gaining acceptance in the medical fields like dermatology, neurosurgery, oncology and gynaecology [2]. A broad range of solid tumours can be treated using modern cryosurgery, for example, tumours of the breast, kidney, liver, prostate and pancreas [3–6]. The use of modern cryosurgery to ablate these tumours presents many advantages over other treatment methods. However, cryosurgery also demonstrates certain inadequacies which need to be addressed so that this technique becomes a routine clinical practice. This chapter provides insight into the technique of cryosurgery and addresses the following points: historical perspective of cryosurgery, advances in cooling techniques, merits and existing problems pertaining to cryosurgical tumour ablation. This section also provides a historical perspective of the cryosurgical practices that existed from the early ages to the modern era.

1.1 The use of low temperature in the primitive age

The first report of the medical use of low temperature to cure ailments is said to be documented in 3500 B.C. in Egypt. The Egyptians used substances like ice that have low temperature and applied it on wounds, thereby, utilising it as a localised anaesthetic [7, 8]. Further, Hippocrates, in 5^{th} century B.C., suggested the application of cold to relieve pain in diseases that affect the bones and joints [8]. Throughout, the middle ages, these practices evolved with time and later in the 17^{th} century cold baths and wet sheets were used to provide relief from fever and inflammation [2]. In the absence of the modern anaesthetic tool during the early 18^{th} century, low temperature was used to aid in the amputations. It was also reported that the bleeding during amputations was controlled if it was covered with ice [8, 9]. However, the use of cryosurgery that provided a controlled low temperature was not available until the 1850s. There were phenomenal advances in the research areas like cryogenics, low-temperature physics and engineering that led to the development of cryosurgery [1].

In the early 1850s, Dr. James Arnott, who was a British physician used freezing for treating cancers. While treating the patients, he used a -12^oC solution of sodium chloride and broken ice cubes to treat the lesions of breast and uterine cavity [10]. After freezing, it was seen that the lesions were white and hard in appearances and there was minimal blood loss. Subsequently, advances in this field had to await the development of cryosurgery devices that provided very low temperatures, and the application of freezing for destruction of tissue was reported at the culmination of the 19^{th} century. The end of the 19^{th} century observed several significant advances in the field of cryogenics [11]. In the same context, Louis Paul Cailletet, a French engineer, produced liquid oxygen by using an adiabatic expansion system in 1877. The year also led to another breakthrough, Raoul Pictet, a Swiss physicist, achieved success in producing liquid oxygen by applying a cascade process. In the early 1880s, a pioneering work was done by S.von Wroblewski and K. Olszenski, who first liquified nitrogen, which was carried forward further by Carl von Linde. With these advancements, industrial liquefaction of air was possible and subsequently in the next few years gases like nitrogen, hydrogen and oxygen were liquefied. Further, a path breaking development took place in 1892, when James Dewar, a British Professor, developed a vacuum-jacket vessel for storing cryogenic fluids. These vessels significantly reduced the evaporation of cryogenic fluids and helped in easy storage for use in therapy and medical applications.

With these tools available, extreme cold temperature could be provided for therapeutic applications, and these advances in cryogenics were encouraging for the field of cryosurgery [1, 2]. Dr. Campbell A. White, for the first time used liquid air to treat skin diseases in 1899 [12]. He collaborated with Professor Charles Tripler who encouraged the use of liquid air in medical practice and produced liquid air for its use in the treatment of skin diseases. Liquid air could treat warts, varicose leg ulcers, boils, herpes and epitheliomas. However, as a cryogenic agent for medical purposes, liquid air was subsequently replaced by solid CO_2 because liquid air was not easily available at a large scale in 1910 as compared to the widespread availability of solid CO_2 [1]. Further, another cryogen, liquid oxygen was used for treating the skin lesions in 1929, but did not become popular for cryosurgery as it could be a potential fire hazard [13]. In 1940s, large scale commercial liquefaction of hydrogen and helium resulted in the production of liquid nitrogen (LN_2) as an abundant and low-cost by product. Liquid nitrogen was used in the clinical practice for the first time by Allington for treating skin ailments [14]. Since the boiling point of liquid nitrogen is lower than solid CO_2 it became a common method of treatment of keratoses, warts and non-neoplastic lesions. Till date, for use in modern cryosurgery, LN_2 is the most effective cryogen. For a better understanding of its thermal and physical behaviour, the properties of saturated LN_2 at 1 atm are provided in Table 1.1 [11].

Table 1.1: Properties of liquid nitrogen at 1 atm [11]

Property at 1 atm	Unit	Value
Normal boiling point	K	77.36
Density	kg/m^3	807.3
Latent heat	kJ/kg	199.3
Specific Heat	$kJ/kg.K$	2.05
Viscosity	$Pa.s$	158×10^{-6}
Thermal Conductivity	$W/m.K$	0.1396

1.2 Cryosurgery in the modern era

In 1961, Dr Irving Cooper fabricated the first cryoprobe which is attributed as the birth of the modern cryosurgery [15]. This design of cryosurgical probe was a closed probe which had a continuous circulation of LN_2 in the inner region of the probe for its cooling. The initial objective of this design was treating neural disorders like Parkinson's and it was observed that the cryoprobe was highly effective in destroying solid tumours seated at depth inside the body. Thus, after the introduction of the first cryosurgical probe (cryoprobe), a rapid growth took place in the field of cryosurgery and numerous novel applications emerged in the 1960s. Rand et al. used cryosurgery in treating neural diseases [16]; Marcover and Miller utilised cryosurgery for orthopedics [17]; Torre and Zacarian et al. worked extensively on cutaneous cryosurgery [18, 19]; Cahan et al. applied the cryosurgical probe to uterus that had a heating element which helped in easy release from the operated tissue [20]. Constant efforts have been made by researchers which led to remarkable advances in the 1970s. However, only till the late 1980s, the cryosurgical technique was well received by the surgeons as an effective surgical technique. The primary opposition to this technique by the surgeons was the inability of this procedure to monitor the ice formation precisely [1].

Unlike conventional surgery, the surgeon is unable to determine the lateral and axial spread of ice visually. The inability to visualise ice makes it difficult for the surgeons in making an accurate judgement on the extent of ice formation [21]. More cooling or lesser cooling ideally causes inadequate freezing or over-freezing. Insufficient freezing does not cause complete cancerous cell destruction, making the treatment less effective; while over-freezing causes complications like destruction to the surrounding healthy tissue and vascular complications. Although the cryoprobes could be placed at a particular location, the understanding of the effect of cooling on the target tissue remains poor. Owing to the problems mentioned earlier, cryosurgery was mainly applied to dermatology and gynaecology [1].

To visualise the thermal history during freezing and the extent of ice formation different cryosurgical monitoring techniques are available. The thermal history measurement during cryosurgery is carried out by measuring the temperature profile during cryosurgery at

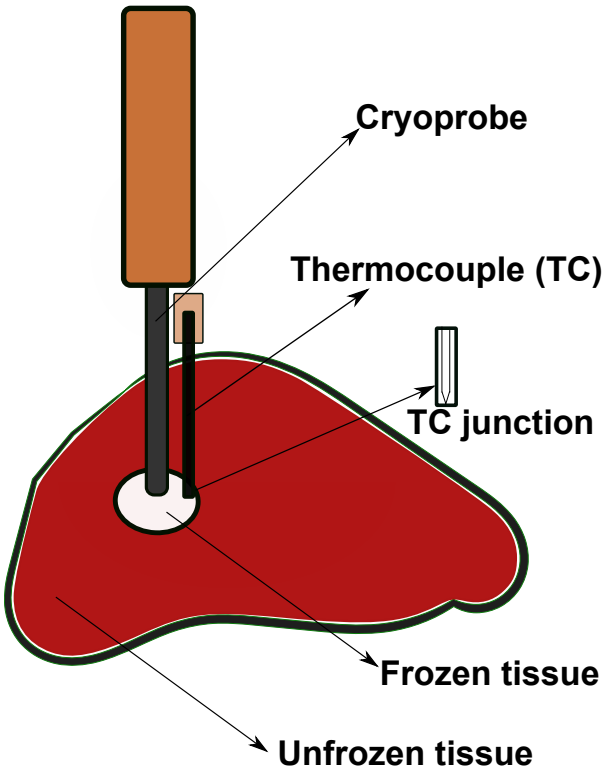

Figure 1.1: Schematic diagram of cryoprobe inserted in a tissue along with thermocouple

finite points in the tissue, where thermocouples are inserted in the region of temperature measurement. Figure 1.1 shows a schematic representation of the temperature measurement during cryosurgery using thermocouples at specific or desired location. In another study, researchers have used the variation in the electrical impedance of the tissue during freezing and also investigated the movement of the freezing front [22]. After a decade, in the late 1970s, it became a routine practice to use thermocouples for measuring temperature during cryosurgery at desired locations [23]. The determination of temperature at specific sites aids

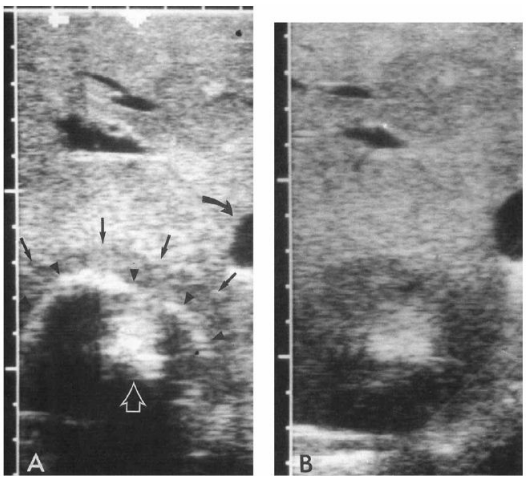

Figure 1.2: Monitoring ice ball during cryosurgery [24]

in a better understanding of the lethal front (-40^oC isotherm) propagation in the target tissue.

However, there are few problems associated with this process of thermal measurement. Since it is invasive, the thermocouple needs to be placed inside the tissue or region to be measured. Further, the temperature is measured at some discrete locations which is inadequate to monitor the temperature of the whole tissue. The developments in the field of medical imaging have helped in the visualising the extent of freezing during cryosurgery (e.g. nuclear magnetic resonance (NMR), computerised tomography (CT) and ultrasound) [25, 26]. Figure 1.2 depicts the practical use of ultrasound during the process of cryosurgery. This figure illustrates that ultrasound can be used to distinguish between the frozen and unfrozen region of the tissue [24] (Figure 1.2(A) and (B), reproduced with permission from Wiley and sons, licence no: 3903701204848). The arrows in the figure 1.2(A) demarcate the presence of the ice ball margin and the frozen part of the tissue generally appears darker in the ultrasound image as compared to the unfrozen one. In comparison to the frozen region, the lighter shaded ablated region is seen after thawing (Figure 1.2(B)). Thus, the technique of ultrasound can aid in the real time propagation of freezing front with more accuracy. Magnetic Resonance Imaging (MRI) is another method that is being used for monitoring the

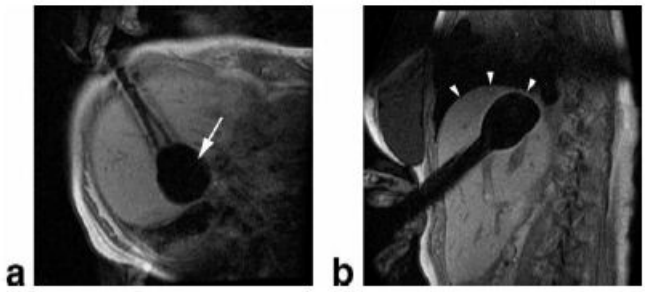

Figure 1.3: Ice ball visulaisation during MRI aided cryosurgery [27]

ice ball formation during cryosurgery. Figure 1.3(b) shows the MRI assisted cryosurgery of liver metastasis and it can be seen the edge of the ice ball is clearly discernible as indicated by the arrows (Figure 1.3(a) and (b), reproduced with permission from Wiley and sons, licence no: 3903710673566) [27].

1.3 Methods of cryosurgical cooling

Cooling is required during cryosurgery as it leads to the generation of a heat sink in the desired tissue that aids in subsequent tissue freezing. Before the 1960s, the methods of cryosurgical cooling had less efficacy. For example, the cotton swab dipped in LN_2 technique was used for treating skin ailments. In this procedure, as seen in Figure 1.4 (Image courtesy: Richard Usatine, reproduced with permission from CRC press, licence no. 3985261071126 [28]), small skin warts or superficial lesions were treated as the depth of penetration during freezing was not more than 2 mm [2, 28]. A study carried out by Zacarian

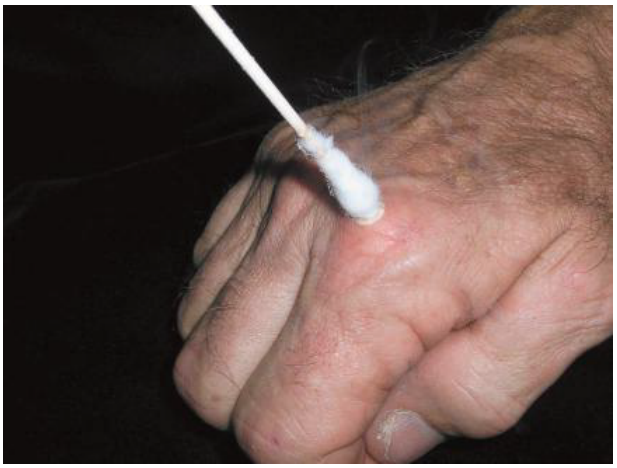

Figure 1.4: Cotton swab soaked in liquid nitrogen being applied to skin surface [28]

showed a higher penetration of freezing [19, 29]. In his work, he utilised a cylindrical copper disc that was dipped in LN_2 apriori to its placement over the skin surface. It was seen that a freezing depth of 7 mm could be achieved using this method. However, the freezing of a large volume of tissue or tissue that is anatomically placed deep rooted inside the body was not easy which resulted in the use of cryosurgery being limited to the fields of dermatology and gynaecology before 1960s [1].

1.3.1 Cryospray

The fabrication of the first cryospray device for application in medicine was suggested by Whitehouse in the year 1907 [30]. A simple spray bottle was designed to spray liquid air on the skin surface for the treatment of skin lesions. Subsequently, the cryogenic fluid, liquid air, was substituted by LN_2. Later, in 1969, a commercial hand-held spray device was developed by Zacarian [31]. Figure 1.5 depicts a cryospray unit (CS1) manufactured by SMT Praha, Czech Republic, a reputed maunfacturer in the field of cryospray and cryosurgery devices (Image reproduced with permission from SMT Praha, Czech Republic). A cryospray device has the following key components:

- a dewar tank for storing liquid nitrogen,
- a delivery pipe,
- a trigger that initiates the cryospray and,
- nozzles of variable diameter.

While using this device, the nozzle to skin surface distance is usually maintained between 1 to 1.5 cm, aiming the centre of the target specified. A cone can be used to limit the spray to the desired region as it prevents splashing to the surrounding tissue and shields the healthy area. Initially, as the spray nozzle is triggered, a combination of fine LN_2 droplets and gaseous nitrogen strike the skin surface resulting in a swifter freezing of the desired region.

Figure 1.5: A cryospray CS1 system manufactured by SMT Praha, Czech Republic

1.3.2 Cryosurgical probe

In comparison to the cryospray, the history of cryoprobe development is short and is available in limited types by the cryogenic fluid. There are two types of systems available, the more prominent one uses liquid nitrogen for cooling; while the other system uses nitrous oxide as a cryogen.

Liquid nitrogen based cryoprobe

The year of 1961 marks the birth of modern cryosurgery as Cooper et al. developed the first modern cryoprobe that could use liquid nitrogen and carried out experiments using their cryosurgical probe to ablate brain tumours [15]. Figure 1.6(a) shows the schematic diagram of the cryoprobe. It consists of three long concentric tubes. There is a presence of vacuum in the gap between the outer and middle tubes and this gap is provided in such a way that there is a thermal insulation. The innermost tube provides liquid nitrogen from a reservoir to the tip of the cryosurgery device, which is made from metal so that there is an efficient heat transfer between the probe and the surrounding tissue that is to be removed using cryosurgery. Since the probe is closed, the liquid that returns after coming in contact with the tip of the cryoprobe needs space. Hence, there is an annular gap between the middle and inner tubes. Further, there is an outer tube that encloses these two concentric tubes. Also, the constant flow of LN_2 leads to a lower temperature at the tip of the cryoprobe. This lower temperature causes

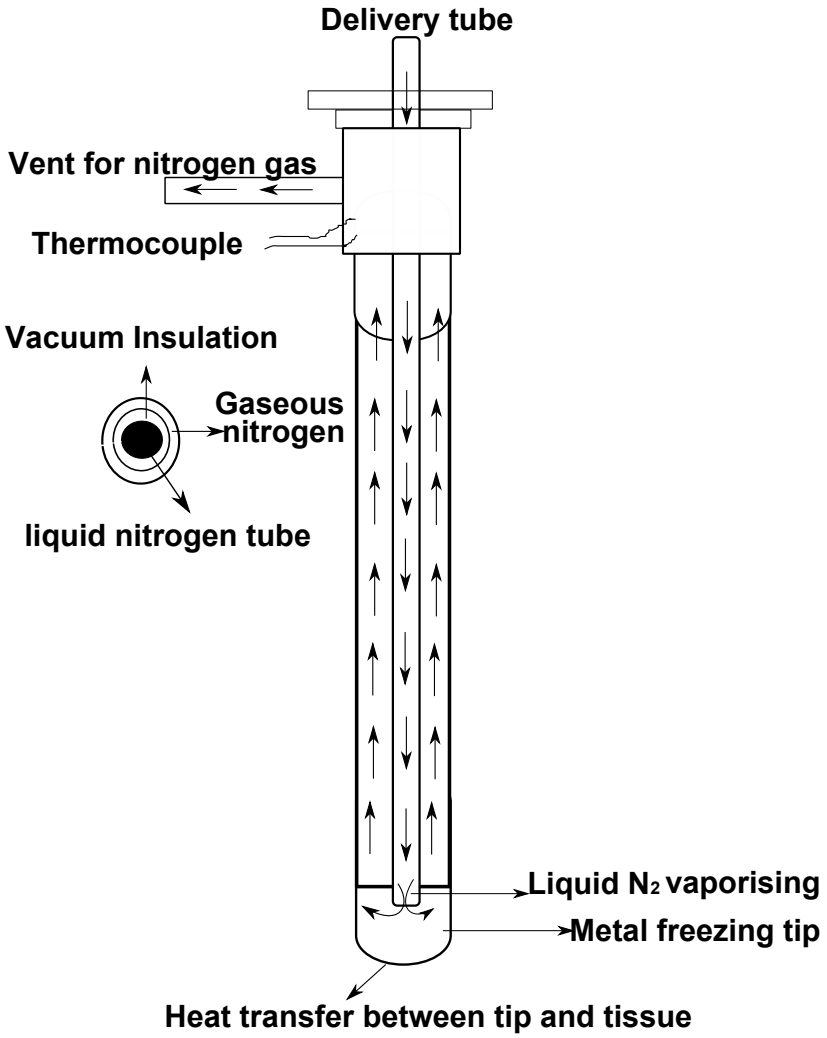

(a) Liquid nitrogen cryoprobe

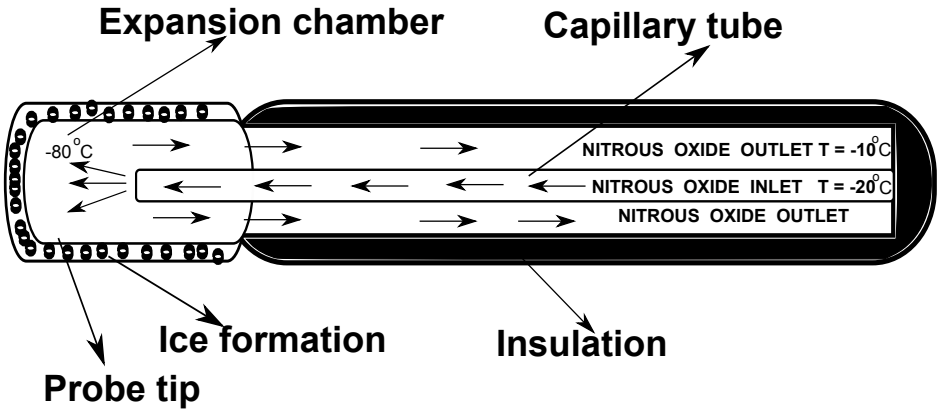

(b) Nitrous oxide cryoprobe

Figure 1.6: Different types of cryoprobe for modern cryosurgery

freezing of tissues, and the ice front propagates from the surface of the probe to the desired tissue. A promising development took place in the 1990s that allowed the use of sub-cooled liquid nitrogen to reduce the gaseous gap (N_2) between the probe wall and liquid nitrogen [32]. The subcooling is carried out by passing the pressurised LN_2 through a cooling coil that is dipped in the semi-solid slush of nitrogen at -209^oC. The flow of nitrogen helps in single phase flow during the cryosurgical ablation that produces a low temperature at the cryoprobe tip. In earlier systems, the boiling of LN_2 released a tremendous volume of gaseous nitrogen that affected the flow of the incoming liquid nitrogen. The primary reason for the development of cryoprobe with a larger outer diameter (OD) before the 1990s was to have a continuous flow of liquid nitrogen in spite of the presence of the gaseous nitrogen. However, a larger OD of the cryoprobe made it less accessible to a particular and specified region as the surface area of contact was more. The usage of subcooled LN_2 decreased the boiling point thus helping in a compact design of a cryoprobe having diameter in the order of 3.4 mm.

Nitrous oxide based cryoprobe

The N_2O based cryoprobe applies Joule-Thomson effect to create a low temperature. Figure 1.6(b) schematically depicts that the shaft of the cryoprobe is insulated. The gaseous N_2O is provided from a source that is high pressure, e.g., 50 bars that pass inside the inner tube. The inner tube has a very tiny orifice of nearly 0.08 mm that helps the pressurised N_2O pass through the expansion chamber where there a pressure drop to 1 bar. The unexpected expansion results in cooling of N_2O and a temperature of -80^oC is achieved inside the chamber. While cryosurgery is being performed, the expansion chamber is in contact with the desired region to be ablated, and a low temperature within the chamber results in freezing and destruction of tissues.

1.4 Advantages of modern cryosurgery

Modern cryosurgery utilises low temperature to destroy undesirable tissue. The basic principle of this technique and the outcome of cryosurgical ablation is different as compared to other treatment methods. This technique is minimally invasive and demonstrates the following advantages over its counterparts such as chemotherapy, surgical ablation and radiation:

1. Cryosurgery is a localised treatment modality. In comparison to other methods of treatment, the use of cryosurgery helps in restricting the low temperature to a specified region, thereby, helping in the minimal destruction of the surrounding healthy tissue. Thus, this merit of cryosurgery has led to its use in removal of tumours of liver, brain, lung and prostate [1].

2. It requires a short duration for the treatment of tumours. A very low temperature is achieved in a single freeze cycle duration during cryosurgery. Even in the case of multiple freeze-thaw cycles, it does not require more than twenty minutes for tumour ablation.

3. There is minimal bleeding during this process since there is no tissue resection carried out in this procedure. It is of significance especially in the case of cryosurgery of hepatic tumours as these tumours are generally located close to major blood vessels [32].

4. Cold serves as a local therapeutic and hence there is no requirement of general anaesthesia during this procedure.

5. This technique provides patient comfort as it is applied for a very short duration of time. Thus, this treatment method improves the quality of patient care considerably.

1.5 Limitations of cryosurgery

Although there have been remarkable developments in the past decades that have improved cryosurgery, still shortcomings exist and need to be addressed accordingly. Currently, the advancement in technique of cryosurgery is stalled because of the following deficiencies:

1. In a real time scenario, it is still a challenging task to monitor the process of cryosurgery continuously. The use of intraoperative ultrasound has aided in visualising the tumour during the freezing of tissue [33]. However, the technique has shortcomings. During freezing, it is not easy to get the fine details behind the edge of the ice ball because the ice ball produces acoustic shadowing.

2. The freezing front can be monitored using current day imaging techniques. But it is the exact location of lethal front (-40^oC) isotherm that is required for complete cancerous cell destruction [32]. Therefore, studies need to be performed to determine the spread of lethal front propagation in real time during the cryosurgery process.

3. Novel strategies are required to improve the efficacy of cryosurgery process. A successful cryosurgical ablation is one which calls for an optimal planning protocol that is capable of predicting the thermal history inside the tissue and improves the efficiency of cooling.

This thesis mainly deals with novel approaches to improve the outcome of cryosurgery through numerical and experimental studies in gel phantoms. Currently, the standard treatment modality of tumour cases includes the use of surgery, radiation, chemotherapy, hormonal therapy, radiofrequency ablation and cryosurgery. Cryosurgery, or tissue

destruction by using very low temperature is an efficient and minimally invasive technique that can be improved immensely by newer methods. This thesis provides an overview of the steps that can be taken to improve the effectiveness of the cryosurgery process through a preliminary study.

1.6 Objectives of the thesis

The primary objectives of this thesis are:

1. To propose a new concept of low thermal conductivity layer around a tumour interface and carry out a parametric study of the freezing process during cryosurgery using numerical modelling.

2. To formulate low thermal conductivity emulsions of perfluorocarbon for effective use as a barrier during cryosurgery.

3. To carry out experiments on gel phantoms using a cryosurgery system and propose a novel concept of adjuvant enhanced cooling in presence of perfluorocarbon layer.

1.7 Scope

The scope of this thesis is as follows:

1. In this study, a parametric analysis of heat transfer process is carried out during cryosurgery of two dimensional (2D) axisymetric spherical tumour in the presence and absence of a low thermal conductivity perfluorocarbon (liquid) layer using numerical modelling. Parameters like offset, i.e (distance between the tip of the cryoprobe and tumour interface), the time taken for complete tumour ablation, the effect of tumour radii on cooling, the effect of a low thermal conductivity layer of perfluorocarbon around the tumour interface, the gap in tumour ablation (i.e. the distance between the lethal front and the tumour interface with respect to time) are optimised. The concept of low thermal conductivity liquid around the tumour interface is new and finds significant practical implications in cryosurgery.

2. Emulsions of perfluorocarbons can be used as an insulation during cryosurgical ablation. Hence, low thermal conductivity emulsions of perfluorocarbon are synthesised. The thermal conductivity is analysed and the most suitable perfluorocarbon emulsion that has the lowest thermal conductivity is chosen for the proposed applicaton in cryosurgery. The zeta potential is also determined to visualise the emulsion stability. These emulsions can be used as an insulation during cryosugery and can prevent the lethal front to cross the gel-perfluorocarbon interface.

3. New experimental methods have been developed for improving the efficacy of cryosurgery of gel phantoms using adjuvants like glycine and alumina in presence of perfluorocarbons, i.e. increased freezing inside a defined geometry due to adjuvants with perfluorocarbon as a barrier to gel freezing.

1.8 Outline of the thesis

A brief description of thesis chapters is summarised below:

Chapter 1 discusses a general introduction of cryosurgery, its history, the cryogens used till date, the types of cooling techniques used for cryosurgical ablation, various cryoprobes used, the advantages and disadvantages of this technique.

Chapter 2 reviews existing literature pertaining to cryosurgery, its advances and the current directions in this field. This chapter also discusses the following key points exhaustively:

1. The variation in freezing of tissue during cryosurgery
2. The mechanisms of tissue damage during cryosurgical freezing
3. The studies related to numerical modelling of cryosurgery process
4. Experimental studies on measurement of temperature distribution and its use in cryosurgery.
5. Perfluorocarbon, its uses, synthesis of perfluorocarbon emulsions and its usefulness in being used as a low thermal conductivity insulation during cryosurgery
6. Studies directed towards the improvement of cryosurgical process.

Chapter 3 discusses a two dimensional axisymmetric model for a multiblock structured grid. The developed model is used to study freezing of spherical tumours of different radii at various active lengths around a single cylindrical cryobrobe. A novel way of calculation of the distance between the lethal front and tumour interface is presented here. Furthermore, the effect of a low thermal conductivity barrier of perfluorocarbon around the tumour interface is evaluated numerically and compared with its absence. A parametric study is carried out that concerns an optimal cooling configuration (i.e. optimal offset), variation in active length of the cryoprobe, role of the low thermal conductivity perfluorocarbon (liquid) layer, change of tumour radii and its effect on cryosurgical freezing, ablation time for optimal offset. This chapter also highlights the results obtained after varying the perfluorocarbon layer thickness and the various chemical substances that can be used for formulating this insulating layer. This chapter also suggests that gap propagation (distance between the lethal front and the tumour interface) can be used as a tool for determining an optimal offset.

Chapter 4 proposes designing of highly concentrated perfluorocarbon emulsions that possess low thermal conductivity and act as an insulation during the cryosurgery process. In the first half of the chapter, formulation of perfluorohexane emulsions is discussed. The thermal conductivity of emulsions is optimised by varying the concentration of perfluorocarbon from (30% (w/v) to 90% (w/v)), an analysis of particle size and zeta potential is also carried out for these emulsion systems. The role of surfactant change is also evaluated. In the second half of this chapter, the perfluorocarbon phase, is varied to perfluorodecalin. The thermal conductivity of the emulsions is measured and subsequently size, zeta potential, functional group analysis and differential scanning calorimetry studies are carried out for the optimal perfluorodecalin emulsions. Subsequently, the lowest thermal conductivity emulsion is utilised as a barrier to gel cooling during cryosurgery of gel phantom.

Chapter 5 focusses on adjuvant containing gels and the use of perfluorohexane as barrier to gel cooling using a cryosurgery system. In the first half of the chapter, research is focussed on the cooling of agarose gel phantoms. To visualise the effect of adjuvant, glycine is added in the agarose gel solution to form the adjuvant containing gel phantoms and the thermal history is measured during the cryosurgery process. To verify the effectiveness of insulating layer, the freezing of glycine containing gels is carried out in presence of perfluorohexane layer as a barrier to gel cooling. The ice ball is also visualised after the completion of freezing process and compared to the normal ice ball. In the second half of this chapter, alumina and alumina-glycine containing gel phantoms are prepared and then cooled using a cryosurgery system. This part of the chapter highlights the increased freezing due to adjuvants, the role of insertion depth in enhancement of freezing, the effect of perfluorohexane solution layer as a barrier to cooling of alumina containing gels. This chapter also discusses the role of glycine-alumina in decreasing the end temperature after cryosurgery substantially. Apart from the above mentioned cases, the thermal profile and ice ball images obtained after the cryosurgery procedure.

Chapter 6 summarizes the key results, lists out the significant inferences and the importance of this study with respect to the contribution made to the existing knowledge. This chapter also highlights the limitation of the present study and the future directions that can be pursued for the betterment of research in this field.

Some of the results of **Chapter 3 and Chapter 5** have been published and mentioned in the dissemination section. Few papers originating from the results of **Chapter 4 and Chapter 5** are either under review or would be communicated to journals shortly (Details mentioned in the dissemination section). Followed by the introduction section of the thesis, the review of literature gives a focussed insight on the effect of temperature decrease during cryosurgery, the mechanisms involved in freezing injury, modelling studies related to cryosurgical freezing, experimental studies for measurement of temperature profile, studies related to perfluorocarbon emulsions and studies carried out to improve the cryosurgery

process. A lot of numerical and experimental studies have been carried out to improve the effectiveness of cryosurgery. However, a lot of drawbacks exist and need to be addressed. This thesis advocates methods to improve the efficiency of cryosurgery procedure through new approaches. Previously reported literature pertaining to the scope and objectives of this thesis shall be reviewed exhaustively in the next chapter.

Chapter 2

Review of Literature

Modern cryosurgery is a surgical technique that has gained acceptance in the field of medicine since its inception in the 1960s. Various research activities have been carried out in the field of cryosurgery. This chapter discusses the literature of the studies carried out in the following areas:

1. Variation in the freezing of tissue during cryosurgery
2. Mechanisms of tissue damage during cryosurgical freezing
3. Numerical modelling studies related to freezing
4. Experimental studies on measurement of temperature distribution
5. Studies related to perfluorocarbons and emulsion preparation
6. Studies directed towards the improvement of cryosurgical process

2.1 Variation in the freezing of tissue during cryosurgery

For optimising the cryosurgical tumour ablation, apart from the development of numerical and experimental studies related to the improvement of the cryosurgical outcome, the effect of freezing needs to be well understood. Studies demonstrate that there are complicated physical, physiological and biological responses that occur in the tissue during freezing, among which these areas deserve significance and exhaustive discussion.

2.1.1 Effect of freezing in tissue at the cellular level

The substantial progress in the low-temperature microscopy has made it possible for biologists to study the changes in freezing at the level of cells and tissues. Three significant events that occur during freezing are: extracellular ice formation (EIF), cellular dehydration, intracellular ice formation (IIF).

Extracellular ice formation (EIF)

During freezing, there is a drop in temperature, and when the temperature lies in between the range of sub-zero to around -20^oC, there is ice formation at the extracellular space [34]. This phenomenon is termed as extracellular ice formation, and the continuous cooling leads to the growth of these ice crystals. Further, in the extracellular space, a low osmotic potential is developed due to freezing that causes the seepage of water present in the intracellular space. Extracellular ice formation has been observed by many researchers during freezing of cells. In a study, it has been reported that EIF is initiated at -1.2^oC while freezing the frog muscle [35]. Further, in another work, researchers have suggested that EIF occurs before intracellular ice formation (IIF) since the liquidus temperature of the extracellular fluid is higher than the intracellular fluid [36]. With advancement in cryosurgical ablation, many findings have suggested the presence of EIF in human tissues. In the same context, Hong et al. have observed large ice crystals around the fat cells after freezing normal and malignant breast tissue samples in LN_2 [37]. Further, researchers have used the directional solidification method to freeze the normal and malignant liver tissues under precisely monitored cooling rates, and it has been observed that EIF occurred in both the cases [38].

Cellular dehydration

Numerous studies carried out by Mazur have reviewed the cellular dehydration due to freezing [39–44]. The presence of a slower cooling rate results in cellular dehydration and the following steps occur during this process. Due to freezing, the temperature decreases to the liquidus temperature of the extracellular space, initiating EIF that increases the solute concentration in the unfrozen fraction of the extracellular space. In principle, a cell adjusts the concentration of water and solute to maintain the chemical equilibrium with the outside surroundings in the absence of any metabolism [45]. Due to selective permeability of the cell membrane, water can pass it while solutes remain outside. This water movement results in a solute concentration difference across the plasma membrane forming an osmotic pressure that drives water transport from inside to outside of cell membrane. At slower cooling rates, sufficient time is available for the water transport and therefore, cellular shrinkage and dehydration eventually occurs. To analyse the freezing within a liver tissue, Rubinsky et al. have used directional solidification [46]. It is seen that the liver cells dehydrate when cooled at a rate of $4^oC/min.$ At lower cooling rates, due to the presence of extracellular ice formation, there is cellular dehydration [47]. Furthermore, a comparison of cellular morphology at different cooling rates suggests that decreasing the cooling rate causes an increased cellular dehydration.

Intracellular ice formation (IIF)

During the freezing process, as the temperature decreases to -40^oC or lower, there is intracellular ice formation [48, 49]. This happens when there is a rapid cooling rate owing to which the freezing water is unable to leave the cells, thereby, causing IIF [34]. It has also been reported that these ice crystals may pass across the cells through intercellular channels [50]. In several studies, Mazur has studied the IIF inside the cells exhaustively [39–44]. In comparison to the dehydration of the cell, IIF usually occurs when the rate of cooling is very high. This leads to the nucleation and growth of ice intracellularly. Early in vitro investigations on IIF in animal tissues have been studied in detail by Love [51]. Mazur has observed IIF in yeast, mouse sperm and human red blood cells [40, 41]. In the last two decades, research groups of Rubinsky and Bischof have carried out studies on IIF in tissues. Under high cooling rates, intracellular ice formation has been observed in normal and malignant breast tissue samples, AT-1 rat prostate tumour [38, 46, 52, 53].

2.1.2 Effect of freezing at the macro level

Considering freezing as a macro level process, a cryosurgical process begins with the cooling of tissue using the cryosurgical probe that causes a decrease in the temperature in the region surrounding the probe. After initial decrease in temperature, phase change occurs and the tissue begins to freeze leading to the formation of ice ball. With time, the cooling progresses and the ice ball encloses the entire volume of the tissue causing damage to the undesired tissue.

Heat transfer in the tissue

Studies related to heat transfer in a biological tissue have fascinated many researchers since 1876 [49]. Numerous research studies have been carried out to quantify the role of blood perfusion and metabolism on the heat transfer in tissue. Some significant reports of heat transfer inside the tissue has been reported by various researchers [54–57]. However, it was Pennes in 1948 who developed the first quantitative bioheat transfer model describing heat flow in tissue [58]. He evaluated the temperature distribution in the human forearm experimentally including the heat conduction terms with two more terms namely the thermal effects of blood perfusion and metabolism. This is one of the most seminal works in the field of bioheat transfer and is also referred to as the "Pennes bio heat transfer equation". Over the last fifty years, Pennes bio heat transfer equation has been successfully used as an important analytical tool. As an analytical tool for bioheat transfer, it finds important application in cancer hyperthermia and thermal models of complete body under environmental stress [59–62]. Till date, Pennes bio heat transfer equation is the most popular and widely utilised equation for solving heat transfer problems related to biological applications and remains an integral part of bioheat transfer [63].

Freezing temperature range of biological tissue

The exact amount of ice and water during freezing at a specific temperature affects the cryosurgery process. In a study, Plank determined ice and water proportion during the freezing of beef muscle at different temperatures by using calorimetry [64]. In another study, Moran found out that the amount of water that converted into ice during freezing of beef, mutton and pork by dilatometry technique [65]. Further, the amount of ice formed during freezing of animal tissues at various temperatures has been determined by the technique of flotation and histology [51]. All these studies are indicative of the fact that freezing in the tissue does not occur at a particular temperature, but at a range of temperature. Generally, the phase change in most biological tissues lies in the range of 0^oC to -10^oC [51].

Vascular stasis during tissue freezing

The first information of the effect of freezing on circulation in tissue has been reported in clinical and experimental works related to frostbite. The tissue cooling during cryosurgery initially results in vasoconstriction i.e., a decrease in the flow of blood in the tissue [34]. The progress in modern cryosurgery in the 1960s led to the beginning of in-vivo studies on the cryosurgery of mammalian tissues. In 1970, Rothenborg carried out experiments to study the cryosurgical cooling of human and rabbit skin by LN_2 cryogen spray [66]. The results of this study suggested that since the diffusion of cooling during cryosurgery is quicker, the walls of capillary have little time to contract before the freezing of blood. The rate of blood perfusion through capillary is constant during cooling and then becomes zero at the start of freezing.

2.2 Mechanisms of tissue damage during cryosurgical freezing

Cryosurgery uses low temperature and freezing to cause tissue destruction. Earlier, the mechanism of tissue destruction was poorly understood, and these shortcomings had prevented the use of cryosurgery by surgeons for treating tumours and other malignancies. The mechanism of tissue destruction has been a topic of discussion among researchers for decades. Till date, many theories have been advocated by scientists. However, the most widely acclaimed views are direct cell injury and vascular injury [34, 48]. These mechanisms are illustrated in Figure 2.1, where elliptical shape indicates healthy cells and star shape suggests the extracellular and intracellular ice.

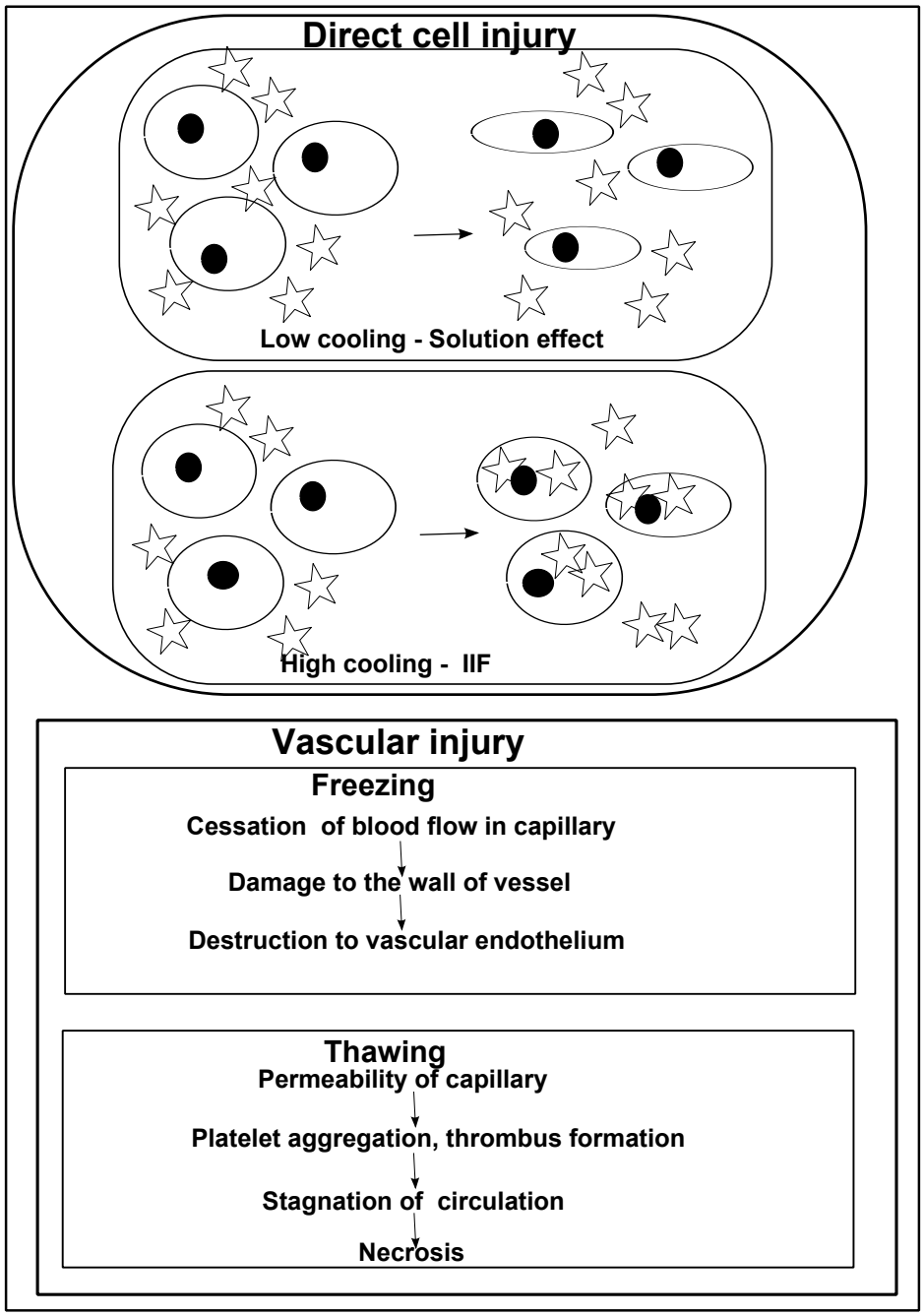

Figure 2.1: A schematic diagram of tissue injury mechanism during cryosurgery

2.2.1 Direct injury to cells

The tissue destruction through direct cell injury occurs primarily due to biophysical events that take place during freezing, i.e. intracellular ice formation and cellular dehydration. The damaging effects of cellular dehydration and solute concentration are termed as the solution effect. Apart from these mechanisms of cellular injury, Ablin has suggested a hypothesis of freezing-initiated immunologic injury [67]. However, there is still controversy surrounding the existence of this mechanism, and therefore this hypothesis is not accepted widely.

Solution effect

As mentioned earlier, freezing of tissues under low cooling rate causes cellular dehydration and a high concentration of solutes, and this is coined as the solution-effect. In the presence of higher concentration of solutes, the enzymatic machinery is destroyed, and there is a destabilisation of the cellular membrane [48]. Further, Gage et al. have advocated that solution effect can injure a cell through several ways. However, a defined interval of freezing during cryosurgery leads to a limited time for the solution effect to occur making it less lethal for the cells [34].

Effect of intracellular ice formation

A higher rate of cooling provides no time for water to move across the cell membrane and causes IIF in the desired tissue. It has been observed that IIF is lethal to cells and this is owing to the fact that these ice crystals aid in disrupting the intracellular cell organelles and membrane [34]. At very low temperatures, smaller ice crystals re-crystallise to form larger ones thereby minimising free energy and surface area. Further, this ice recrystallisation increases the chances of intracellular ice damaging the plasma membrane and other organelles [48].

2.2.2 Vascular injury

The primary cause of vascular injury is anoxia and tissue necrosis due to vascular stasis. In a research work, Cohnheim suggested that frostbite necrosis is a result of hemostasis [68]. During cryosurgery, there are circulatory changes that cause vascular stasis. As the ice formation starts, blood circulation ceases and the blood vessel is affected. This damage includes wall distension and direct cell injury to endothelial cells [48]. Once the ice thaws, there are a plethora of changes in the micro-circulation e.g. increases in permeability of the capillary wall, aggregation of platelets and thrombus formation. In the case of freezing, thrombus occludes the capillary and small blood vessels resulting in vascular stasis [34].

2.3 Numerical modelling studies related to freezing

A good numerical model related to cryosurgery should adequately address all the physical events during the process of tissue freezing. It should also take into account the thermal effects such as heat loss due to blood perfusion, the effect of metabolic heat generation, metabolism inside the unfrozen region of the tissue, release of latent heat during phase change and heat conduction inside the frozen region of the tissue. Considering above mentioned requirements, Comini et al. developed the first mathematical model in 1976 [69]. Since then, researchers across the globe have carried out several studies on the

numerical modelling of cryosurgery process [53, 70–76]. Various numerical strategies and mathematical models have been used to determine the thermal history during cryosurgical ablation.

2.3.1 The governing equation

The studies mentioned earlier suggested that the conduction process dominates the heat transfer within the frozen tissue region. It is understood as there is no blood perfusion and metabolism in the frozen region. The heat diffusion and the thermal distribution in the unfrozen tissue can be calculated by Pennes heat transfer equation [53, 69, 71, 72]. Pennes equation is applied in cases of biological heat transfer especially when the tissue originates from an animal source, and this equation is popularly termed as Pennes biot heat transfer equation. For example, this equation has been utilised to study heat transfer in the case of dunning AT-1 rat prostate tumour, angioma, human brain and tumour in the dorsal skin of a Copenhagen rat [48, 53, 69, 72].

2.3.2 Boundary conditions

The following boundary conditions have been used by the researchers at the cryoprobe tip, e.g. constant temperature, transient temperature dependence conditions or constant cooling rate. [4, 8, 48, 51, 53, 70, 71, 73, 76].

2.3.3 Modelling studies on cryosurgery

The technique of cryosurgery needs very precise control for ablating the tissue. If freezing is not sufficient enough then it might lead to recurrence of cancer in cases of malignancies, thus, while extreme over freezing results in more volume of tissue being destroyed lesser ablation might lead to its recurrence. A numerical study carried out by Comini considered the practical anatomic structure of angioma on an infant's head [69]. However, most numerical studies assume tissue to be isotropic and homogenous, which renders inability to locate components like blood, nerves in the calculation domain. Advances in imaging techniques such as magnetic resonance imaging (MRI), ultrasound, X-ray and electrical impedance tomography (EIT) have facilitated in performing cryosurgeries with ease and made this technique popular, but each one of them has its limitations [26, 77–80]. Each imaging procedure available currently helps in visualising the ice ball interface, but it is unable to predict the exact location of the lethal front or critical temperature isotherm which is extremely crucial for determining the extent of damage to cancerous cells. To tackle these problems and provide online monitoring of temperature at a finite number of points within the tissue, thermocouples are being used. But the exact placement and positioning of these thermocouples again require details like precise location of critical temperature isotherm.

To solve this issue, models have been developed not only to determine the temperature around the cryoprobe but also within the iceball that is formed during this process. The earliest model that was developed was for a single cryoprobe on a one-dimensional plane which assumed immediate cooling around the probe [81]. This model proposed conduction as the significant driving force of heat transfer inside biological tissues. Newer and complex models were developed later to conduct a parametric study of freezing of tissue in a two-dimensional and axisymmetric cylindrical cryoprobe using finite difference scheme. Also, an exact time-dependent location of the ice ball was visualised, but the temperature within it was not calculated [72]. In the same context, Rewcastle et al. proposed a three-dimensional finite difference method that simulated freezing and temperature evolution in a medium with a multiprobe arrangement [73]. In another study, Deng et al. have carried out a study on selective freezing of tissues. In this numerical work, it is seen that the injection of solutions of high thermal conductivity results in a better clinical outcome during cryosurgery [82]. To improve the efficacy of the cryosurgical procedure, Rossi et al. have suggested a method of computerised planning for prostate cryosurgery that advocates variation in the insertion depth of cryoprobes [83].

Researchers have recently utilised mathematical tools to reconstruct the temperature field for wireless temperature sensors. The results of the study demonstrate that this technique can help in determining the lethal front temperature to a significant degree of certainty [84]. Another significant research work recreated a database of prostate models that can later help in computerised planning and training of cryosurgical procedures [85]. Further, a cryosurgery tutoring aid has been developed that helps in optimising a geometrical constraint like cryoprobe placement and predicting temperature distribution [86]. A new potential field analogy method (PFAM) is combined with the temperature field reconstruction method (TFRM) to determine the temperature profile in the frozen area. The results of this integrated approach (PFAM and TFRM) suggest that this is an efficient tool to calculate the thermal history in the frozen region during ultrasound-assisted cryosurgery [87].

2.3.4 Numerical schemes

Several numerical schemes have been utilised for discretising the governing Pennes biot heat transfer equation and the phase change phenomena is handled as mentioned below.

2.3.5 Discretisation methods for solving the numerical schemes

Several researchers have used the finite difference scheme for solving these problems [48, 53, 71, 72]; while the use of finite element method has been advocated by Budmann et al. , Weill et al., and Wan et al. [70, 74, 75]. In another study, Smith et al. have suggested the use of finite volume based numerical approach to solve similar problems [47].

2.3.6 Handling the phase change processes

Various numerical methods have been used to handle the tissue freezing process, e.g. front tracking method [53, 75], source term method [76], enthalpy method [72, 74] and apparent heat capacity method [70, 72, 73]. The principles of these methods are described in the following section:

Front tracking scheme

This methodology solves the conduction problem in the frozen region of the domain and the Pennes equation in the unfrozen region. The boundary condition, i.e., Stefan conditions, are required to define the temperature continuity and heat flux at the interface. While calculating, the position of the freezing front has to be updated at each time step, which requires extra work for grid refresh or local refinement. Further, this method gives superior output for a pure substance, in which the phase change occurs at a single point in terms of temperature value. Due to this reason, Bischof et al. assumed the freezing point of dunning AT-1 Rat prostate tumour to be 0^oC (273 K), however, tissues generally freeze over a range of temperature [53, 69, 72].

Enthalpy method

This method uses enthalpy (H) as the variable in the transient term in the heat conduction equation instead of temperature (T) or the Pennes biot heat transfer equation. The presence of two dependent variables (H and T), needs an additional equation for addressing the relationship between H and T. Once the enthalpy at the current time step is determined, H at the current time is also known, corresponding temperature field can be updated by solving the additional equation prior to proceeding to the next time step. In comparison to the front tracking scheme, the enthalpy method helps in solving phase change problem in a fixed grid.

Apparent heat capacity method

This method considers the phase change process by incorporating the effect of latent heat effect into the change of variation of an apparent heat capacity, thus, the integration of the specific heat over temperature of phase change is equivalent to the latent heat. This strategy makes an assumption that the apparent specific heat varies linearly in the region of phase change [70, 72, 73].

2.3.7 Factors affecting the outcome of cryosurgery

Several studies that have discussed mechanisms of cryo injury to tissue have revealed that the thermal history has significant impact on cryosurgical injury. In the same context,

Hoffmann and Bischof have suggested that the thermal history is in turn affected by four parameters[48]:

1. Rate of cooling
2. End temperature
3. Hold time (Time taken below the lethal temperature)
4. Thawing rate

These parameters have a significant impact over the outcome of cryosurgery. Hence, these parameters are discussed concisely in the following sections.

Cooling rate

The rate of cooling plays a crucial role in determining the mechanisms of direct cell injury: Intracellular ice formation (IIF) results in high cooling, while at lower cooling rate solution effect is dominant. Since IIF is highly fatal to the survival of freezing cells, the cryosurgical procedure or planning should be designed in such a way that cryosurgery protocol results in generation of significant IIF. Hence, the cryoprobe should have a higher cooling capacity to produce an elevated rate of cooling. Due to this reason, the LN_2 cryoprobe should be utilised to ablate invasive tumours [23]. Moreover, it is seen that the method of multiple cryoprobes can be used for a larger tumour, as a higher cooling rate occurs near the tip of the cryoprobe [34]. Therefore, further technology improvement needs to de carried out for developing high performance multiprobe cryosurgery systems. For example, Chang et al. have developed a novel cryosurgery system using subcooled liquid nitrogen that produces a lower temperature of -206^oC which is better than the conventional cryosurgery systems [88]. These techniques, i.e. multiprobe and sub-cooled systems provide higher destruction and produce a higher cooling rate, thus, enhancing the outcome of cryosurgery significantly. Further, experimental studies show a significant dependence of cooling rate in association with IIF. In a study, Bischof et al. have revealed that a cooling rate of $50^oC/min$ produces intracellular ice formation in Dunning AT-1 rate prostate tumour cells[53], while in human liver tissue IIF occurs at a cooling rate of $22^oC/min$ [47].

Lethal or critical temperature

For a cryosurgical procedure to be effective, the rate of freezing should be optimal so that the tumour ablation is uniform with minimal damage to the surrounding healthy tissue. It is well known that lower temperature in the tissue leads to higher destruction and for a complete destruction a lethal or critical temperature should be achieved. It has been reported that the critical temperature for cell destruction must be in the range of -40^0C to -50^0C [9, 10, 89–96]. This critical temperature is achieved due to the ice formation during

Table 2.1: Some important in vivo experimental studies showing lethal temperature for various tissues

$1^{st} Author$	Year	Tissue	Lethal temperature
Gage	1966	Osteocytes, bone, dog	-2^oC [97]
Gage	1978	Melanocytes, skin, dog	-4^oC [94]
Gage	1982	Skin, dog	-40^oC [92]
Neel	1971	Sarcoma, mouse	-60^oC [101]
Rivoire	1996	Liver,pig	-15^oC [90]

the cooling of tissue. Many cryosurgical studies have been conducted on determining the lethal temperature and it has been observed that it is a tissue dependent parameter [34, 97]. Moreover, experiments carried out by researchers indicate that malignant cells are more resistant to freezing induced destruction than the normal cells [98–100]. Considering the differences in the quantitative values of temperature at which complete cell/tissue destruction occurs, Gage et al. have suggested that it is safe to lower the temperature between -40^oC to -50^oC for achieving the goal of complete cellular damage [92]. Table 2.1 provides the list of some significant studies that were carried out to determine the lethal temperature.

Thawing rate

Till date, studies point out that a slow thawing rate can strengthen the destructive effect and cause higher damage [34, 48]. Experiments indicate that longer thaw duration results in increased solution-effect and higher growth of ice crystals [102, 103]. Some experimental evidences also reveal that a slow thawing plays a critical role in cell death than rapid a cooling protocol [101, 104, 105].

Hold time

Hold time is referred to as the time at which the desired tissue has been frozen to a temperature lower than the lethal temperature [48]. Increasing the hold time actually results in a higher amount of intracellular ice formation and provides sufficient time for recrystallisation of intracellular ice crystals [125]. In terms of solution effect, the increment in the hold time allows the equilibration of the osmosis between the intracellular and extracellular spaces, thereby, increasing the cellular dehydration. Further, in different in vivo experiments, the destructive effect of the increase of hold time has been observed by researchers [91, 94, 96].

2.4 Experimental studies on determination of temperature profile during cryosurgery

Temperature plays an important role in determining the tissue injury mechanism and the clinical outcome of tumour ablation during cryosurgery. Numerous experiments have been carried out on tissues and tissue mimicking gel phantoms to investigate the temperature distribution inside the tissue during cryosurgery, which will be discussed in this section of the thesis.

2.4.1 Experimental studies on tissue mimicking gel phantoms

Researchers have made gel phantoms to mimick the thermophysical properties of tissue [106]. In this study, agarose has been used to form the tissue mimicking gel phantoms. Cooper et al. for the first time carried out an experiment to investigate the thermal history during cryosurgery [7]. A clear gel consisting of 1.5% gelatin and 98.5% water was utilised for the preparation of tissue phantom and liquid crystal technique aided in the measurement of temperature distribution in the gel. In this case, the cooling was produced by a single LN_2 cryoprobe. Budman et al. also studied thermal profile in a tissue phantom containing 2% gelatin and 98% water [70]. Cryoprobes of LN_2 and pressurized N_2O were used to cool the tissues respectively and temperature is determined by the thermocouples present at the different locations near the cryoprobe. Experiments have been compared with the analytical solution, and the numerical findings have been obtained by using finite element method. Similar kind of experiments have been conducted by Augustynovvicz et al. on the gelatin gel phantoms of different concentration [107]. The use of gel phantom to mimick the thermophysical property of tissue makes the real time measurement of temperature at multiple locations easy since the location of the thermocouple inside the gel is visible through visual observation. Furthermore, the thermophysical properties of gel phantoms are similar to that of biological tissue. Therefore, there is no significant difference in heat flow dynamics during cryosurgery and these results provide a preliminary finding that can be applied in a real time clinical trial of cryosurgery.

2.4.2 Experimental studies on tissues

Apart from gel phantoms, experiments have also been performed by researchers on tissues and is discussed in the following section.

In vitro studies

Several tissues (animal and human) have been studied by in vitro experiments to explore the effect of cryosurgery and analyse the thermal history due to the tissue cooling (Table 2.2).

Table 2.2: Few significant in vitro experimental studies on tissues during cryosurgery

$1^{st} Author$	Year	Tissue	Parameter investigated
Onik	1984	Beef liver	Temperature profile and ice ball [26]
Homasson	1994	Rat tissue culture, human serum and whole blood	Temperature profile and ice ball [108]
Augustynovvicz	1985	Beef tissue	Thermal history, rate of cooling and ice ball [107]
Lam	1998	Porcine liver	Temperature,rate of cooling and ice ball [109]
Yang	2000	Mouse bladder-tumour cell line	Temperature distribution, ice ball [110]

Onik et al. conducted cryosurgical freezing on beef liver [26]. The technique of ultrasound has been used to monitor the extent of ice formation or the frozen region during cryosurgery. In a research study, Augustynovvicz et al. utilised cryoprobe to focally freeze beef, muscle and liver while the tissue was immersed in a water bath at 37^oC [107]. Further, this study measured temperature by placing thermocouples at different locations and the measurement of cooling curves aided in estimating the thermal history and the iceball growth. A study carried out by Homasson et al. revealed the use of N_2O based cryoprobe for cryosurgical ablation of rat tissue culture, human serum and blood [108]. In this work, the tissue impedance and temperature readings have been measured at fixed positions, and the ice ball growth has been observed and determined visually. Lam et al. have reported the study of freezing of fresh porcine liver experimentally [109]. In this study, the ice ball growth and temperature measurements have been carried out exhaustively. Yang et al. cultivated mouse bladder tumor cell line MBT-2 as the target of the cryosurgical freezing produced by a LN_2 based cryoprobe. Tissue temperature was measured by 16 thermocouples arranged on a horizontal plane and the temperature distribution and variation were studied [110].

2.5 Studies related to perfluorocarbons and emulsion preparation

Perfluorocarbons are chemically inert, non-toxic and find a plethora of applications in biomedical engineering [111]. These are highly fluorinated compounds that are capable of dissolving a large amount of respiratory gases like oxygen and carbon dioxide [112, 113]. In a study, researchers have used perfluorocarbon nanoparticles for molecular imaging while performing magnetic resonance imaging (MRI) [114]. Nanoemulsions of perfluorocarbons are currently available that increase the cell labelling efficiency during imaging [115]. Apart from these applications, perfluorocarbons have been used for supporting liquid breathing [116]. In another study, Fraker et al. have evaluated the crucial role played by the particle size of perfluorocarbon emulsions in the oxygen transfer rate[117]. The study indicated that there is a reduction in oxygen diffusion with the increment in particle size of the perfluorocarbon emulsions. Recently, researchers have synthesised perfluorocarbon emulsions that can help in imaging of cells and tissues [118, 119]. Furthermore, perfluorocarbon nanoprobes have been designed that aid in optical imaging of cells, however, less light penetration through the tissue prohibits the use of this kind of visual labelling in non-invasive experiments [120].

Perfluorocarbons are hydrophobic and immiscible with biological fluids like water and plasma. Therefore, emulsification is necessary and done before it is utilised for in vivo or biological applications. Emulsification is carried out with the help of surface active molecules termed as the surfactant. In a study, Freire et al. formulated perfluorocarbon emulsions of 50% (w/v) to study the ageing processes and a detailed investigation of mechanism revealed the presence of both coalescence and molecular diffusion in the emulsions. Generally, with time, the growth of perfluorodecalin emulsion particles occurs due to two molecular level processes namely molecular diffusion and coalescence [121, 122]. In another significant study, researchers have reported the stabilisation of emulsions with the help of adsorption of solid particles at the oil and water interface. It has also been seen that thermal variation in these emulsions leads to surfactants desorption from the oil and water interface. However, in the case of solid particles, this anchorage at the interface is permanent [123]. Barnett et al. have utilised perfluorocarbon nanoparticles for non-invasive imaging of human cadaveric islets. The results presented in the study suggest that both perfluorooctyl bromide and perfluoropolyether labelled cells are fluorinated efficiently for visualisation using F-MR (magnetic resonance) imaging. The inner core of perfluorocarbon nanoparticle can be used for the delivery of melittin in vivo. The results of this study demonstrate that the use of perfluorocarbon core can help in preventing toxicity to vaginal and sperm epithelium, yet acting as a potential virucide for the targeted region [124]. In another experiment, nuclear magnetic resonance technique has been explored to determine the size of an emulsion

droplet. Further, it can also aid in visualising a single droplet and distinguish it from a cluster of droplets, thereby, helping in the identification of coalescence from flocculation [125]. All these studies point out that the perfluorocarbons can be identified easily with the help of various imaging techniques, thus, suggesting that it can be practically utilised in the medical applications. In the current study, one unique facet of perfluorocarbon molecule is explored; the thermal conductivity of perfluorocarbon is low and can be used effectively for insulating the tumour during cryosurgery. These emulsions can be utilised to formulate new low thermal conductivity emulsions of perfluorocarbons tailored for use as insulation during the cryosurgery process.

2.6 Studies directed towards the improvement of cryosurgical process

A plethora of in vivo and in vitro studies have been carried out to improvise cryosurgery and increase its effectiveness. Cryosurgery has been used to perform hepatic surgery for colorectal masses and porcine kidney tumours [126, 127]. Another in vivo study showed that phosphate buffered saline solution of antifreeze proteins type-I at a concentration of 10 mg/ml can cause cell death and acts as an adjuvant. The spicular nature of ice crystals formed due to these proteins rupture the cell and cause its membrane to lose integrity [128]. Several chemical adjuvants, used in chemotherapy, like peplomycin and adriamycin, have been used along with this procedure and have shown good results[129]. Recently, it has been shown that eutectic freezing can also elevate tissue damage during cryotherapy [130]. Further, if a solution of high thermal conductivity or low latent heat is injected into the tumour, with the same probe configuration, a larger ice ball has been produced [82]. In another study, experimental results demonstrated that injection of appropriate solution like water, aluminium oxide nanoparticles in water, ethanol and 10% solution of dimethyl sulfoxide enhanced the tumour killing during cryosurgery without affecting the freezing process [131].

Studies have been carried out to investigate the role of the vasculature in enhancing cryosurgical cell death. Pre-conditioning of the tumour before cryosurgery using TNF-α, which is a vascular cytokine, has shown promising results. The cryo lesions diameter increased significantly when the cryosurgery was performed after injection of this cytokine [132]. Thus, showing that even vascular adjuvants increase the efficacy of cryosurgery significantly. Chua and Chou suggested that employing more number of freeze-thaw cycles facilitates greater cell destruction within the tissue [106]. These techniques improve the cryosurgical process to some extent but lack in minimising the damage to the surrounding healthy tissues. To further enhance cryosurgery by decreasing the healthy tissue damage, the use of a cryo heather is recommended, a device which aids the cryoprobe by heating the tissue to shape the freezing of ice ball [133]. A recent numerical study carried out

by Ramajayam and Kumar has proposed a novel approach for the improvement of the cryosurgical outcome[134]. The study suggests the use of a layer of perfluorocarbon around the tumour interface during cryosurgery. This strategy has two benefits: it helps in increasing the rate of tumour ablation and prevents the destruction to the surrounding healthy tissue. Furthermore, this parametric study indicates that perfluorocarbon (PFC) can act as a barrier to heat transfer during the cryosurgery of a tumour.

As discussed previously, researchers have carried out extensive numerical studies for improving the efficacy of cryosurgery process [1]. Earlier studies have focussed on developing one-dimensional models for heat transfer process during cryosurgery [69]. With advances in technology, three dimensional models have been developed to determine the location of lethal and ice front [73, 83]. Another study carried out by Deng et al has concluded that injection of solutions of high thermal conductivity can better the outcome of cryosurgery [82]. In another significant study, a new potential field analogy method (PFAM) is combined with the temperature field reconstruction method (TFRM) to determine the temperature profile in the frozen area [84]. However, none of the prominent studies mentioned above have focussed on a combinative approach that suggests the use of adjuvants to increase the efficacy of the cryosurgery inside the tumour and at the same time prevent the damage due to the surrounding healthy tissue using a perfluorocarbon layer. In the present study, a parametric analysis (offset, time taken for complete tumour ablation etc) of heat transfer process is carried out for a two dimensional (2D) axisymetric spherical tumour in the presence or absence of a low thermal conductivity perfluorocarbon (liquid) layer using numerical modelling during cryosurgery. The concept of low thermal conductivity liquid layer around the tumour interface is new and finds significant practical implications in cryosurgery and hence requires investigation similar to the once carried out in this study. Secondly, although pure perfluorocarbons possess suitable thermal conductivity, perfluorocarbon emulsions can also be used for the proposed application as it would help in reducing the amount of the pure perfluorocarbon used without compromising its lower thermal conductivity significantly. Studies suggest the use of perfluorocarbon based emulsions in various biomedical applications [115, 117, 120]. However, this study reports the use of perfluorocarbon emulsions as an insulating layer during cryosurgical tumour ablation, thus, providing a low cost substitute for improving the efficacy of cryosurgery. The use of different adjuvants during cryosurgery has been advocated by researchers earlier [128–130]. However, the use of glycine and alumina as an adjuvant during cryosurgery in presence of a thermal barrier of perfluorocarbon layer has not been reported. This gap in literature is filled by this current study which will provide a two-fold benefit of a lower end temperature inside the gel phantom owing to the adjuvants during cryosurgery and at the same time limit the freezing to the desired region by using a perfluorocarbon layer. Thus, providing a combinative strategy for enhancing the freezing while minimising the damage to the surrounding region. In conclusion, this chapter discusses the indequacies that exist in

the field of cryosurgery and also proposes the steps that can be taken to improve the efficacy of cryosurgery. The subsequent chapters shall discuss the results of the new approaches used to improve the cryosurgical outcome so that this technique reaches clinical practice and becomes a routine procedure in the near future.

Chapter 3

An approach to improve cryosurgery: a numerical study

3.1 Introduction

Although a lot of research has been done on improving cryosurgery process but still a lot of drawbacks exist and to overcome the same, a novel concept is proposed that can improve the efficacy of modern cryosurgical process substantially. The primary objective of this chapter is to carry out a parametric study of the freezing process during cryosurgery of tumours in the presence of a perfluorocarbon (liquid) layer of low thermal conductivity at the tumour interface by using numerical modelling. It should be noted that the liquid layer can be made by using perfluorohexane, a perfluorocarbon, which is widely used in the field of medicine for liquid breathing. This liquid has a very low thermal conductivity of 0.067 $W/m.K$ and very low solubility in water. Tumour cells have unique cell surface receptors which are quite different from their normal counterparts. Different type of tumour cells express different antigens; these tumour antigens can be targeted by monoclonal antibodies, which is already in practice in biological research [135]. It is proposed that this monoclonal antibody can attach to an adaptor protein on the other end [136]. The adaptor protein used can bind to a thermosensitive ligand which can bind preferentially at the temperature of tumour interface. This thermosensitive ligand can then be linked to perfluorocarbon by using an adaptor. Figure 3.1 mentioned below illustrates a schematic representation of the proposed approach that can be used in a real time scenario.

For this approach to be successful in the clinics, first, the tumour interface needs to be identified using the current day imaging technique like Magnetic resonance imaging (MRI), X-Ray. Subsequently, a thin space can be created around the tumour interface by a surgeon using laparoscopy which is a minimally invasive technique. This has to be followed by the injection of perfluorocarbon in the created space around the tumour. The perfluorocarbon (PFC) will not enter the tumour because it is hydrophobic and the inner environment is hydrophilic, thereby, preventing the mixing of PFC inside the tumour tissue. Secondly, the mass diffusivity of PFC is 5×10^{-5} cm^2/s which is very low and this is very favourable for

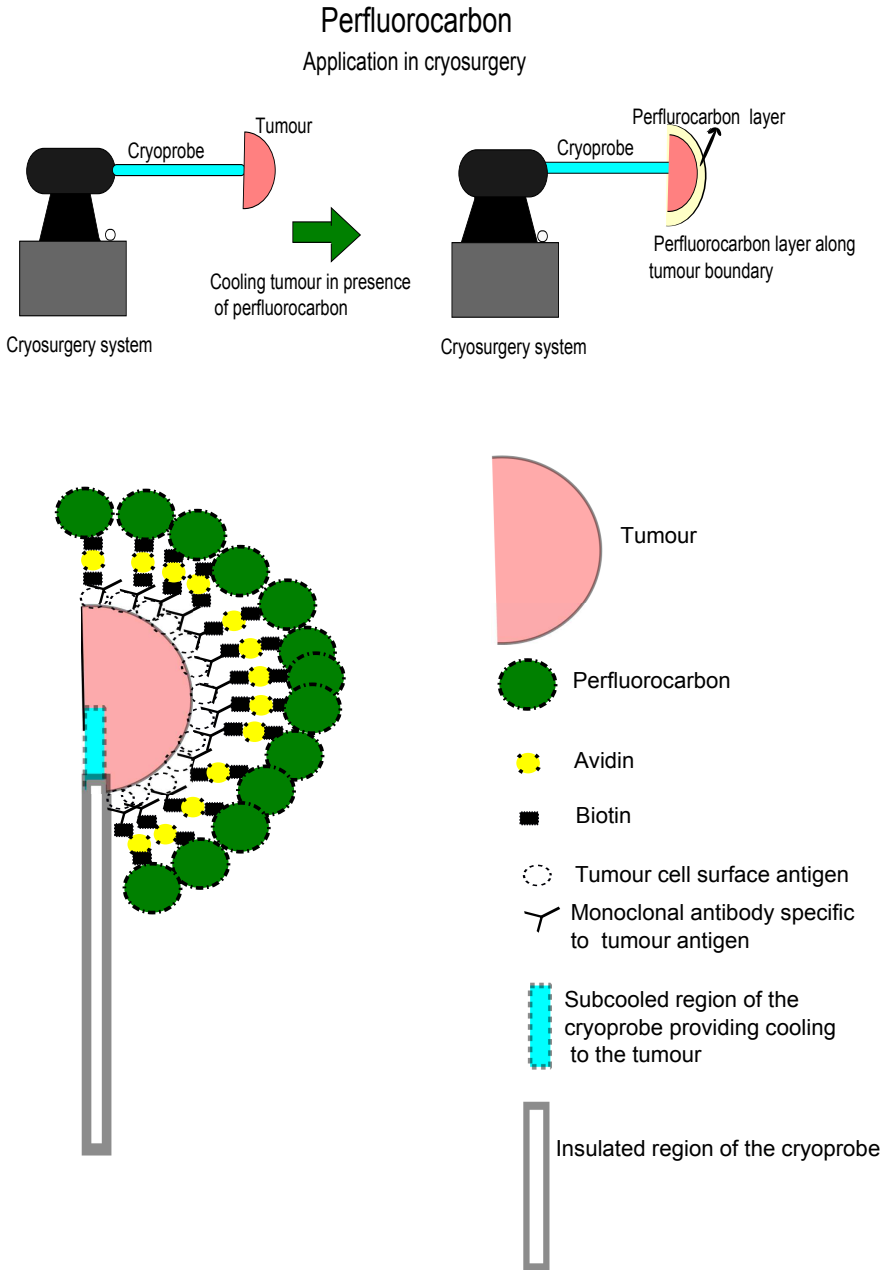

Figure 3.1: A proposed approach to improve the efficacy of cryosurgery

the proposed application as once the PFC is filled in that space, owing to meagre diffusivity, it would not enter the tumour tissue. One more reason which would make this perfluorocarbon layer approach successful it the time needed to complete the procedure, generally, a complete cycle of ablation takes 10-20 minutes and the PFC layer filled in that space surrounding the tumour needs to be maintained till that particular time. Once the freezing cycle is completed, PFC can be drained out in a minimally invasive way. After surgery, the removal of PFC layer will give a measure of the ablated zone. The avidin-biotin interaction for attaching PFC at the tumour interface can be made reversible. Modified versions of avidin resins and modified forms of biotin labeling reagents are commercially available which can make the reaction readily reversible. Therefore, once the cryosurgery process is complete, the bound avidin-biotin and PFC can be removed and drained out using minimally invasive techniques.

In this chapter, a parametric study is carried out for determining the optimal cooling configuration (i.e. optimal offset) and the effect of change in active length of the cryoprobe on the freezing process for various tumour radii. Further, studies have also carried out to investigate the role of the low thermal conductivity perfluorocarbon (liquid) layer around the tumour interface, the effect of increase in tumour radii on cryosurgical freezing and the ablation time for various optimal offsets. The results thus obtained provide a deeper insight into the fundamentals of heat transfer occuring during this process and also aid in design of an optimal protocol for cryosurgical planning. The other objective of this chapter is to numerically evaluate the effect of perfluorohexane layer as an insulation around the interface of the tumour. Further, the determination of the optimal thickness of perfluorohexane (liquid) layer is evaluated for the prevention of the destruction to the neighbouring healthy tissue. Beyond a critical thickness, the increase in thickness of the perfluorohexane layer does not change the heat transfer characteristics during cryosurgery. On the other hand, decreasing the thickness below the critical limit leads to the destruction of the healthy tissue present at the tumour interface. Furthermore, in this study, the effect of a change in thermal conductivity of the liquid which is used as an insulating layer at the tumour boundary is also determined. The change in thermal conductivity affects the propagation of lethal front. With the increase in thermal conductivity of the insulation layer (liquid) at the tumour boundary, the lethal front is unable to reach the tumour interface. Hence, the propagation of the lethal front is also studied during the cryosurgical process. The gap between the lethal front and the tumour boundary can be used in the identification of an optimal offset. This offset is the most optimal configuration that leads to uniform cooling inside the tumour, thus, reducing the tumour ablation time. Therefore, the results of this chapter also provide optimised parameters which will help in improving the effectiveness of the cryosurgical procedure.

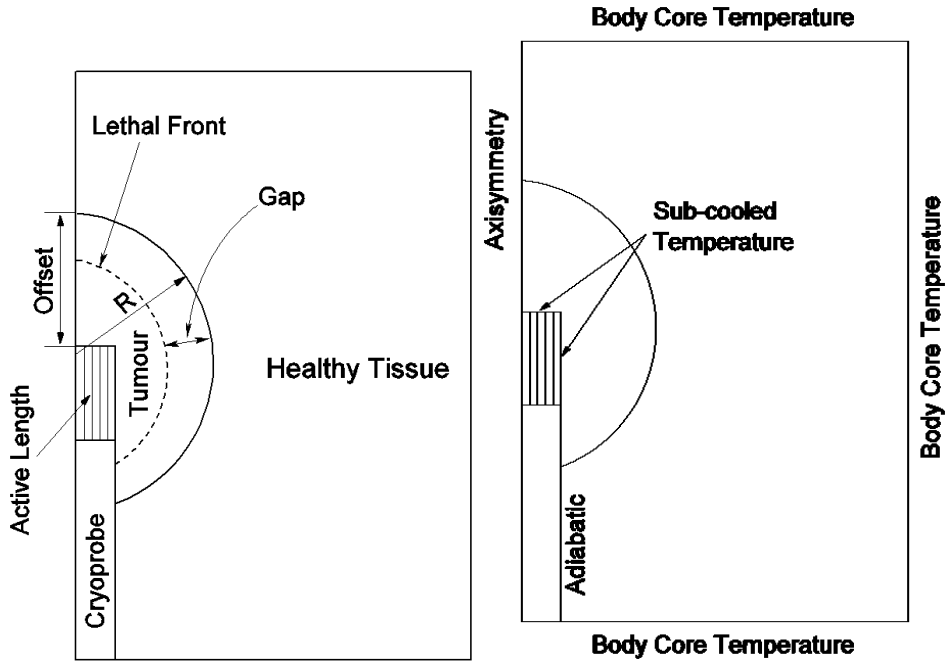

(a) Terminology (b) Boundary conditions

Figure 3.2: Schematic representation of terminology and boundary conditions used in the study

NOMENCLATURE

c	specific heat $(J/g.K)$	m_b	blood perfusion rate
H	specific total enthalpy (J/kg)		per m^3 of tissue per blood
h	specific sensible enhthalpy (J/kg)	**Subscript**	
k	thermal conductivity $(W/m.K)$	b	blood
L	specific latent heat (J/g)	f	frozen tissue
Q_m	metabolic heat generation (W/m^3)	l	point at which freezing starts
T	temperature (^oC)	s	point at which freezing ends
t	time (s)	u	unfrozen tissue

3.2 Mathematical formulation

A two dimensional (2D) axisymmetrical model for a multiblock structured grid is developed in FORTRAN 77 compiler (in house code). The developed model is used to study freezing of tumours of three different radii namely 10 mm, 12.5 mm, and 15 mm for three different active lengths around a single cylindrical cryobrobe of radius 3 mm. The terminology and boundary conditions used in this study are depicted in Figure 3.2(a) and Figure 3.2(b). In Figure 3.2(a), it can be seen that a cryoprobe is inserted into a tumour of particular radius. The lethal front is the -40^oC temperature isotherm which ensures complete cancerous cell destruction. The term "gap "mentioned in this study is the distance between the -40^oC

isotherm and the tumour interface. Further, active length is the length of the cryoprobe which provides the cooling to the tissue. For each active length of the cryoprobe, an offset (the minimum distance between the interface of the tumour and the tip of the cryoprobe) is identified, termed as the optimal offset. This optimal offset provides a uniform cooling of the cancerous tissue, thereby, destroying the complete tumour at a particular interval of time. The boundary conditions that are considered here are realistic and practical. A condition of axisymetry exists around the cryoprobe which is inserted into the tumour. In other words, it means that only one half of tumour is being considered and the other half is just the exact match of it in terms of geometry of the tumour, insertion of depth of cryoprobe and the boundary conditions assumed. The region near the active length of the cryoprobe has sub cooled temperature as this is the region that provides cooling to the tumour. The region of the cryoprobe which faces the healthy tissue and is just below the active length has adiabatic conditions because below the active length, the cryoprobe is insulated and hence the temperature gradient between the insulated surface and the surrounding healthy tissue which is in contact is zero. The upper boundary, lower boundary and the right hand side of the domain has temperature equivalent to 37^oC which is the core body temperature. This is due to the fact that the tissue surrounding the tumour which is healthy and metabolising properly has temperature equal to the core body temperature. It is very important to note that there exists a perfluorocarbon (liquid) layer around the interface of tumour which possesses very low thermal conductivity and which is mathematically defined as the sum of the radius of the tumour and the thickness of that layer.

3.2.1 The governing equation

The classic Pennes bio heat transfer equation has been used to study the heat transfer dynamics during cryosurgery. The equation in its usual form is given as

$$\frac{\partial(\rho H)}{\partial t} = \boldsymbol{\nabla} \cdot (k \boldsymbol{\nabla} T) + \dot{m}_b c_b (T_b - T) + \dot{Q}_m \tag{3.1}$$

where ρ is the density of the tissue, $H = h + \int c\, dT$, is the total specific enthalpy, h is the specific sensible enthalpy, c is the specific heat at constant pressure, $\dot{m}_b$ is the blood perfusion rate, T is the temperature, and $\dot{Q}_m$ is the volumetric metabolic heat generation rate which is taken as 10890.0 W/m^3. The thermophysical properties of rat prostate tissue have been listed in Table 3.1.

The Pennes equation is similar to the general heat diffusion equation with exception of the second and the third terms appearing in the right hand side of equation 3.1. The second and third terms on the right hand side of the equation represent the internal heat sink due to blood flow and heat generated due to metabolism, respectively. It has been assumed that blood enters the target tissue with fixed temperature T_b. It has been observed that for a particular

Table 3.1: Thermo-physical properties of biological tissue [137]

ρ_u	1000 kg/m^3	L	194×10^3 J/kg
ρ_f	998 kg/m^3	c_b	4200 J/kg^{o}C
c_{pu}	3347 J/kg^{o}C	k_u	0.50208 W/m^{o}C
c_{pf}	1673. J/kg^{o}C	k_f	1.7528 W/m^{o}C
T_l	-1°C	T_s	-8°C

body mass and activity, the heat generated due to metabolic process is relatively constant. The numerical solution of equation 3.1 is obtained for the following assumptions: heat transfer in the tissue is purely by diffusion; phase transition occurs over a wide temperature range between -1^oC (upper limit) and -8^oC (lower limit) [138]; thermal conductivity varies drastically with the temperature; blood perfusion acts as heat sink and metabolism is the heat source for the unfrozen tissue. Further, researchers working on cryosurgery generally use the Pennes bio heat transfer equation that is based on the fourier model of heat conduction owing to a prolonged exposure time (10-20 minutes) that is sufficient enough to reach thermal equilibrium without a thermal lag. Therefore, non-fourier based model may not be appropriate in this particular case.

The method proposed by Voller and Prakash uses the following approach [139]. In this method, the enthalpy is associated with the liquid fraction in the mushy zone where the general form of local solid fraction ($f_s(T)$) varies as $f(T) = L$, when $T > T_l$; $f(T) = L(1-f_s)$ when $T_l > T \geq T_s$; and $f(T) = 0$ when $T < T_s$ where ΔH is the enthalpy, L is the latent heat of fusion, T_l is the temperature at whoch the freezing starts i.e. liquidus temperature, T_s is the temperature at which the freezing ends i.e. the solidus temperature, the transition region temperature lies between the solidus and the liquidus temperature.

3.2.2 Solution approach

The computational domain with variation in grid densities is shown in figure 3.3. It should be noted that Figure 3.3 corresponds to the configuration when the central probe is also present. Different colours of the boundary are representative of the different blocks used in the simulation. The axis of the physical domain is also shown in the figure. The axial length of the computational domain is taken as 100 mm while radial distance is taken equal to 60 mm. The above mentioned distances are found sufficient to impose the basal body temperature, 37^oC, condition at the extremities of the domain. It should be noted that grids are laid in such a way that grid density is higher near the large temperature gradient zone (i.e. near the cryoprobes) and it is lower at the extremities of the domain. A multiblock grid system having three blocks of 57×66, 57×34, and 30×34 control volumes is found sufficient to resolve the temperature fields and the frozen and the unfrozen fronts during the freezing process for the case of configurations with a single cylindrical cryoprobe around a tumour. For example, Figure 3.4 shows the variation of gap between the lethal front and the

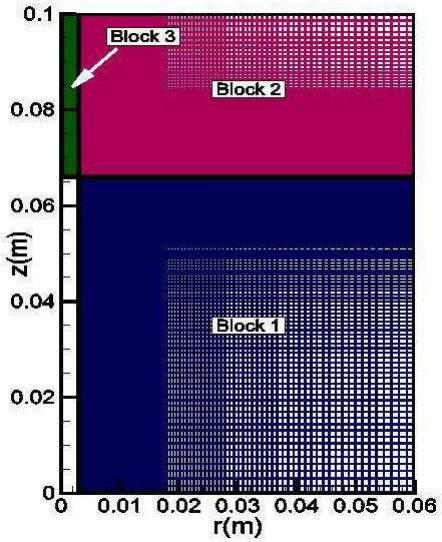

Figure 3.3: The computational domain with multiblock orthogonal structured nonuniform grid

radius of tumour with time for two sets of grid densities, fine and coarse. It can be noticed that with increase in the number of control volumes the change in predictions is almost negligible. The diffusion equation with phase change, blood perfusion, and metabolism is discretised on a structured multiblock orthogonal grid system using finite volume approach. The diffusive term and the unsteady term are discretised using central difference scheme and the implicit three time level method (a quadratic backward approximation) respectively giving rise to second order accuracy in space as well as in time. Detailed discussion about implicit three time level scheme and the structured multiblock grid system adopted here can be found in Ferziger and Peric [140]. Fixed grid enthalpy method given by Voller and Prakash [139] is utilised to solve the phase change problem. This method suggests an enthalpy formulation based on fixed grid for the numerical solution of convection-diffusion controlled phase change problems where phase change occurs at a distinct temperature range which is true in case of biological tissues. The defect or gap between the radius of the tumour and the lethal front is quantified in terms of an angle (θ) , which is calculated as follows:

Figure 3.5 shows the different parameters which are used to calculate the angle (θ). It should be noted that first the coordinate of the centre of the circle (because of the spherical tumour) (xc, yc) is determined to calculate the angle (θ); xc is the coordinate of the leftmost part of the computational domain, which is equal to zero in this study. Further, it should be noted that for all the cases considered in this study, the tip of the cryoprobe is placed at the same axial location of 0.066m from the bottom of the computational domain. Let us consider a case for which the active length of the cryoprobe is equal to y (in metre) and the offset is equal to x (in metre) as shown in Figure 3.5. Then the vertical coordinate of the centre, i.e. yc is given as

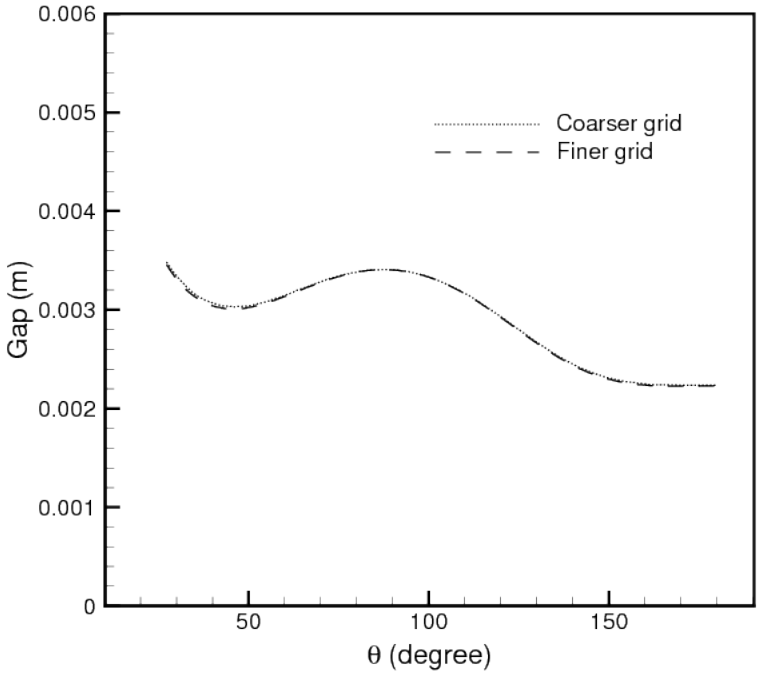

Figure 3.4: Grid independency test

$$\text{yc} \;=\; 0.066 + \text{x} - R_t \tag{3.2}$$

where R_t is the radius of tumour. The points of intersection of lethal front with the control volume faces are explicitely calculated after each time step. Such an intersection point is represented by a cross mark ($\times$) in Figure 3.5 with a coordinate of (xl, yl). Once the point of intersection and the centre of the tumour are known, the angle (θ) is easily calculated using the following formula,

$$\theta \;=\; arctan\left(\frac{\text{xl-xc}}{\text{yl-yc}}\right) \tag{3.3}$$

This approach is new and quite effective because, it not only predicts the gap between the lethal front and tumour interface efficiently but also provides the angular position at which this is occuring (Equation 3.3). This information is really important for the surgeons to manipulate the surgical parameters (i.e. the active length of the cryoprobe, offset of the cryoprobe etc) so as to make this process more effective. Generally, defect is calculated using the volume enclosed by the lethal front (Equation 3.4) and is quantified by the following relationship [83]:

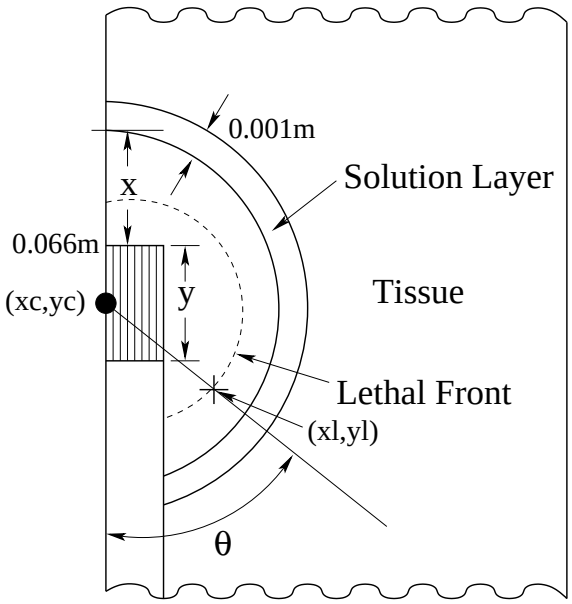

Figure 3.5: Different parameters used to calculate θ

$$G = \frac{1}{V_t}\int_{V_s} w dV_s; \tag{3.4}$$

where w = 1, when $T < -40^oC$ and w = 0, when $T > -40^oC$. Even the above mentioned approach is used to get an idea of the defect volume but the new method proposed in the present study also accounts for the angular position, thus, providing a new approach to calculate the gap between the lethal front and the tumour boundary (Equation 3.3).

3.2.3 Code validation

The present numerical code is validated by comparing the numerical predictions with the published experimental results of Rewcastle et al.[141]. They considered a tissue-simulating gel (1.4% gelatin solution) in a cylindrical perspex geometry where the temperature of a freezing gel was recorded by placing thermocouples at a distance of 10 mm from the axis of the probe. The phase change took place in the temperature interval of $[-1^oC, -8^oC]$. Further, blood flow and metabolic heat generation were absent for the gel. Figure 3.6 shows a comparison between the computed temperatures, at the location of thermocouples having coordinates (10 mm, 36 mm), (10 mm, 46 mm), (10 mm, 56 mm), and (10 mm, 66 mm) and the experimental temperatures obtained by Rewcastle et al. These numerical results agree very well with the experimental results.

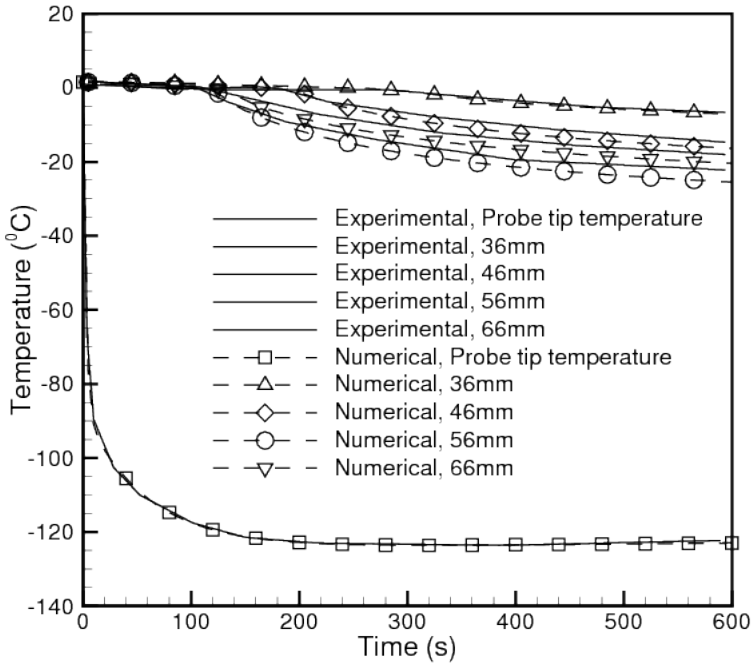

Figure 3.6: Validation of the code by experimental result depicting variation of temperature with time

3.3 Results and discussion

The governing 2D-axisymmetric equations for a single cyilndrical cryoprobe inserted into tumour of different radii covered by a layer of a low thermal conductivity liquid (called as perfluorocarbon (liquid) layer in the subsequent sections) are discretised using finite volume method. The parametric study has been done for tumour radii of 10 mm, 12.5 mm, and 15 mm with the varying active length of the cryoprobe. For a tumour radius of 10 mm, the studied active lengths are 6 mm, 8 mm, and 10 mm while for tumour radii of 12.5 mm and 15 mm these activelengths are 8 mm, 10 mm, and 12 mm and 10 mm, 12 mm, and 14 mm respectively. The perfluorocarbon (liquid) layer thickness is 1 mm for all the studied cases but the variation in offset led us to conclude an optimal offset for each set. The gap is presented in a novel way with the help of angle (θ); i.e. the difference between the -40^oC isotherm and the interface of the tumour corresponding to each angular location. The thermophysical properties considered for the numerical simulation are listed in Table 3.1. The parameters which are kept constant for the entire numerical computations are: the radius of the probe (3 mm) and the thickness of the perfluorocarbon (liquid) layer (1 mm). In all the contour plots, the lethal (-40^oC) and freezing (0^oC) fronts are represented by a dashed line and a solid line respectively. The time required to destroy the tumour completely and the corresponding optimal offset positions of the cryoprobe are determined for various

cases.

3.3.1 Ablation of the tumour in the absence or presence of perfluorocarbon (liquid) layer

For studying the role of perflurocarbon (liquid) layer on tumour ablation the parameters considered are: radius of tumour = 12.5 mm, active length of the cryoprobe 10 mm, and the offset = 8 mm. The variation of gap between the lethal front and the radius of the tumour during cryosurgical freezing in the presence and absence of perfluorocarbon layer is shown in Figure 3.7. It is observed that the variation of gap is almost similar in the beginning of the freezing process, i.e. at t = 20 s and t = 100 s (Figure 3.7(a) and 3.7(b)).

This is expected, as at the start of freezing process there is a substantial difference between the temperature of the cryoprobe and tissue. Hence, the cooling is fast. After few seconds, more volume of tissue is frozen and the lethal front progresses further towards the boundary of the tumour. But eventually the gap ceases to decrease further which can be visualised in Figure 3.7 for the time instances of t = 800 s and t = 950 s. This is due to the fact that the healthy tissue surrounding the tumour acts as a heat sink; initially, the heat transfer rate is high but there is a particular point in time when the heat given off by the surrounding healthy tissue is equal to the cooling provided by the cryoprobe in the tumour. This leads to a gap of approximately 2 mm between the lethal front and the tumour boundary for the case when the solution layer is not present (Figure 3.7(a)). This issue needs to be addressed because not only does it require higher surgical time but it also leads to ineffective tissue destruction of tumours. In this current study, a liquid layer of specific thermophysical property like perfluorocarbons is injected at the boundary of tumour. This liquid layer has low thermal conductivity and low mass diffusivity. Thermal conductivity is a crucial parameter in the cryosurgical process. This novel approach is really beneficial as it will help the physicians in ablating the tumours with more precision without any damage to the surrounding healthy tissue.

The lethal front does not reach the boundary of the tumour even after 950 s of freezing in the absence of perfluorocarbon (liquid) layer but in the presence of this layer the gap reduces to zero within 210 s of the freezing process as seen in Figure 3.7(b). This implies that the lethal front has reached the interface of tumour. Furthermore, if the tumour is continued to cool even till 950 s, it is clearly seen that the gap is still zero. There is slight decrease in the gap between t = 210 s and t = 850 s but there is hardly any change in the value of gap between t = 850 s and t = 910 s. This reflects that the lethal front is unable to penetrate through the perfluorocarbon (liquid) layer because of its distinct thermophysical property. Comparison of Figures 3.7(a) and 3.7(b) depicts the key role played by the perfluorocarbon layer during the heat transfer process in cryosurgery. In the former case, the tumour ablation is incomplete whilst in the latter one, perfect tumour destruction occurs very swiftly in comparatively lesser

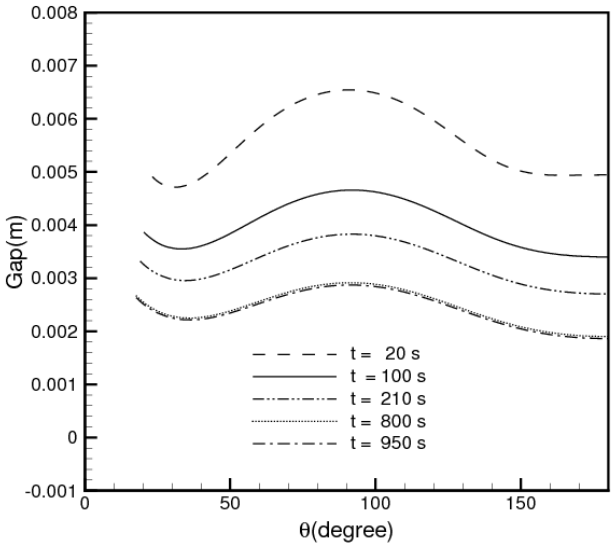

(a) Without perfluorocarbon layer at the tumour interface

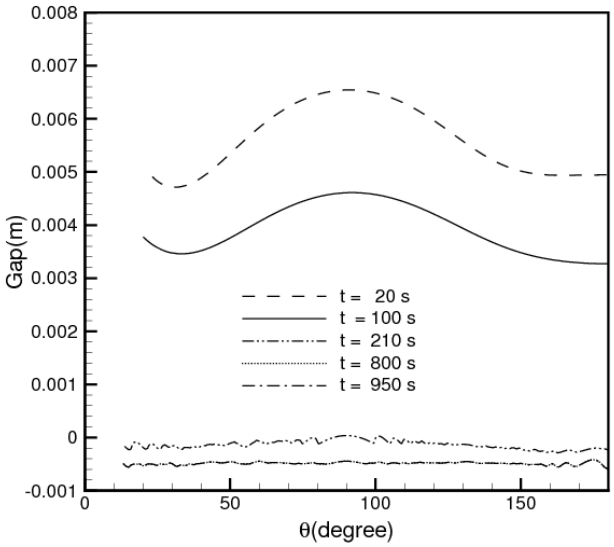

(b) With perfluorocarbon layer at the tumour interface

Figure 3.7: Comparison of gap between lethal front (-40^oC) and radius of tumour (m) with respect to θ (degree) in the absence or presence of solution layer; parameters considered for this case are: radius of tumour = 12.5 mm, active length = 10 mm and offset = 8 mm.

time interval. Also, in presence of perfluorocarbon (liquid) layer across the tumour interface there is minimal or no heat transfer to the nearby healthy tissue. Thus, encapsulation of the tumour with a perfluorocarbon (liquid) layer not only reduces the surgical time drastically but also prevents the damage to the tissue surrounding it.

3.3.2 Identification of an optimal offset

The parameters that have been utilised in this study are: radius of tumour = 12.5 mm, active length of the cryoprobe = 10 mm, and offsets = 7 mm, 9 mm and 8 mm. Offset is the distance between the tip of the cryoprobe and the interface of the tumour and active length of the cryoprobe is that length of cryoprobe which provides the cooling. The variation in offset at constant active length of the cryoprobe and fixed size of tumour leads to a change in the depth of insertion inside the tumour. During cryosurgery, the surgeon finds it difficult to place the cryoprobe at an offset which provides the most symmetrical ice front propagation. The study of various offsets would help the cryosurgeons in optimising this process in a better way.

When the offset is less, the probe is inserted deeper into the tissue, hence, the change in temperature is more in upper half of tumour. Here, it is expected that upper half of the tumour should be cooled faster than the bottom half which can be seen in figure 3.8(a). At t = 100 s, it is noticed that a gap of around 5 mm exists between the lethal front and the bottom half of tumour while the in the upper half this gap is 1 mm. Due to this particular offset, cooling is non-uniform inside the tumour which leads to uneven tumour destruction as mentioned earlier. With time, the gap is reduced to zero in around 210 s in case of optimal offset (Figure 3.7(b) whilst in this case there exists a gap of 3.2 mm in the bottom half of the tumour at the same time point (Figure 3.8(a)). The lethal front remains inside the perflurocarbon (liquid) layer even at the end of a freezing cycle of 950 s. As mentioned earlier, this layer acts as a barrier to heat transfer between tumour and surrounding healthy tissue.

In case of an offset of 9 mm, the cooling is more profound in the bottom half of the tumour with a gap of 2.6 mm and in the upper half of the tumour, there exists a gap of nearly 4.6 mm as seen in Figure 3.8(b) after a freeze time of 100 s. As the offset is more than the earlier case, the depth of probe insertion is less inside the tissue which leads to non-uniformity in cooling inside the tumour thereby cooling the bottom half of the tumour more faster than the upper half of the tumour. After a freezing time of 210 s, the tumour is still not completely ablated as it is in the case of optimal configuration (Figure 3.7(b)). A gap of 1.4 mm exists between the lethal front and the upper tumour interface as seen in Figure 3.8. One noteworthy inference which can be made from the comparison of Figures 3.8(a) and 3.8(b) is that between these two offsets there exists an offset at which tumour receives homogenous or uniform cooling throughout its whole volume. This particular offset is termed as an optimal offset for that configuration. In this case, the optimal offset for the

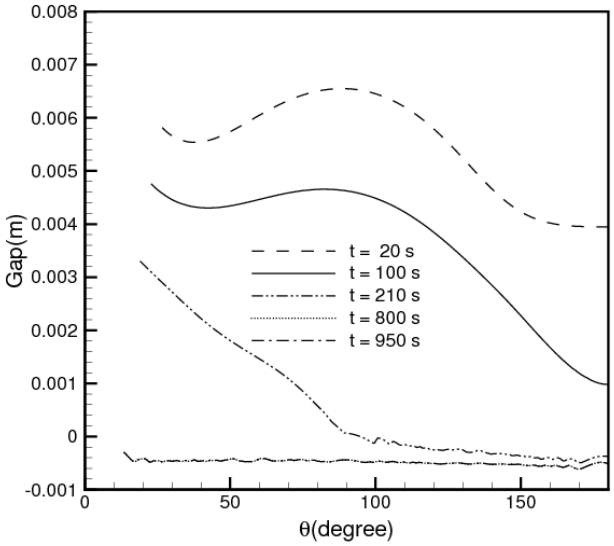

(a) Offset = 7 mm

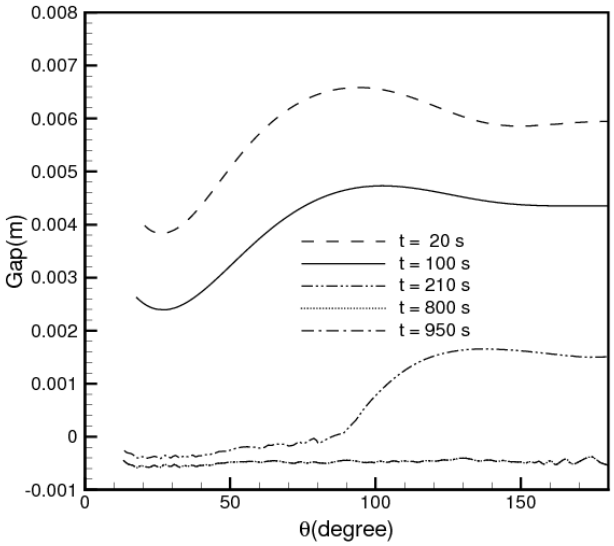

(b) Offset = 9 mm

Figure 3.8: Comparison of gap between ice front (-40^oC) and radius of tumour (m) with respect to θ (degree) when radius of tumour is 12.5 mm, active length is 10 mm

corresponding configuration is identified to be 8 mm. The determination of an optimal offset would enable the cryosurgeons to reduce the surgical time greatly, thereby increasing the comfort level for patients and making it a more popular treatment modality. Figure 3.7(b) illustrates the symmetrical nature of gap between the lethal front and the tumour interface when the offset is optimal. In other words, it implies that the gap at both the upper and bottom half of the tumour is nearly the same. Eventually when the gap is zero at 210 s, the tumour is enclosed by the lethal front perfectly. The ablation is not only uniform throughout the tumour due to the optimal offset but it is also quicker in comparison to other offsets for the similar configuration keeping other parameters same.

The ice front propagation is a significant aspect of this study which can be visualised by the contour plots. Figures 3.9 (a)-(d) illustrate the propagation of the lethal (-40^oC) and freezing (0^oC) fronts with time. As mentioned earlier, the dashed and the solid line represent the lethal (-40^oC) and freezing (0^oC) front respectively. The shaded portion shows the perfluorocarbon (liquid) layer of thickness 1 mm. When the freezing starts inside the tissue, ice fronts are formed which move with certain velocity. These fronts, namely the lethal and the freezing fronts, have nearly same velocity initially (Figure 3.9(a)). With the passage of time, the freezing front, owing to higher velocity than the lethal front moves swiftly and reaches the boundary of the tumour as seen in Figure 3.9(b). Later on, near the end of the ablation period, the lethal front moves faster than the freezing front (Figure 3.9(c)). It is expected as in the beginning of the freezing process the temperature gradient near the probe is quite high which results in the propagation of ice fronts with almost same speed. With time, this gradient decreases and there is also an increase in the thermal conductivity of the tumour (tissue) with the decrease in temperature. Therefore, when a certain amount of tissue is frozen, the thermal conductivity of the frozen volume increases resulting in less resistance to the heat transfer by the frozen volume. And, the heat has to be given off by the tissue ahead of the freezing front; as a consequence, the freezing front moves faster than the lethal front in the middle of ablation period. Because of the distinct properties of the perfluorocarbon (liquid) layer, heat diffusion across the perflurocarbon (liquid) layer is very less. Therefore, after reaching the boundary of this layer, the freezing front ceases to advance further. But, on the other hand, with the passage of time the distance between the boundary of tumour and the lethal front decreases suggesting an increase in temperature gradient. Hence, the lethal front moves faster at the end of ablation period. The ablation period for this case is 210 s which has earlier been seen in Figure 3.7(b). Another interesting point which can be noted is that even after 400 s, the lethal front is unable to cross the tumour boundary due to the presence of the perfluorocarbon (liquid) layer which has unique thermophysical property as stated earlier (Figure 3.9(d)). The propagation of the freezing front (0^oC) and lethal front (-40^oC) with respect to time gives a clear idea about the velocity of these fronts inside the tumour at different intervals of time.

Figure 3.10 shows the propagation of freezing front and lethal front with respect to time

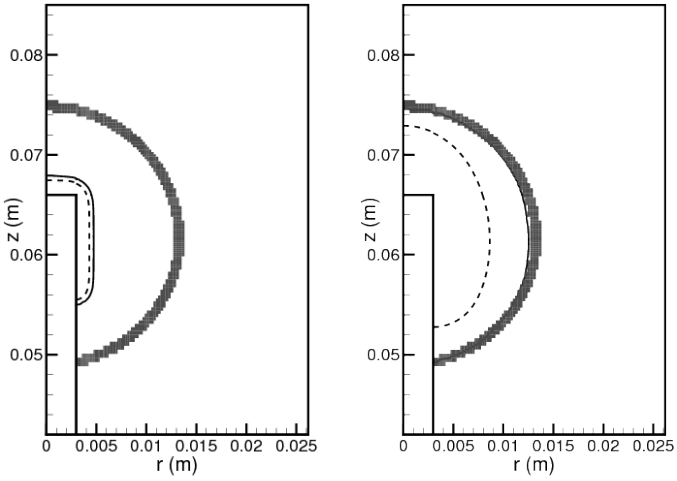

(a) Ice front at t = 2 s (b) Ice front at t = 150 s

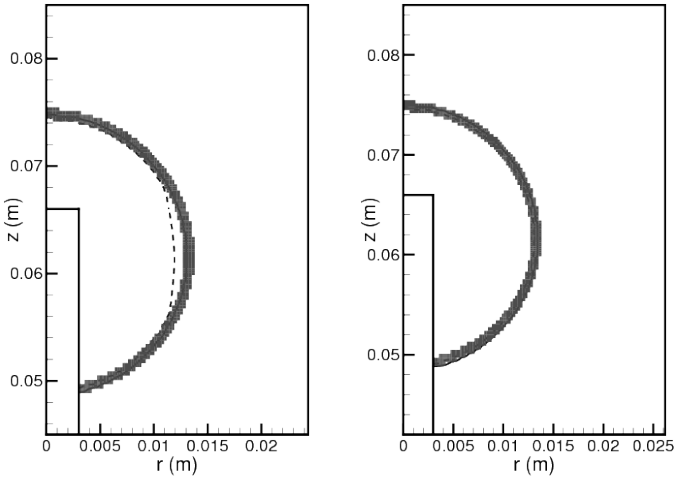

(c) Ice front at t = 200 s (d) Ice front at t = 400 s

Figure 3.9: Ice front propagation for the radius of tumour = 12.5 mm, active length = 10 mm and optimal offset = 8 mm, dashed line and solid line represent lethal and freezing front respectively

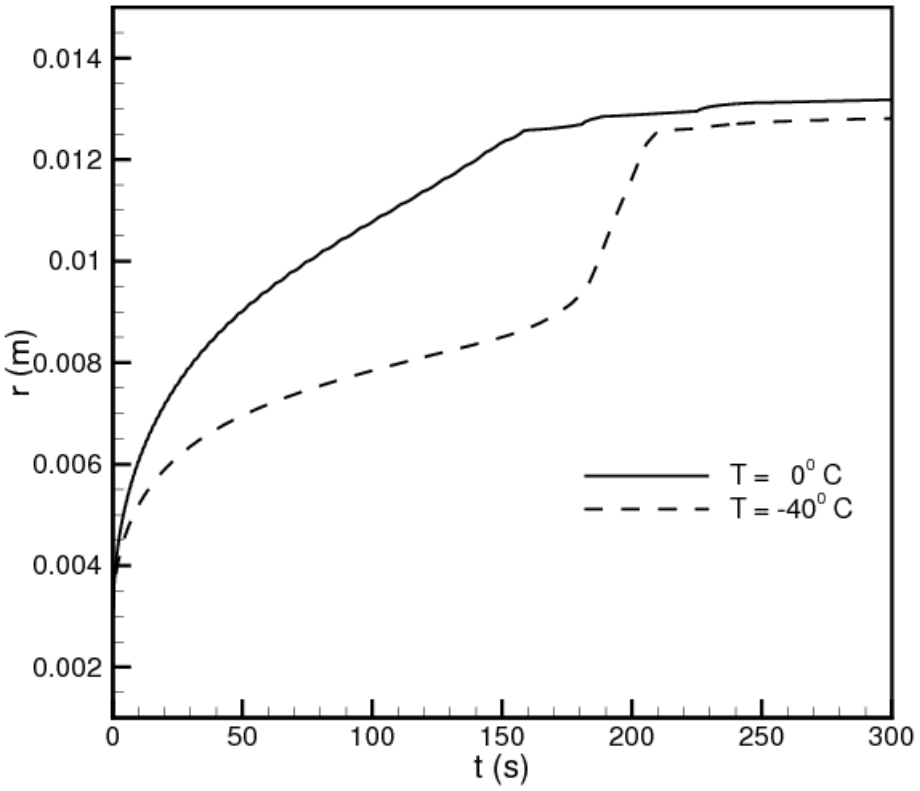

Figure 3.10: Evolution of freezing front (0^oC) and lethal front (-40^oC) inside the tumour with respect to time when radius of tumour is 12.5 mm, active length is 10 mm and optimal offset is 8 mm

when radius of tumour is 12.5 mm, active length is 10 mm and optimal offset is 8 mm. The plot is obtained for an axial location coinciding with the tip of the cryoprobe, i.e. at an angular location of $\theta = 90^o$. At the start of freezing, it is noticed that both the freezing front as well as the lethal front possess the same velocity, as stated earlier. However, one significant observation can be made from Figure 3.10. It is observed that, initially, the fronts which were moving with the same velocity now travel different distances with respect to time, thereby attaining different velocites. The freezing front moves faster than the lethal front and the reason for this has been mentioned earlier. One key inference which can be noted from the figure is that the lethal front moves faster at two intervals of time. Initially, when the freezing begins it has a high velocity, loses little pace in the middle region of the tumour, but as it nears the interface of the tumour there is a steep increase in the velocity of the lethal front. This is because of the high temperature gradient which exists at the beginning of freezing and in the end when the lethal front is near the interface, as explained previously. At 210 s, the lethal front reaches the boundary of the tumour and its velocity becomes zero. Owing to distinct properties of the perfluorocarbon (liquid) layer, the lethal

front ceases at the interface and the healthy tissue necrosis around the tumour boundary is prevented. Therefore, the identification of an optimal offset not only lessens the surgical ablation time drastically but also leads to a uniform lethal front propagation which causes complete tumour necrosis.

3.3.3 Non uniform cooling due to increase in active length

The parameters that have been used for this discussion are: radius of tumour = 15 mm with an active length of 10 mm, 12 mm, and 14 mm with their respective optimal offsets. As stated earlier, active length is that length of cryoprobe which provides cooling to the tissue. Hence, its increase leads to a faster ablation of the tumour. But the faster ablation of the tumour is achieved with the non-uniform cooling of the tumour. The change in active length implies a variation in insertion depth of the cryoprobe inside the tissue. The region closer to the cryoprobe receives the maximum cooling due to a large temperature gradient and the heat diffuses out towards the boundary of the tumour with the increase in duration of freezing. For this particular tumour radius of 15 mm, with an optimal offset of 10.65 mm corresponding to the active length of 10 mm, the variation of gap between the lethal front (-40^oC) and the radius of tumour with time is illustrated in Figure 3.11(a).

In the beginning of freezing at t = 40 s, the ice formation leads to a decrease in gap and the value of gap is 7 mm near the bottom and upper half of the tumour and around 8 mm in the middle of the tumour. The ice formation is more or less uniform througout the angular position (θ) inside the tumour. The uniformity, in the way ice forms, is due to the proper placement and positioning of the cryoprobe inside the tumour. If this positioning is improper, it leads to certain region of the tumour receiving more cooling than the rest leading to non-uniform distribution of heat inside the whole volume of the tumour. With time (at t = 400 s), the lethal front inches towards the boundary of tumour thereby decreasing the gap. This gap reduces to zero at t = 580 s. It means that the lethal front has reached the interface ensuring a perfect ablation. Even if freezing is continued beyond this point, the lethal front stays inside the perfluorocarbon (liquid) layer preventing the surrounding tissue from harm's way.

When the active length of the cryoprobe is changed to 12 mm for the same radius of tumour, the gap between lethal front and tumour interface is non-uniform as seen in Figure 3.11(b). Initially, at t = 40 s itself, it can be seen that the gap is around 6 mm near the bottom and upper half of the tumour. But in the middle of tumour, the gap is more pronounced and is about 8 mm in magnitude. It is expected as the increase in insertion depth of probe inside the tissue leads to a higher temperature difference over a comparatively smaller distance along the axial direction as compared to along the radial direction. At around 450 s, complete tumour necrosis is achieved as the lethal front coincides with the boundary of the tumour. Even after 600 s, the lethal front does not cross the tumour boundary and the perfluorocarbon

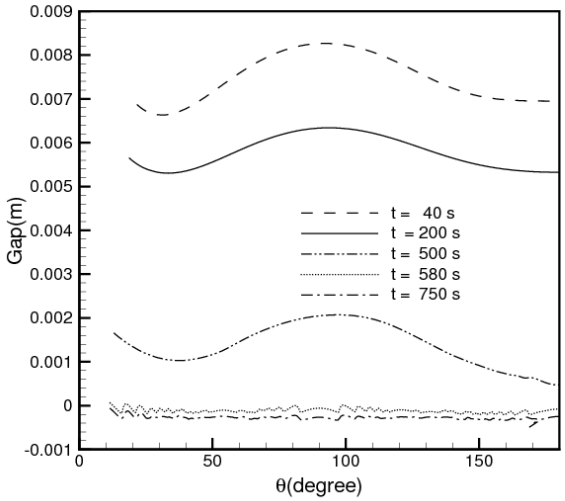

(a) Active length = 10 mm

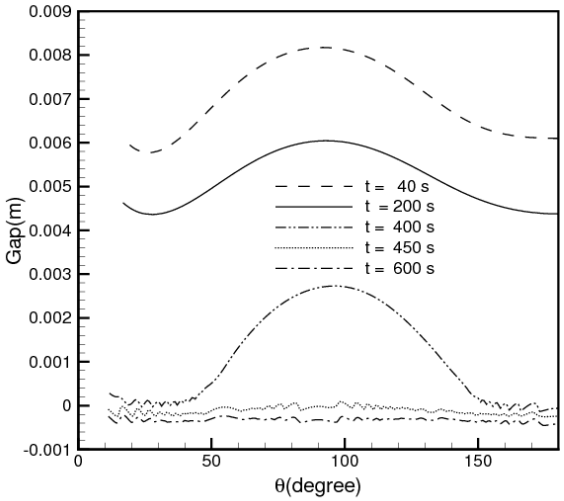

(b)Active length = 12 mm

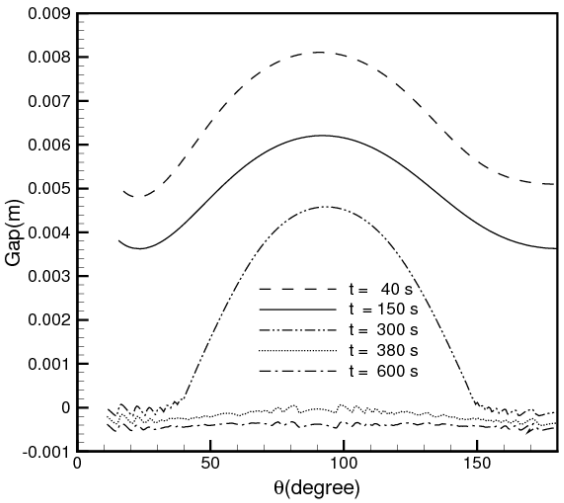

(c) Active length = 14 mm

Figure 3.11: Comparison of gap between lethal front (-40^oC) and radius of tumour (m) with respect to θ (degree) for different active lengths with their respective optimal offsets (i.e. 10.65 mm, 9.8 mm and 8.88 mm) for a tumour radius of 15 mm

(liquid) layer prevents its advancement. Similarly, further increase in active length to 14 mm yielded the same outcome which is clearly noticed in Figure 3.11(c). One significant inference which can be made from Figures 3.11(a)-(c) is that as the active length increases there is a bump in the gap profile in the middle region of the tumour. This bump becomes more pronounced with further increase in the active length.

The ice front locations, at a particular point of time during freezing, at t = 300 s, depicts the uneven ice formation which can be seen in Figure 3.12. When the active length of cryoprobe is varied for the same tumour radius of 15 mm with its respective optimal offsets, the ice ball formation becomes more uneven inside the tumour with the increase in active length of the cryoprobe. For an active length of 10 mm (Figure 3.12(a)), the ice ball formation is almost spherical as reflected by almost a circular arc. This is quite obvious as for the given configuration, the cooling zone is almost at the same distance from the periphery of tumour. But, with the increase in active length of the probe, keeping other parameters same, the distance *between* the cooling zone and the tumour boundary decreases along the axial direction. Therefore, heat is diffused quickly in that direction as compared to heat diffusion along radial direction. As a result, the shape of ice ball becomes elliptical with major axis along axial direction. This is the reason for the presence of a bump in the middle of gap profiles in Figures 3.12(b) and 3.12(c). It should be noted here that the figures correspond to the optimal offsets for the respective configurations. And, as per definition of optimal offset, these configurations give maximum tissue ablation in minimum freezing time with uniform (as much as possible) ice formation. So, it can be concluded that when the cryoprobe is inserted deeper into the tumour with a larger active length, though the tumour ablation is faster, the temperature gradient is more along the axial direction as compared to the gradient along radial direction leading to non-uniform ice formation. It can, hence, be said that for a particular tumour radius lower active length ensures a more uniform ice ball formation.

3.3.4 Effect of variation of tumour radii on its ablation

This part of the study is carried out using the following parameters: radius of the tumour = 10 mm, 12.5 mm, and 15 mm with active length of 10 mm. The effect of variation of tumour radius on its ablation has been studied for each active length. This aspect is crucial for the surgeons as more the volume of tumour, higher is the surgical time required for its ablation. For a cryosurgery to be really effective, the surgical time should be preferably less as it helps in avoiding vascular and other surgical complications. Hence, it becomes important to study the effect of variation of tumour radii on its ablation. The increase or decrease in radius implies a change in volume of the tissue that is to be frozen. When tumour of radius 10 mm is ablated using an active length of 10 mm, the optimal offset is identified to be 5.5 mm.

Figure 3.13 shows the gap between the lethal front and the radius of tumour for the above mentioned parameters. When the freezing begins, the gap between the lethal front

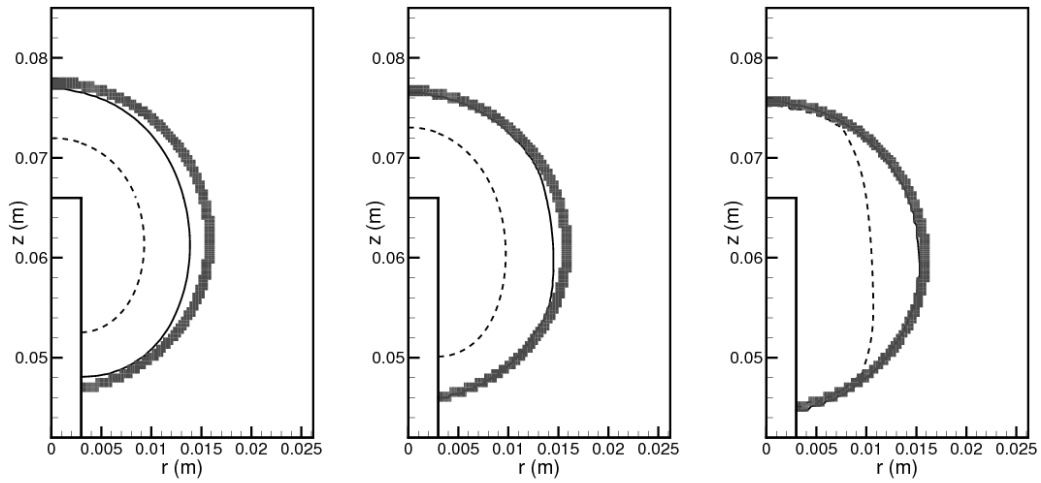

(a) Active length = 10 mm (b) Active length = 12 mm (c) Active length = 14 mm

Figure 3.12: Ice front propagation in tumour radius of 15 mm for various active lengths with their respective optimal offsets (10.65 mm, 9.8 mm and 8.8 mm) at t = 300 s

and interface starts to reduce. At t = 20 s, this is 2.4 mm for the top and bottom part of the tumour, except in the middle region where it is more and about 4 mm in magnitude. This causes a marginal bump in the gap profile. With time, at around 80 s, the lethal front reaches the tumour boundary making the gap between the lethal front and tumour interface zero. Beyond this point, as mentioned earlier, the perfluorocarbon (liquid) layer present at the interface prevents the propagation of the lethal front further and hence even after 200 s the gap remains zero. When a comparison is done between different tumour radii of 10 mm (Figure 3.13(a)), 12.5 mm (Figure 3.13(b)) and 15 mm (Figure 3.13(c)) for the same active length of 10 mm, an interesting inference can be made: the bump in the gap profile decreases with increase in the tumour radius for the respective optimal configurations, keeping the active length same. Similarly, a comparison of gap profile with respect to angular location θ (degree) for different tumour radii of 10 mm, 12.5 mm, and 15 mm with an active length of 10 mm yielded the same result.

Figures 3.14(a)-(c) shows the location of ice fronts at a time instance of 0.8 times the corresponding total ablation time for the respective tumours with their optimal parameters, i.e. at t = 64 s, 168 s, and 464 s for tumour radii of 10 mm, 12.5 mm, and 15 mm respectively corresponding to their optimal offset. It is observed that as the radius of tumour is increased from 10 mm to 12.5 mm, the time taken by the lethal front to ablate the tumour is more. This is understood as the volume of tumour increases with increase in its radius. Similar results are obtained when the radius is further increased to 15 mm. In the former case (Figure 3.14(a)), the lethal front is near the tumour interface and touches the top and bottom part of the tumour interface but in the other two cases (Figure 3.14(b) and Figure 3.14(c)) the front has to still travel a considerable distance to reach the boundary of tumour. This clearly depicts that the

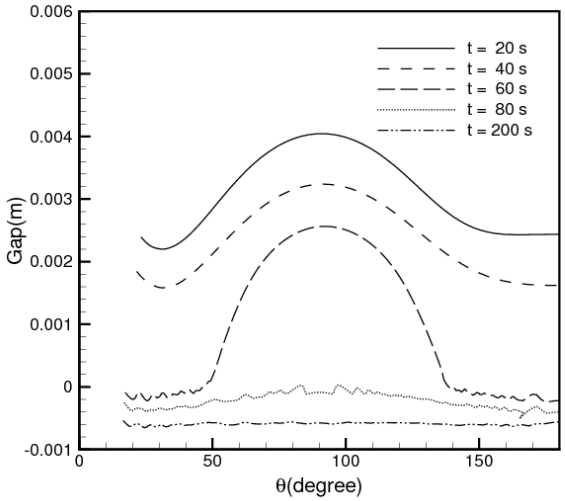

(a) *Radius= 10 mm*, Offset = 5.5 mm

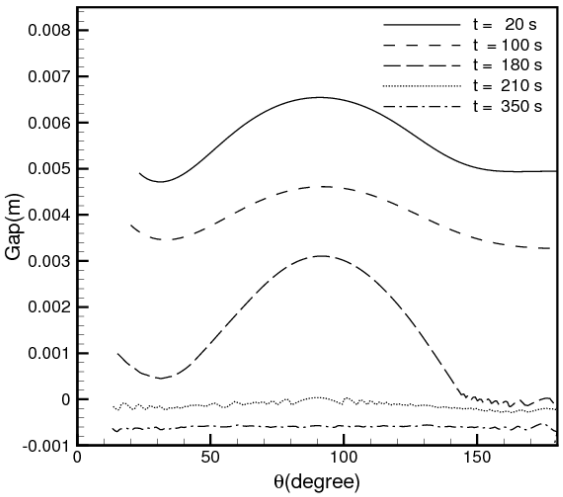

(b) *Radius= 12. 5mm*, Offset = 8 mm

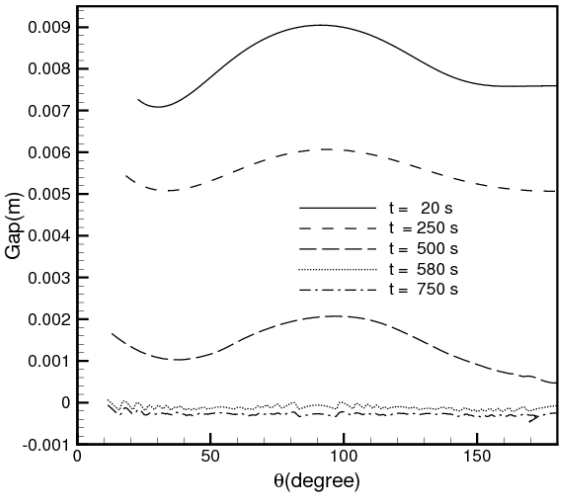

(c) *Radius = 15 mm*, Offset = 10.65 mm

Figure 3.13: Comparison of gap between lethal front (-40^oC) and radius of tumour (m) with respect to θ (degree) for different tumour radii of 10 mm, 12.5 mm, and 15 mm for their respective optimal offset (5.5 mm, 8 mm and 10.65 mm) at the same active length of 10 mm

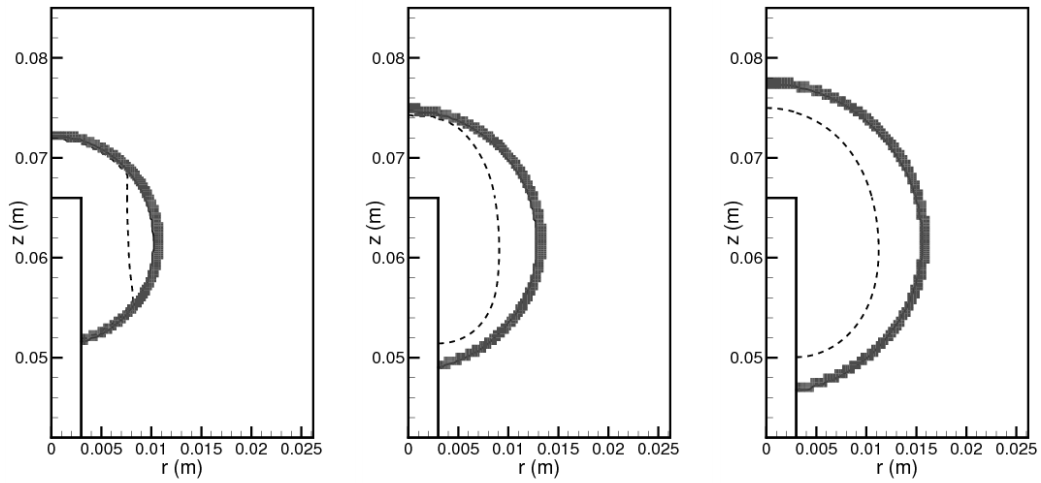

(a) Tumour radius = 10 mm (b) Tumour radius = 12.5 mm (c) Tumour radius = 15 mm

Figure 3.14: Ice front propagation in tumour radii of 10 mm, 12.5 mm, and 15 mm for the same active length of 10 mm with their respective optimal offsets (5.5 mm, 8 mm and 10.65 mm) at an instance of 0.8 times the total ablation time

front propagation is faster in the former one owing to the lesser volume of the tumour. When a comparison is done between the shape of ice ball enclosed by the lethal front, an important and significant inference can be made; the shape changes from an ellipsoid to spherical with the increase in the tumour radius for a given active length of the cryoprobe with their optimal offsets. Also, the determination of optimal offset corresponding to various radii becomes really crucial for a surgeon as it will help in determining an optimised cryosurgical treatment protocol.

3.3.5 Decrease in distance between the lethal front and tumour interface (gap) suggesting an optimal offset

The results of gap propagation have been obtained using the following parameters: radius of tumour = 10 mm with an active length of 6 mm, and an offset of 6 mm, 7.6 mm and 10 mm respectively. The gap in tumour ablation corresponding to an offset indicates the distance between the lethal front and the tumour interface. In the case of an offset of 6 mm, in Figure 3.15(a), it is seen that with time, the gap decreases linearly. Also, when the offset is less, i.e. 6 mm, the cryoprobe is inserted deep into the tumour, therefore, the upper half of the tumour receives more cooling than the lower half. Furthermore, the gap in lethal front and interface of the tumour is due to inefficient cooling in the lower half of the tumour. On the contrary, when the offset is more i.e. 10 mm, the cryoprobe insertion is less deep into the tumour (Figure 3.15(b)); this lesser cryoprobe insertion means that the lower half of the tumour receives more profound cooling than the upper half, thereby, leading to

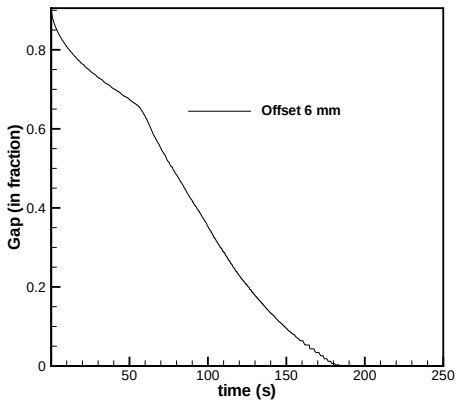

(a) Offset = 6 mm

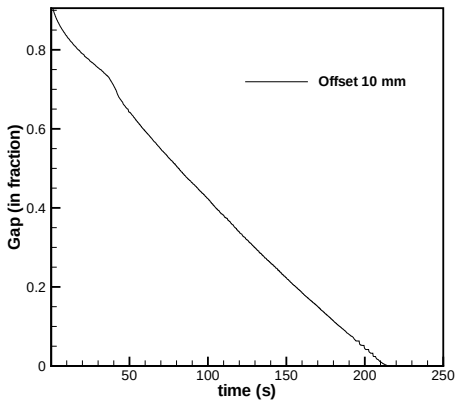

(b) Offset = 10 mm

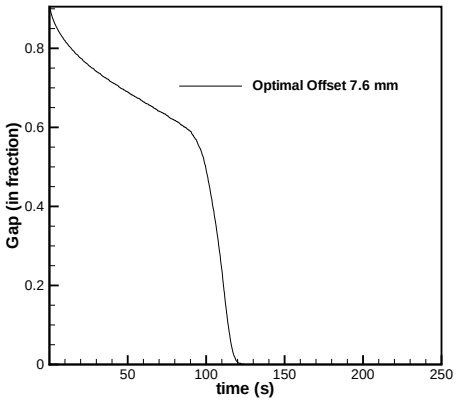

(c) Offset = 7.6 mm

Figure 3.15: Reduction in gap in tumour radius of 10 mm with an active length of 6 mm, offset of 6 mm, 7.6 mm and 10 mm respectively

Table 3.2: Variation of optimal offset due to change in activelength for different tumour radii

Radius of tumour = 10 mm			
Active length (mm)	6	8	10
Optimal offset (mm)	7.6	6.6	5.5
time (s)	122	100	80
Radius of tumour = 12.5 mm			
Active length (mm)	8	10	12
Optimal offset (mm)	9	8	7
time (s)	270	210	180
Radius of tumour = 15 mm			
Active length (mm)	10	12	14
Optimal offset (mm)	10.65	9.8	8.88
time (s)	580	450	380

a gap in tumour ablation. From these results, it can be observed that there exists an optimal configuration between these two offsets where the cooling is uniform throughout the whole tumour leading to a faster ablation. In Figure 3.15(c), it is seen that the distance between the lethal front and tumour boundary is zero in a lesser time interval of 120 s at an offset of 7.6 mm (also an optimal offset in comparison to other offsets of 6 mm and 10 mm for the same tumor radius of 10 mm). The gap at the tumour boundary is zero in a lesser time interval as compared to offsets of 6 mm (Figure 3.15(a)) and 10 mm (Figure 3.15(b)) which ablate completely at 180 s and 220 s respectively. At the optimal offset of 7.6 mm, the whole volume of tumour receives uniform cooling. Thus, the calculation of "gap"would help the surgeon in identifying the most optimal configuration (i.e. optimal offset) for faster and more efficient ablation of tumours.

3.3.6 Ablation time for optimal offset

The ablation time for different configurations with optimal offset for the studied cases are reported in Table 3.2. It is seen that for a tumour of a particular radius as the active length of the cryoprobe increases, the time taken for ablation decreases suggesting that increased sub-cooled surface area of cryoprobe provides a higher cooling rate for cell destruction. However, higher cooling rate comes at the cost of non-uniform propagation of the ice front in most cases. In general, due to the increase in active length the non-uniformity in gap profile is elevated. A noteworthy observation which can be concluded from the results is that for a 2 mm increase in active length, the decrease in optimal offset is approximately 1 mm, i.e. optimal offset decreases linearly with an increase in the active length for a given

radius of the tumour. With increase in radius, the time taken for complete necrosis increases for the same active length of the cryoprobe. This is understood from the fact that if the volume of tumour is more, corresponding to it the time taken to reach the critical isotherm or lethal temperature is more. Also, the most important inference which can be made from this study is that for different tumour radii, with the same active length, the time taken for complete ablation by the larger tumour is nearly 2.7 times the time taken by the smaller one for every 2.5 mm increase in the tumour radius. For example, if we compare the ablation time for tumour radii of 10 mm and 12.5 mm for the same active length of 8 mm, we can notice that the time taken for ablation of a tumour having a radius of 12.5 mm is 2.7 times the time taken for ablation of a tumour of 10 mm (270 s for 12.5 mm tumour and 100 s for 10 mm tumour).

3.3.7 Optimisation of perfluorocarbon layer thickness

This section of the study has been carried out for a radius of 10 mm with the varying active length of the cryoprobe. For a tumour radius of 10 mm, the active lengths of 6 mm and 8 mm were used in this study. The perfluorocarbon layer thickness is changed from 0.5 mm to 1 mm and subsequently to 3 mm. One interesting inference which can be drawn is the existence of an optimal thickness of perfluorohexane (perfluorocarbon) layer. Below this layer thickness, the freezing front (0^oC temperature isotherm) crosses the tumour interface. The parameter which is kept constant for the entire study is the radius of the probe (3 mm). In all the contour plots, the lethal (-40^oC isotherm) and freezing (0^oC temperature isotherm) fronts are represented by a dash line and a solid line respectively. The time required for the destruction of the tumour completely and the corresponding optimal offset positions of the cryoprobe are determined for various cases, however, only a few important results are discussed in this study.

For studying the role of perfluorohexane (liquid) layer thickness on tumour ablation the following optimised parameters are considered: radius of tumour = 10 mm, the active length of the cryoprobe = 8 mm, and the offset = 6.6 mm [134]. The ice front propagation is a significant aspect of this study, which can be visualised by the contour plots. These contour plots help in determining the location of the ice fronts at various intervals of time. Figure 3.16(a) illustrates the propagation of the lethal (-40^oC isotherm) and freezing (0^oC temperature isotherm) fronts with time. The shaded portion shows the perfluorohexane layer of thickness 0.5 mm, 1 mm and 3 mm. When the freezing starts inside the tissue, ice fronts are formed which move with a certain velocity. After a few minutes, the ice ball encloses the whole volume of tumour reaching its interface. Figure 3.16(a)-(c) present the lethal and freezing front propagation when the layer thickness is 0.5 mm. Initially, at around 20 s, the results present the lethal front to be located near the probe surface (Figure 3.16(a)). With time, at around 100 s, Figure 3.16(b) shows that the lethal front reaches the tumour

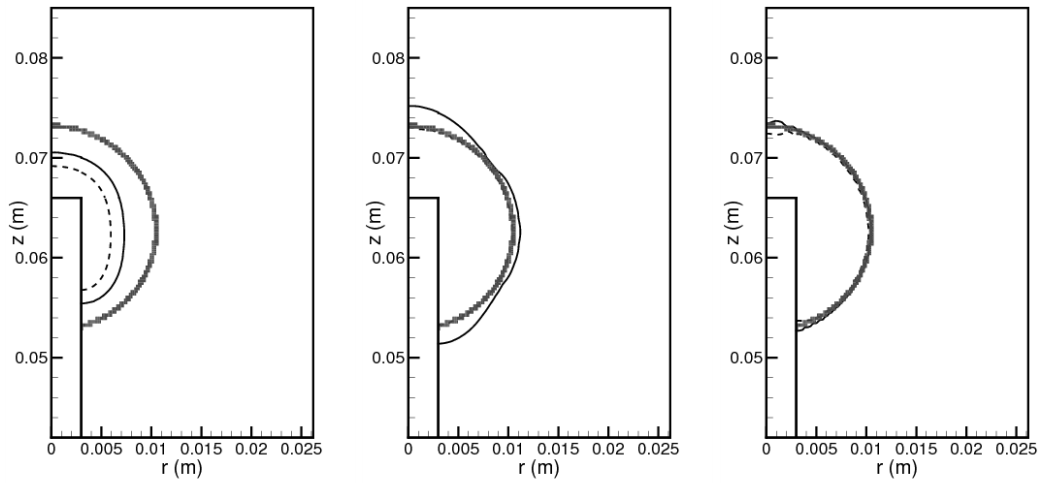

(a) t = 20 s (b) t = 100 s (c) t = 200 s

Figure 3.16: Ice front propagation in tumour radii of 10 mm, active length = 8 mm and optimal offset = 6.6 mm for a perfluorohexane layer thickness of 0.5 mm

interface. Although the lethal front is at the tumour interface, the freezing front which should have ceased at the interface due to the presence of thermal barrier of perfluorohexane layer penetrates the healthy tissue near the tumour margin as seen at 200 s (Figure 3.16(c)). This is due to the lesser thickness of the perfluorohexane layer (i.e. 0.5 mm). Owing to the imperfect insulation of perfluorohexane (which has low thermal conductivity), the freezing front cools the healthy tissue around the tumour interface.

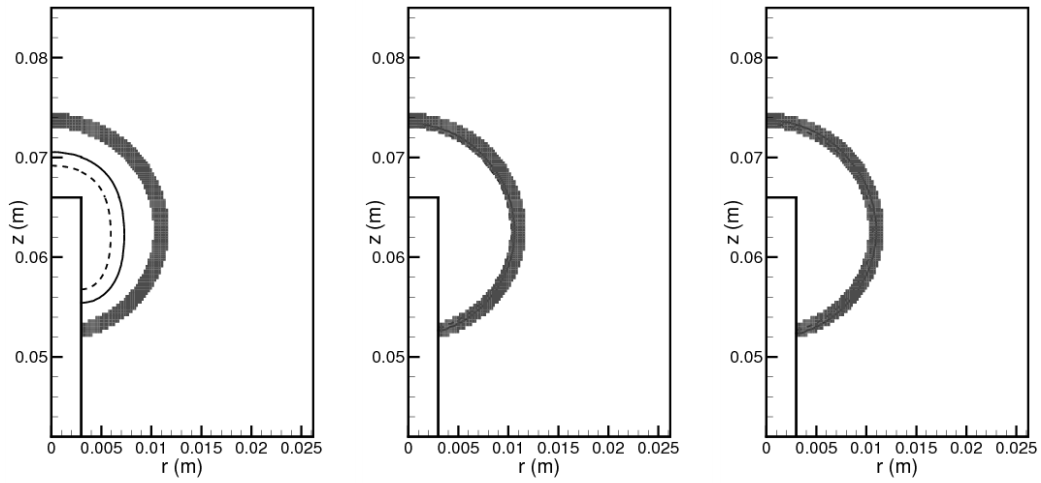

(a) t = 20 s (b) t = 100 s (c) t = 200 s

Figure 3.17: Ice front propagation in tumour radii of 10 mm, active length = 8 mm and optimal offset = 6.6 mm for a perfluorohexane layer thickness of 1 mm

When the thickness of the perfluorohexane layer is increased to 1 mm keeping all the

other parameters same, an interesting observation is made (Figure 3.17(a)-(c)). Although, earlier results presented the freezing front affecting the healthy tissue near the tumour interface after 200 s, Figure 3.17(c) suggests that the increase in layer thickness to 1 mm results in cessation of the freezing front at the tumour boundary. Thus, suggesting that owing to the increase in its thickness, a good insulation is provided by the perfluorohexane layer. Similar to the presentation in Figure 3.17, results demonstrate that further increment in the perfluorohexane layer thickness to 3 mm also leads to a perfect insulation (Figure 3.18(a)-(c)). With time, it can be seen that the lethal front reaches the tumour interface (at 100 s approximately, Figure 3.18(b)). At 200 s, the freezing front remains inside the perfluorohexane layer. This is in contrast to the findings obtained earlier when the perfluorohexane layer thickness is 0.5 mm. At 200 s, in this particular case, (Figure 3.16(c)), the freezing front penetrates the neighbouring tissue surrounding the tumour, whereas in the case of a layer of 1 mm and 3 mm, the freezing front is unable to cross the tumour margin at the same time point (Figure 3.17(c) and Figure 3.18(c)). The increase in thickness of the perfluorohexane layer beyond 1 mm has no change in velocity of the ice fronts. Below this thickness, owing to freezing, there might be the destruction of the healthy tissue at the tumour boundary. Therefore, to summarise, all results obtained in this section of the study suggest a perfluorohexane layer thickness of 1 mm or more at the tumour interface for perfect insulation during the cryosurgical freezing. Practically, since imaging techniques like CT can provide a lower spatial resolution of 3 mm and micro-CT up to 10 μm, it will be possible to measure the perfluorohexane layer experimentally. Therefore, any thickness of perfluorohexane layer which is beyond 1 mm can be used in clinical practice.

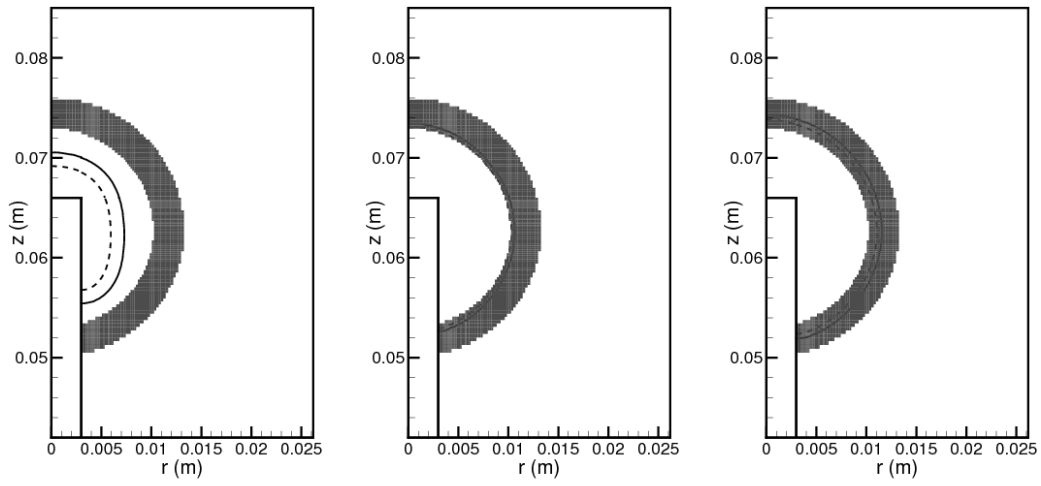

(a) t = 20 s (b) t = 100 s (c) t = 200 s

Figure 3.18: Ice front propagation in tumour radii of 10 mm, active length = 8 mm and optimal offset = 6.6 mm for perfluorohexane layer thickness of 3 mm

3.3.8 Variation in the thermal conductivity of liquid layer around the tumour interface

The liquid layer around the interface of the tumour should possess low thermal conductivity. In this particular section of the study, the emphasis is put on the identification of various chemical substances that can be used as an insulation at the tumour boundary during the cryosurgical process. Figure 3.19 shows the role that thermal conductivity of the liquid at the tumour interface plays during cryosurgical freezing. The comparison of "gap" with respect to θ (degree) is studied using the following optimised parameters; active length = 6 mm, optimal offset = 7.6 mm, the radius of tumour=10 mm and the liquid layer thickness=1 mm. The parameter that is varied is the thermal conductivity of the liquid layer at the tumour margin. In the first case, (Figure 3.19(a)) the liquid layer is maintained at the tumour interface using perfluorohexane (k = 0.067 W/m.K) layer. Results demonstrate that at t = 40 s, the gap is found to be 3.8 mm approximately from the upper and lower boundary of the tumour. With the passage of time, the gap reduces and is zero at 140 s. This is due to the increase in the volume of ice ball with respect to time. Beyond this point, the lethal front does not cross the tumour boundary. The low thermal conductivity acts as a barrier to heat transfer, preventing the damage to the neighbouring healthy tissue. When octafluoropropane (i.e. k = 0.12 W/m.K nearly twice of perfluorohexane) is used for maintaining the layer at the tumour boundary, the gap reduces to zero at t = 170 s (Figure 3.19(b)). This is due to the increase in thermal conductivity of the liquid layer which leads to more heat loss to the surrounding healthy tissue. Hence, more time is required for complete ablation of the tumour. When the thermal conductivity is further increased (water, k = 0.596 W/m.K) an interesting inference can be made, i.e. even after 300 seconds, a gap of 1.4 mm exists in the upper and lower half of the tumour. Further, results presented show that at 950 s the upper and lower boundary of the tumour is not completely ablated (Figure 3.19(c)). This is owing to the thermal conductivity of water, which is very high when compared to perfluorohexane and octafluoropropane. The heat loss to the surroundings is more and the tumour ablation is incomplete. Thus, the thermal conductivity of the liquid layer around the tumour interface plays a crucial role in increasing or decreasing the rate of freezing inside the tumour.

Figure 3.20 shows the distance travelled by the lethal front with time in the presence of a layer of perfluorohexane, octafluoropropane and water at the tumour boundary. The slope of this graph depicts the velocity of the lethal front. In the case of perfluorohexane as a layer (solid line in Figure 3.20), the thermal conductivity is low, leading to a high velocity of the lethal front. Initially, a large thermal gradient results in the high velocity of the lethal fronts. Subsequently, as the front travels further, due to a decrease in temperature gradient its velocity lessens (Figure 3.20). Results indicate an interesting trend when the layer of liquid at the tumour interface is made of octafluoropropane. As the thermal conductivity of octafluoropropane is higher than perfluorohexane, there is a gradual decrease in the velocity

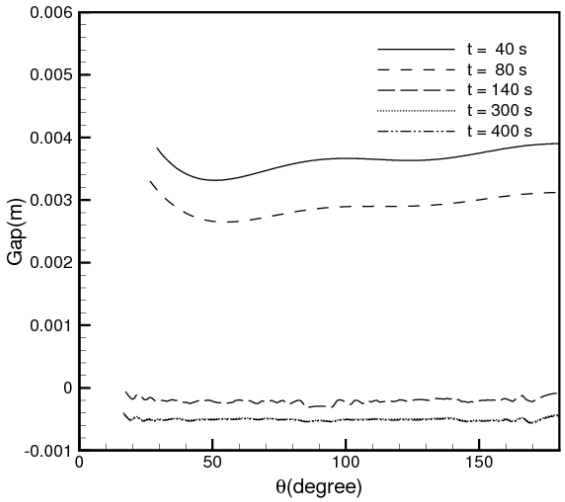

(a) Perfluorohexane layer

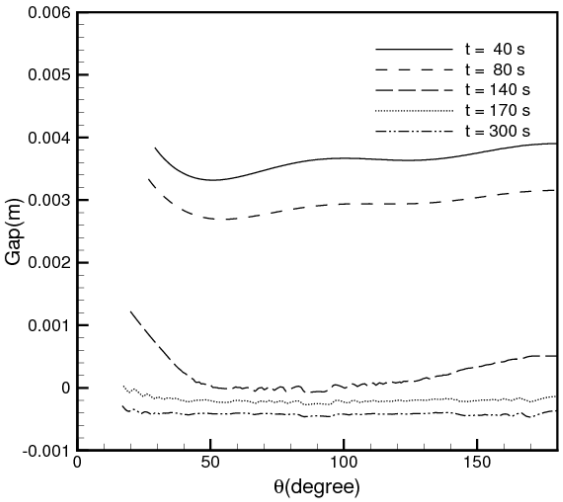

(b) Octafluoropropane layer

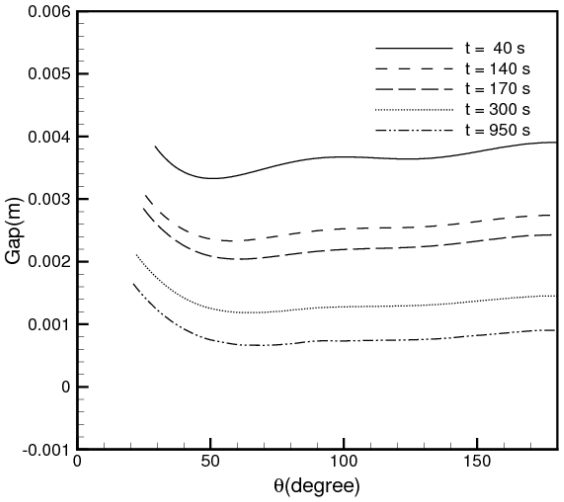

(c) Layer of water

Figure 3.19: Comparison of gap between lethal front (-40^oC) and radius of tumour (m) with respect to θ (degree) for different substances at the tumour interface

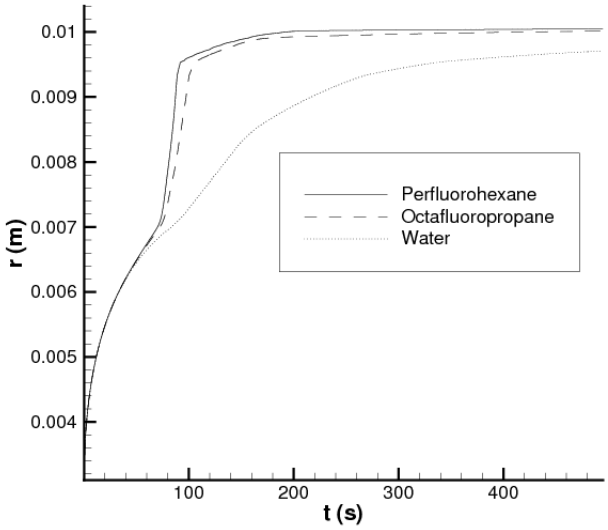

Figure 3.20: Distance travelled by the lethal front with time when the liquid layer around tumour interface is made of perfluorohexane, octafluoropropane and water $\theta = 90^o$

(i.e. a marginal decrease in slope as seen in dash lines in Figure 3.20 which represents the distance travelled by lethal front when octafluoropropane is used as the insulating layer), which becomes constant later. Further, when water is used as a layer around the tumour interface (dotted lines in Figure 3.20), the velocity decreases considerably due to its higher thermal conductivity which results in substantial heat loss to the surrounding healthy tissue. This heat loss leads to incomplete ablation of the tumour. The results also suggest that the velocity of the lethal front is drastically reduced in the case of water as compared to the velocity of lethal fronts obtained in the presence of a layer of perfluorohexane and octafluoropropane. Therefore, it can be concluded that the thermal conductivity of the liquid layer affects the velocity of lethal front significantly.

3.4 Summary

In this chapter, a novel approach is proposed which utilises perfluorocarbon (liquid) layer as an insulating barrier at the tumour interface during cryosurgery. The developed 2D-axisymmetric model for a single cylindrical cryoprobe inserted into tumours of radii 10 mm, 12.5 mm, and 15 mm covered by a layer of a low thermal conductivity liquid is used to study the heat transfer characteristics during cryosurgery process. It is observed that for each tumour radius with a given active length of the cryoprobe there exists an optimal offset which gives maximum tumour necrosis in less time. The important conclusion which can be drawn from this study is that for a 2 mm increase in activelength, the decrease in optimal offset is approximately 1 mm, i.e. optimal offset decreases linearly with an increase in the active length for a given radius of the tumour. Also, the time taken for complete ablation

by the larger tumour is nearly 2.7 times the time taken by the smaller one for every 2.5 mm increase in the tumour radius with same active length of the cryoprobe. The absence or presence of a perfluorocarbon (liquid) layer of low thermal conductivity around a tumour affects the heat transfer process during cryosurgery immensely. In its absence, the time taken for ablation is more or sometimes the risk of healthy tissue surrounding the tumour being damaged is greater. During its presence, the time taken to achieve lethal temperature is reached quickly and even after a long interval of time the lethal front is unable to cross the perfluorocarbon layer suggesting that using this cryosurgical protocol a surgeon will be ablate the tumour faster without causing any damage to the surrounding healthy tissue. Practically, this appproach can be implemented using the following methodology. Each cancerous tumour expresses a unique type of protein through its surface receptor. It is suggested that if this protein can be used in binding to its complementary one (a lock and key type binding) which has an affinity for the perfluorocarbon solution layer then a layer can be maintained around the surface of the tumour. This would help in selectively targeting different cancers at the molecular level using cryosurgery thus improving the effectiveness of the cryosurgical treatment tremendously.

From this study, it is also observed that for a particular tumour radius with a given active length of the cryoprobe there exists an optimal configuration which gives a lesser defect and a faster tumour ablation. The other important conclusion that can be drawn from this study is that there exists an optimal perfluorohexane layer thickness which not only leads to a faster tumour ablation, but it also prevents the damage to the healthy cells around the tumour interface. This optimal thickness is found to be 1 mm. Further, the increase in thickness of perfluorohexane layer does not affect the velocity of these ice fronts. The most suitable substance for making the liquid layer around the tumour boundary is perfluorohexane when compared to octafluoropropane and water. The decrease in gap is evident and is least in the case of an optimal offset of 7.6 mm at a minimum ablation time. Thus, identifying the optimal thickness of the layer, the exact substance needed for making the liquid layer and the calculation of gap would help the surgeons in determining the most optimal configuration. Furthermore, the use of these optimised parameters during cryosurgery will increase the efficiency of the tumour ablation significantly.

Chapter 4

Designing emulsions for improving the efficacy of cryosurgery

4.1 Introduction

Perfluorocarbons have been earlier used for many biological applications. However, one unique aspect of this material that has not been explored is its suitable thermophysical properties. This study proposes to utilise the perfluorohexane and perfluorodecalin emulsions for a novel application in cryosurgery. Perfluorocarbons possesses very low thermal conductivity (0.057 W/mK, perfluorodecalin, and 0.067 W/mK, perfluorohexane). Perfluorocarbon-like perfluorodecalin and perfluorohexane have low thermal conductivity and can be emulsified with the help of a surfactant. Emulsion systems of perfluorocarbons are required as inside a biological system there is an existence of a hydrophilic environment; emulsification of perfluorocarbons results in oil in water emulsion, which is hydrophilic as water is the outer continuous phase [121]. In this regard, this study reports the formation of novel materials (low thermal conductivity emulsions of perflurohexane and perfluorodecalin) for use as a barrier to cooling during cryosurgery. Hence, it is crucial to evaluate the thermophysical properties of these perfluorohexane and perfluorodecalin emulsions as seen earlier in the previous chapter. Two crucial aspects have been studied in this chapter. The first aspect is the study of thermal conductivity. After determining the optimal emulsion that has lower thermal conductivity, particle size analysis, zeta potential, functional groups and specific heat of the optimal emuslion formulations are analysed; the other important aspect of this chapter is the application of this emulsion in cryosurgery of gel phantoms.

4.2 Materials and methods

4.2.1 Materials

Perfluorohexane (95% C_6F_{14} Sigma-Aldrich) and Perfluorodecalin ($C_{10}F_{18}$, 95% pure, Sigma-Aldrich), a perfluorocarbon, is utilised as the primary phase for the preparation of emulsions. For emulsion preparation, a surfactant is needed and the role of the surfactant is to reduce the interfacial tension that exists between the dispersed and the continuous phase. In this study, Span 20 (Sorbitan Monolaurate, Loba Chemie) and lecithin (L-α- Phosphatidylcholine from egg yolk,60% (TLC)) is utilised as the surfactant for the formulation of the perfluorocarbon emulsions. Deionized double-distilled water is the other phase required for the preparation of these emulsions.

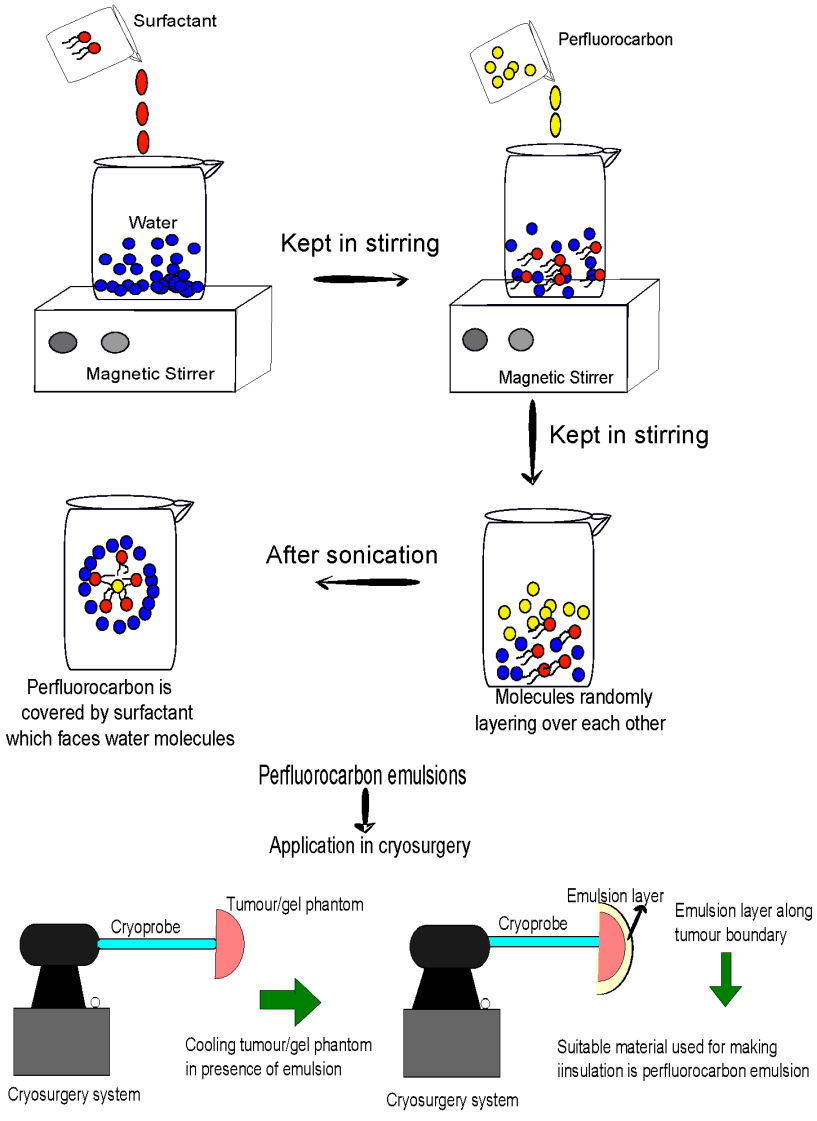

Figure 4.1: Schematic representation of emulsion preparation

Table 4.1: Composition of perfluorohexane emulsions

Concentration (w/v)	Emulsion	Weight of perfluorohexane (g)	Surfactant (5%)	Weight of surfactant (g)	Volume of water (ml)
30%	PFH 30	2.4	Span 20	0.4	8
50%	PFH 50	4	Span 20	0.4	8
70%	PFH 70	5.6	Span 20	0.4	8
90%	PFH 90	7.2	Span 20	0.4	8
30%	PFHL 30	2	Lecithin	0.4	8
50%	PFHL 50	4	Lecithin	0.4	8
70%	PFHL 70	5.6	Lecithin	0.4	8
90%	PFHL 90	7.2	Lecithin	0.4	8

4.2.2 Preparation of perfluorocarbon emulsions

The preparation of perflurocarbon based emulsions of different concentration (i.e. 30% (w/v), 50% (w/v), 70% (w/v) and 90% (w/v)) is carried out by using probe sonication (Vibrionics Ultrasonic processor, India). The concentration of the surfactants is 5% (w/v) and the surfactants used for emulsion formulation are Span 20 and lecithin. The other phase that is utilised for emulsion preparation is water. The emulsion preparation requires three cycles of probe sonication: the first cycle consists of sonication for two minutes, followed by a gap of a minute. The second cycle is carried out for a minute, followed by another gap of a minute and the third and final cycle consists of a minute of sonication.

During this entire process of sonication, ice cubes are kept in a tray and the sample tubes are placed on ice to avoid the excess heat generation due to sonication. After carrying out trials for optimising the duration of sonication, it is seen that 4 minutes is sufficient for homogenous mixing of the two phases. The operating frequency of probe sonicator for emulsion preparation is 20 kHz. The sample preparation is carried out in three independent trials for checking the consistency of method of emulsion formulation and the mean values of the measurements are reported. The standard deviation of the measurements is also mentioned along with the mean values. Table 4.1 and Table 4.2 summarises the composition of the various perfluorohexane and perfluorodecalin emulsions prepared for use as an insulating layer during cryosurgery. The schematic diagram of the emulsion preparation is shown in Figure 4.1.

4.2.3 Experimental verification of thermal conductivity of emulsions

The determination of thermal conductivity for perfluorocarbon based emulsions is carried out experimentally using the KD2 Pro Thermal analyser (Decagon Devices Inc, US). This probe utilises the principle of line source method for estimation of thermal conductivity of the emulsion samples. The thermal conductivity measurements are carried out in triplicates

Table 4.2: Composition of perfluorodecalin emulsions

Concentration (w/v)	Emulsion	Weight of perfluorohexane (g)	Surfactant (5%)	Weight of surfactant (g)	Volume of water (ml)
30%	PFD 30	2.4	Span 20	0.4	8
50%	PFD 50	4	Span 20	0.4	8
70%	PFD 70	5.6	Span 20	0.4	8
90%	PFD 90	7.2	Span 20	0.4	8
30%	PFDL 30	2	Lecithin	0.4	8
50%	PFDL 50	4	Lecithin	0.4	8
70%	PFDL 70	5.6	Lecithin	0.4	8
90%	PFDL 90	7.2	Lecithin	0.4	8

using a KD2 probe thermal analyser. Subsequently, the mean, standard deviation is calculated, based on that the uncertainty in thermal conductivity is obtained and mentioned along with the mean value in the results section.

4.2.4 Estimation of particle size and zeta potential using Zetasizer system

Dynamic light scattering (DLS) is carried out to evaluate the particle size after perfluorohexane and perfluorodecalin emulsion preparation (Zeta sizer Nano ZS system, Malvern Instruments, US). This apparatus helps in calculating the hydrodynamic radius of the particle through the Stokes-Einstein equation. Since these emulsions are highly concentrated, samples are diluted before this measurement to avoid the effects of multiple scattering. Three independent trials of the experiment are carried out for reliability and reproducibility in measurements. The mean values of the size measurements are reported and the standard deviation is also noted down. The Nano ZS system measures particles in the size of 0.3 nm to 10 μm. For this analysis, 0.1 ml of perfluorodecalin emulsion is taken in a sample tube and diluted to 10 ml with the addition of deionized water. After dilution, 2 ml of the sample is placed in the measurement cell and a particle size distribution of reasonable accuracy is obtained.

In this study, the zeta potential of perfluorohexane and perfluorodecalin emulsions are calculated by using the same Zetasizer Nano ZS system. This instrument measures the electrophoretic mobility of the perfluorodecalin emulsions and then automatically determines the zeta potential using Schmoluchowski equation. In this current work, the zeta potential of the perfluorocarbon emulsions is analysed after its preparation. For the measurement of zeta potential, the emulsions are diluted with deionized water (0.1 ml of perfluorohexane or perfluorodecalin emulsion is diluted to 10 ml in water). Further, for any practical use as insulation during cryosurgery perfluorohexane and perfluorodecalin

emulsions should possess consistent thermophysical property and therefore, phase separation should not occur in the emulsions. Also, the study reported by Riddick provides the nature of colloidal stability for various values of zeta potential [142]. It suggests reasonable stability of emulsion for a zeta value of -60 to $-40\ mV$. The stability is moderate if zeta potential is between -40 to $-30\ mV$, a threshold of light dispersion for a zeta value of -30 to -15 mV and precipitation in the case of zeta value lying between -15 to $-5\ mV$.

4.2.5 Thermal conductivity estimation theoretically

The theoretical estimation of thermal conductivity of the perfluorocarbon emulsions is done using Maxwell equation (Equation 4.1)[143, 144].

$$\frac{k_{effective}}{k_o} = \frac{k_p + 2k_o + 2\phi(k_p - k_o)}{k_p + 2k_o - \phi(k_p - k_o)} \tag{4.1}$$

where k_p is the particle phase, in this case, perfluorocarbon (perfluorodecalin or perfluorohexane), k_o is water phase, ϕ is the phase volume fraction (perfluorodecalin/perfluorohexane) and $k_{effective}$ is the effective thermal conductivity of the perfluorocarbon emulsions.

4.2.6 Measurement of specific heat using differential scanning calorimetry

Using a differential scanning calorimeter (DSC) DSC200 F3 Maia system, Netzsch, Germany, the specific heat of the most optimal emulsion samples (i.e. PFD 30, PFD 50, PFD 70, PFD 90) are estimated. Further, the differential scanning calorimetry uses C_p ratio method for the estimation of specific heat [145]. During the analysis, a nitrogen environment is maintained at a flow-rate of 40 ml/min and a cooling rate of $10.0^oC/min$ is specified in the temperature range of 40^oC to 0^oC. In reality, the temperature of the emulsion layer around the tumour interface must be equivalent to the core body temperature of 37^oC. With the help of values of thermal conductivity, average density and specific heat of the perfluorodecalin emulsions, the thermal diffusivity of the emulsions is also evaluated at 37^oC.

4.2.7 Cryosurgery of gel phantoms in presence of emulsion layer

Cryosurgery of 1% (w/v) agarose gel which has a thermal conductivity of 0.541 W/m.K is performed in presence of an emulsion layer of perfluorodecalin as a barrier to gel cooling. This is further illustrated in Figure 4.2. The cooling is carried out with the help of cryosurgery set up (KCH 450A, SMT Praha, Czech Republic) and the thermal history is recorded with the help of thermocouples coupled with the data acquisition system (NI USB 9213). The real time monitoring of the freezing process is done using LABVIEW (NI Systems, USA).

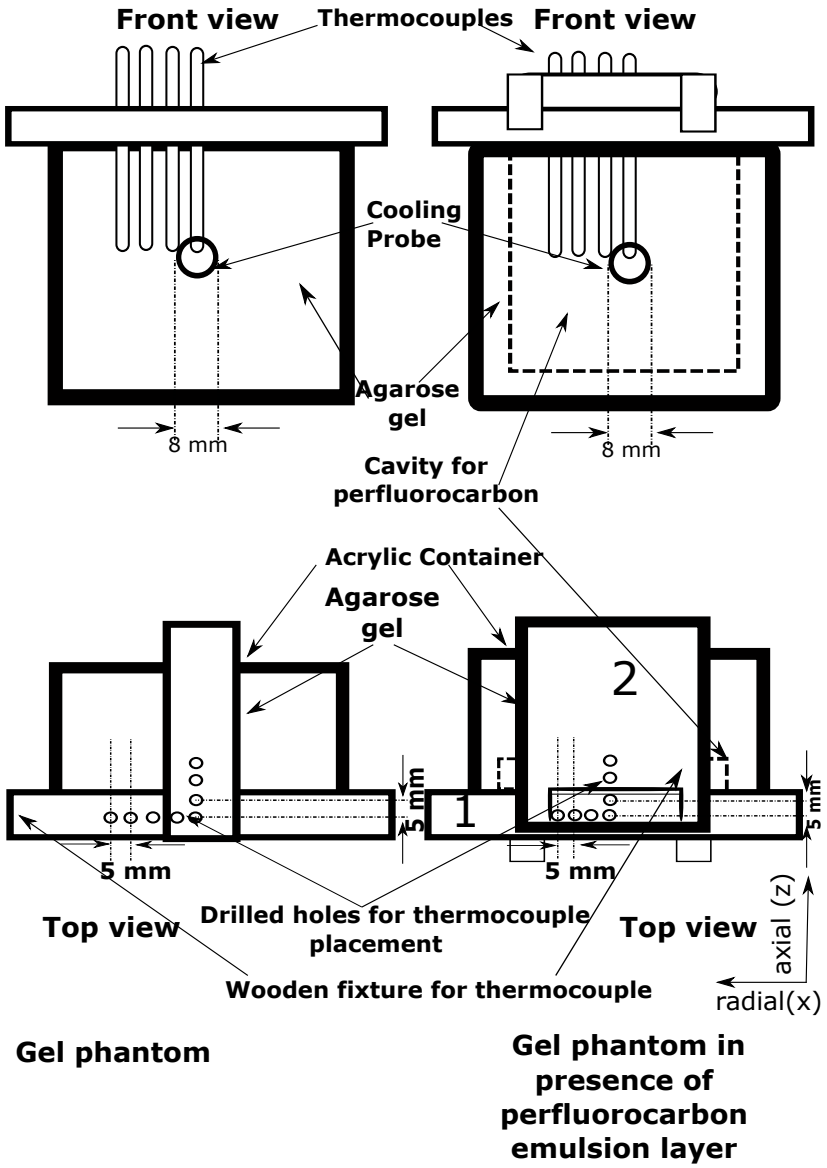

Figure 4.2: Schematic diagram of experimental set up for performing cryosurgery of gel phantoms in absence and presence of perfluorocarbon emulsions

The complete arrangement of radially and axially placed thermocouples are shown in Figure 4.2. Further, it can be seen that an acrylic fixture is inserted before pouring the agarose gel inside the acrylic container. The thermocouple fixture contains four thermocouples placed at the probe and radially at 5 mm, 10 mm and 15 mm from the probe and one thermocouple is placed axially at 5 mm from probe, inside the solidified gel. After the removal of the acrylic fixture, there is a cavity formed as seen in Figure 4.2. This cavity is filled with perfluorocarbon emulsion layer and a second thermocouple fixture is placed which contains the thermocouples placed at 10 mm and 15 mm axial location from the probe. Subsequently, after the placement of these thermocouples in the emulsion layer, the cryosurgery system is used for cooling the gel phantom.

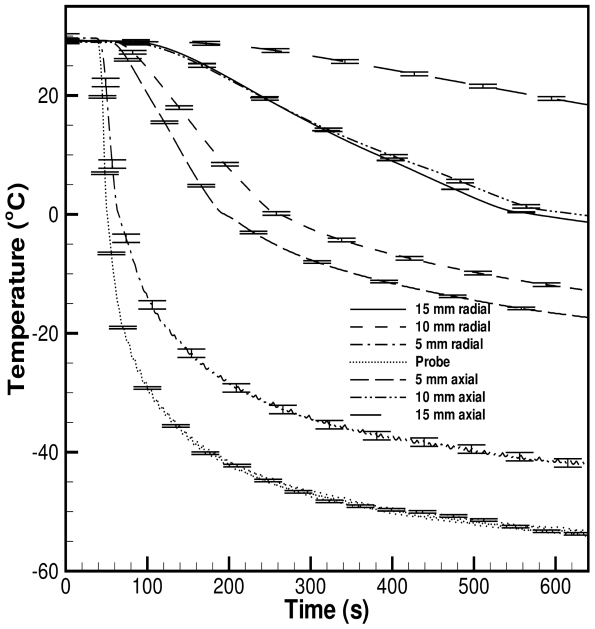

(a) Repeatability in thermal measurement

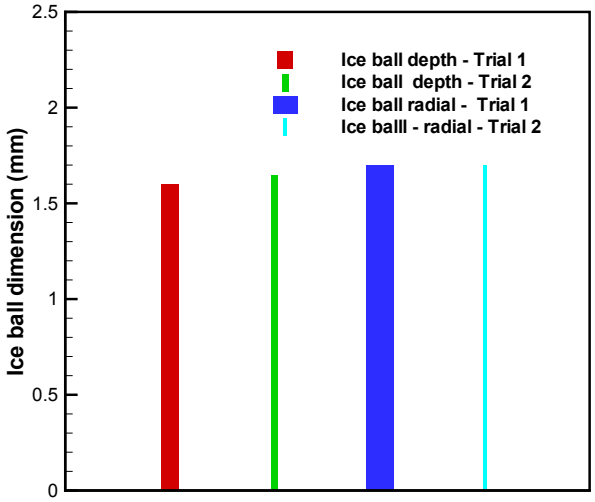

(b) Repeatability in ice ball measurement

Figure 4.3: Repeatability in freezing to verify the accuracy of measurement

Repeatability of freezing in gel phantoms during cryosurgery

The repeatability of temperature measurements during cryosurgery is important and to ensure the same, freezing experiments of 1% (w/v) agarose gels are carried out in duplicates. The mean temperature is obtained with respect to time and standard deviation from mean is calculated to verify the closeness of the obtained values at each thermocouple location (Figure 4.3(a)). A good similarity is seen in the temperature values obtained in the two trials of freezing during cryosurgery.The measurements suggest that the temperature is nearly the same at each thermocouple location in the two freezing trials, therefore, reproducible measurements of temperature can be obtained using this experimental design. The bar graph depicting the repeatability in obtaining the ice ball measurements is shown in Figure 4.3(b). This clearly indicates that repeatable neasurements of temperature and ice ball are obtained with the help of current experimental set up.

4.3 Results and discussion

In the first half of this section, efforts have been made to optimise the formulation of low thermal conductivity emulsion using perfluorohexane as the primary phase with the other phase as water. Followed by these experiments, the amount of perfluorohexane has been varied and perfluorodecalin has been utilised. From the aspect of thermal conductivity, although investigation has been done on perfluorohexane emulsions but perfluorodecalin emulsions seem to posses better thermophysical properties and stability. Therefore, after a preliminary investigation on perfluorohexane emulsions, a deeper analysis of perfluorodecalin emulsions has been carried out for application in cryosurgery process.

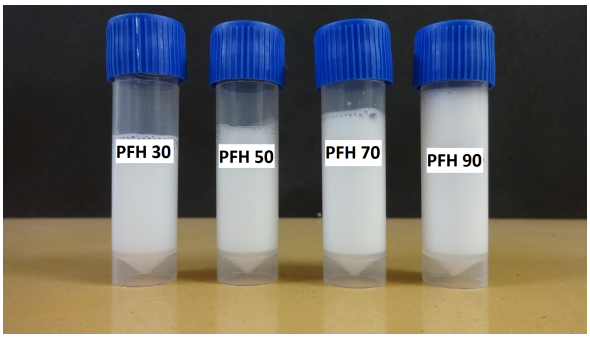

Figure 4.4: Images of perfluorohexane emulsion samples obtained through a digital camera (SONY, WX 80)

Table 4.3: Experimental thermal conductivity measurement of perfluorohexane emulsions

Sample	Thermal conductivity (W/mK)
PFH 30	0.51 ± 0.01
PFH 50	0.42 ± 0.01
PFH 70	0.36 ± 0.003
PFH 90	0.30 ± 0.01
PFHL 30	0.51 ± 0.003
PFHL 50	0.45 ± 0.006
PFHL 70	0.41 ± 0.01
PFHL 90	0.37 ± 0.009

4.3.1 Size analysis of perfluorohexane emulsions in presence of different surfactants

The particle size analysis using dynamic light scattering reveals that PFH 30, 50, 70 and 90 emulsions (Span 20 based) have a z-average diameter of 245.3 nm, 339.4 nm, 427.8 nm and 517.2 nm respectively (The z-average diameter is calculated by DTS 5.0 software, provided by Malvern Instruments, US). Figure 4.5(a) shows the particle size distribution for PFH emulsions after its preparation. It is interesting to observe that with the increase in concentration of perfluorohexane (from 30% (w/v) to 90% (w/v)), there is peak broadening indicating a wider particle size distribution and a larger particle size. From the figure, it is clear that there is a concentration dependent increase in z-average diameter. Further, the shift of the peak maxima to the right hand side of horizontal x-axis indicates a higher particle size which corroborates well with the z-average diameter mentioned earlier.

The change of surfactant to lecithin reveals that PFHL emulsions (i.e., 30% (w/v), 50% (w/v), 70% (w/v) and 90% (w/v)) have a z-average diameter of 205.9 nm, 258.9 nm, 441.6 nm and 483.8 nm. Figure 4.5(b) shows the particle size distribution when lecithin is used as a surfactant at various concentration of perfluorohexane. It is observed that the increase of concentration of perfluorohexane leads to increase in the peak height and a marginal shift to the right hand side of the horizontal x-axis. When compared to PFH emulsions, PFHL emulsions also have a similar z-average diameter. The presence of an ionic surfactant instead of a non ionic one does not affect the emulsion formation. After the characterisation of the emulsion particle size, the most important property with regard to heat diffusion, i.e. thermal conductivity is determined. Based on the most optimal thermal conductivity, the suitable emulsions are screened out and further analysis is carried out on the emulsions that possess lower thermal conductivity.

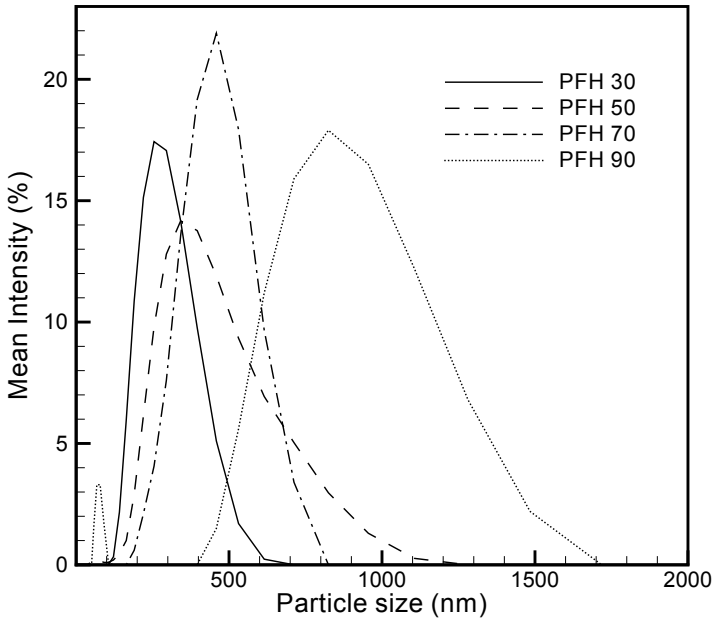

(a) Perflurohexane emulsions made using Span 20

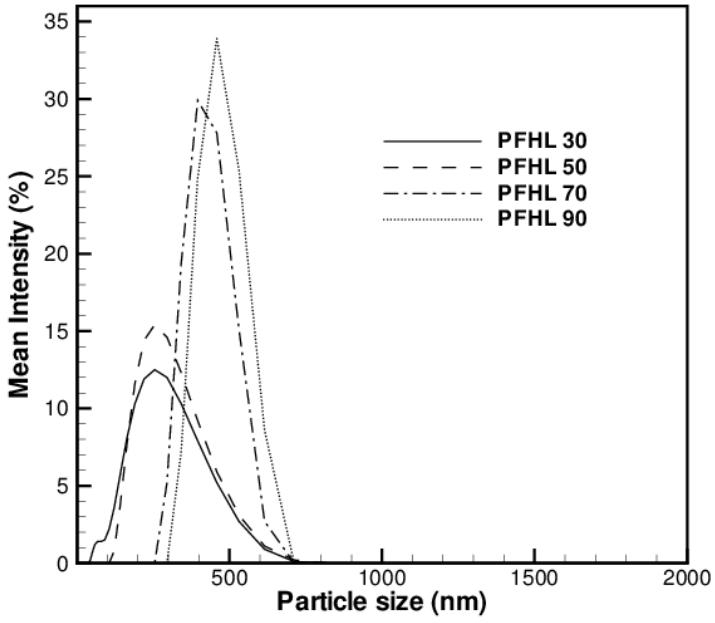

(b) Perfluorohexane emulsions made using lecithin

Figure 4.5: Effect of change of surfactant in particle size of perfluorohexane emulsions

4.3.2 Optimisation of thermal conductivity of perfluorohexane emulsions

The thermal conductivity of the emulsions is determined using KD2 pro thermal analyser and the values are reported in Table 4.3. It is observed that the thermal conductivity of perfluorohexane emulsion prepared with Span 20 is lower than the ones prepared with lecithin. The value of thermal conductivity for the emulsions prepared with Span 20, i.e., PFH 30, 50, 70 and 90 are found to be 0.51 $\pm$ 0.01 W/m.K, 0.42 $\pm$ 0.01 W/m.K, 0.36 $\pm$ 0.003 W/m.K and 0.30 $\pm$ 0.01 W/m.K respectively. On the other hand, as stated earlier, the thermal conductivity of PFHL emulsions (with lecithin) is higher than PFH emulsions and found to be 0.51 $\pm$ 0.003 W/m.K, 0.45 $\pm$ 0.006 W/m.K, 0.41 $\pm$ 0.01 W/m.K and 0.37 $\pm$ 0.009 W/m.K. From all the thermal conductivity measurements, a common trend is observed; the thermal conductivity decreases with the addition of perfluorohexane in the emulsion system. It is obvious as the phase that has low thermal conductivity is increasing in concentration and contributing to the lowering of thermal conductivity of the bulk emulsion. In terms of practical application as an insulating barrier, lower thermal conductivity emulsions would be more useful than the ones with higher thermal conductivity, therefore, perfluorohexane emulsions with Span 20, at the highest concentration, i.e. 90% (w/v) would be more suitable as compared to perfluorohexane emulsions based on lecithin as the surfactant. Therefore, for further analysis, PFH emulsions are formulated at different concentration with specific interest towards formulating low thermal conductivity emulsions.

4.3.3 Theoretical estimation of thermal conductivity for perfluorohexane emulsions

The thermal conductivity values of perfluorohexane emulsions have also been estimated using maxwell equation as stated earlier in the methodology section. The value of k_p, i.e. the thermal conductivity of perfluorohexane which is the dispersed phase is 0.067 W/m.K and the value of k_o, i.e. the thermal conductivity of water (which is the other phase) is 0.596 W/mK. ϕ is the volume fraction of the dispersed phase, which is 0.3, 0.5, 0.7 and 0.9 (30% (w/v), 50% (w/v), 70% (w/v) and 90% (w/v)). Using these values of thermal conductivity and volume fraction, $k_{effective}$ is determined and the values are reported in Table 4.4. It is clearly seen that the thermal conductivity of the emulsion decreases as the concentration of perfluorohexane is increased. PFH 30 emulsions possess a thermal conductivity of 0.50 W/mK. With increase in perfluorohexane concentration to 90% (w/v), the thermal conductivity is found to be 0.37 W/m.K. This is understood as the amount of perfluorohexane is increasing in the emulsion system.

Table 4.4: Theoretical determination of thermal conductivity for perfluorohexane emulsions

Sample	Thermal conductivity (W/mK)
PFH 30	0.50
PFH 50	0.44
PFH 70	0.40
PFH 90	0.37

Table 4.5: Experimental determination of thermal conductivity for perfluorodecalin emulsions

Sample	Thermal conductivity (W/mK)
PFD 30	0.505 $\pm$ 0.01
PFD 50	0.408 $\pm$ 0.04
PFD 70	0.35 $\pm$ 0.004
PFD 90	0.29 $\pm$ 0.003
PFDL 30	0.526 $\pm$ 0.003
PFDL 50	0.463 $\pm$ 0.006
PFDL 70	0.40 $\pm$ 0.01
PFDL 90	0.37 $\pm$ 0.009

4.3.4 Analysis of zeta potential of perfluorohexane emulsions

The zeta potential of PFH emulsions is subsequently determined using Zetasizer ZS (Malvern instruments, US) as it is a good indicator of suspension stability. Figure 4.6(a)-(d) indicate the graphs of zeta potential measurements for PFH emulsions at different amount of perfluorohexane (30% (w/v),50% (w/v), 70% (w/v) and 90% (w/v)). When the concentration of perfluorohexane is 30% (w/v), the zeta potential is found to be -32.7 mV. Figure 4.6(a) shows that the peak is narrow and has a highly negative charge. As stated earlier in methodology, higher magnitude of charge results in a higher repulsion between emulsion droplets, thus, preventing coalescence or merger, improving stability. With increase in amount of perfluorohexane in the emulsions to 50% (w/v), the zeta potential is -41 mV suggesting higher charge at surface of emulsion droplet (Figure 4.6(b)). Further addition of perfluorohexane in the emulsions to 70% (w/v) and 90% (w/v) reveals a zeta potential measurement of -52.1 mV and -60.7 mV (Figure 4.6(c)-(d)). Hence, it is clearly evident that with rise in the perfluorodecalin concentration, the magnitude of negative charge is increasing indicating a higher stable perfluorohexane emulsion.

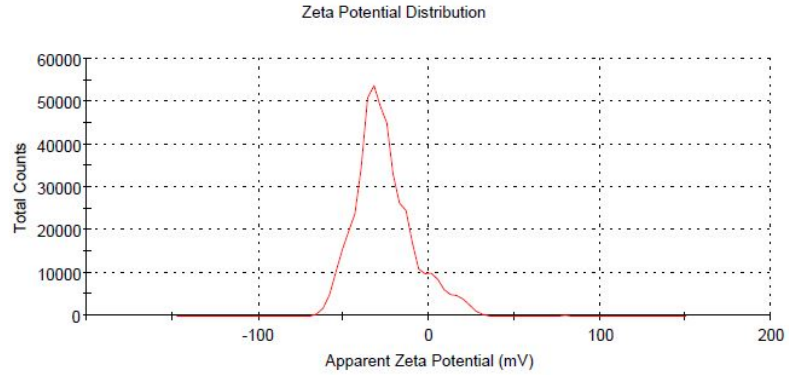

(a) Zeta potential- PFH 30

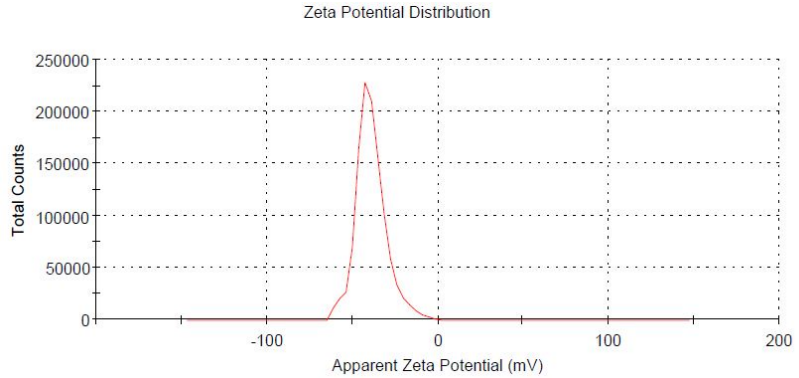

(b) Zeta potential- PFH 50

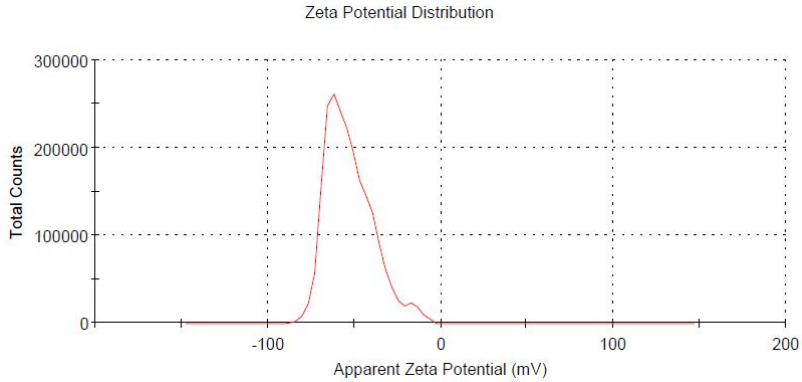

(c) Zeta potential- PFH 70

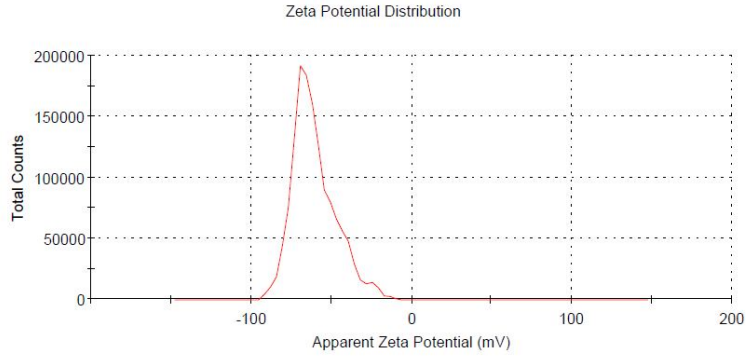

(d) Zeta potential- PFH 90

Figure 4.6: Determination of surface charge of perfluorohexane emulsions

4.3.5 Optimisation of thermal conductivity of perfluorodecalin emulsions

In the earlier half of the chapter, research has been carried out for the formulation of low thermal conductivity emulsion systems of perfluorohexane. However, apart from perfluorohexane, there are other perfluorocarbons that can be used for the same purpose, even perfluorodecalin that has lower thermal conductivity i.e. 0.057 W/m.K can be utilised for the formation of low thermal conductivity fluids. Hence, perfluorodecalin emulsions have been formulated that can help in acting as a barrier to gel cooling during cryosurgery (Figure 4.8). The determination of thermal conductivity of perfluorodecalin emulsions is carried out by KD2 pro thermal analyser and the values are shown in Table 4.5. The thermal conductivity for the perfluorodecalin emulsions prepared with Span 20, i.e., PFD 30, 50, 70 and 90 are found to be 0.505 $\pm$ 0.01 W/m.K, 0.408 $\pm$ 0.01 W/m.K, 0.35 $\pm$ 0.004 W/m.K and 0.29 $\pm$ 0.03 W/m.K respectively. On the other hand, the thermal conductivity of PFDL emulsions (with lecithin) is higher than PFD emulsions and determined to be 0.526 $\pm$ 0.003 W/m.K, 0.463 $\pm$ 0.006 W/m.K, 0.40 $\pm$ 0.01 W/m.K and 0.37 $\pm$ 0.009 W/m.K. From the thermal conductivity values, it is evident that its value decreases with the increase of perfluorodecalin in the emulsion. It is understood as the phase that possesses lesser thermal conductivity (perfluorodecalin) is contributing to the lowering of its magnitude. Further, it is seen that the perfluorodecalin emulsion prepared with Span 20 has lower thermal conductivity than the ones prepared with lecithin. With regard to its application as an insulating barrier during cryosurgery of gel phantoms, lower thermal conductivity emulsions would be more useful than the ones with higher thermal conductivity. Hence, perfluorodecalin emulsions with Span 20, at 90% (w/v) would be more apt for the cryosurgical application as compared to perfluorodecalin emulsions made by using lecithin as the surfactant. Therefore, for further studies, PFD emulsions are analysed in depth with respect to its prospective application in cryosurgical practice.

4.3.6 Effect of perfluorodecalin concentration on the particle size

Particle size analysis of these perfluorodecalin emulsions (PFD 30, 50, 70 and 90) are carried out after the emulsion formulation. Before the particle size measurements, the perfluorodecalin emulsions are diluted as mentioned in the methodology section. A comparison of the particle size of PFD 30, 50, 70 and 90 emulsion demonstrates a marginal increment in the z-average diameter of the emulsions with the rise in the concentration of perfluorodecalin (Figure 4.7). The results demonstrate that PFD 30 emulsion shows a maxima at 190.1 nm (12.73% intensity). Further, in this case, the z-average diameter of PFD 30 is found to be 170.5 $\pm$ 10.69 nm (DTS 5.0 software, z- average diameter is obtained from cumulants analysis of the measured correlation curve). With the rise in perfluorodecalin

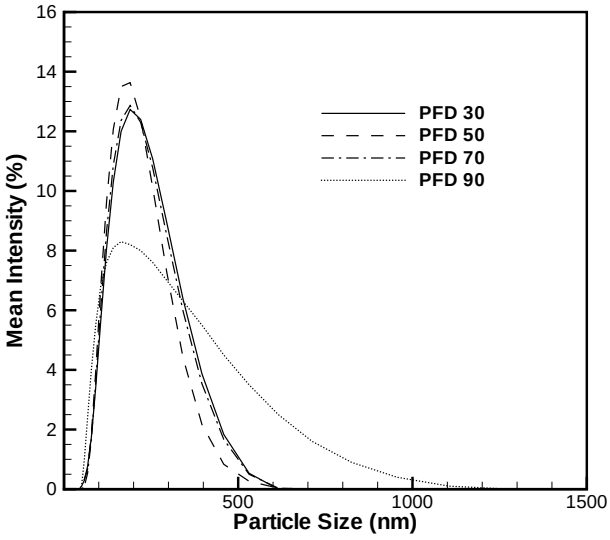

Figure 4.7: Effect of perfluordecalin concentration on the particle size of emulsions after preparation (Span 20 as surfactant)

concentration to 50% (w/v), PFD 50 emulsion suggest a maxima at 220.2 nm (13.63 % intensity) and the z-average diameter for PFD 50 emulsion is 191.7 ± 3.98 nm. With more addition of perfluorodecalin phase in the emulsion to 70% (w/v) and 90% (w/v), the maxima is observed at 220.2 nm (12.86 % intensity and 14.8 % intensity respectively) and the z-average diameter is determined to be 199.1 ± 4.01 nm and 206.1 ± 5.1 nm. Hence, even in these case, with rise in the amount of perfluorodecalin, there is a marginal increase in z-average diameter. Another significant observation reveals that for PFD 90 emulsions, there is a mild broadening in the particle size distribution in comparison to PFD 30, PFD 50 and PFD 70 emulsion.

The dynamic light scattering studies (particle size analysis) also provide the values of polydispersity index of the perfluorodecalin emulsions. The polydispersity index points out the very low heterogeneity in the particle size distribution of the emulsions. In this study, the polydispersity index is found to be 0.186 ± 0.008 for PFD 30 emulsion at the day of preparation. Also, with rise in perfluorodecalin phase in emulsion, polydispersity is marginally lower for PFD 50 emulsion and determined to be 0.164 ± 0.052. Further increase of perfluorodecalin to 70% (w/v) and 90% (w/v) results in a value of polydispersity index that is similar to the previous cases. Hence, for all perfluorodecalin emulsions (PFD 30, PFD 50, PFD 70 and PFD 90), it is evident from the polydispersity index values that the emulsions are monodisperse in nature.

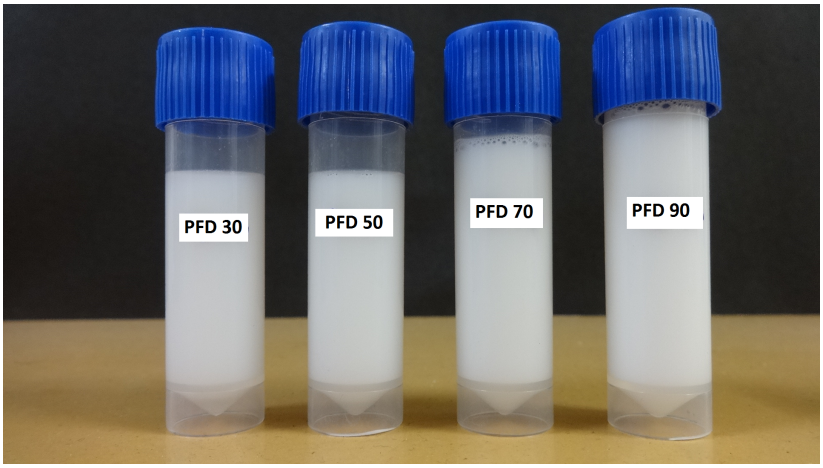

(a) PFD emulsions

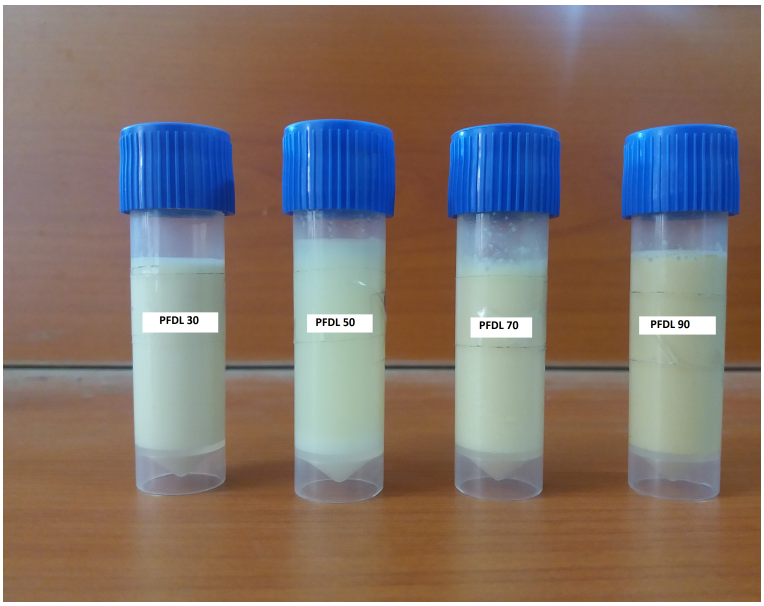

(b)PFDL emulsions

Figure 4.8: Images of perfluorodecalin emulsions with Span 20 (PFD) and lecithin (PFDL) as surfactant (obtained through a digital camera (SONY WX 80))

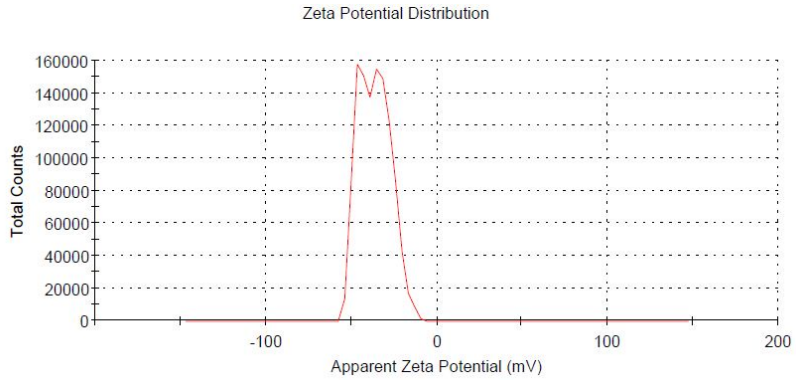

(a) Zeta potential- PFD 30

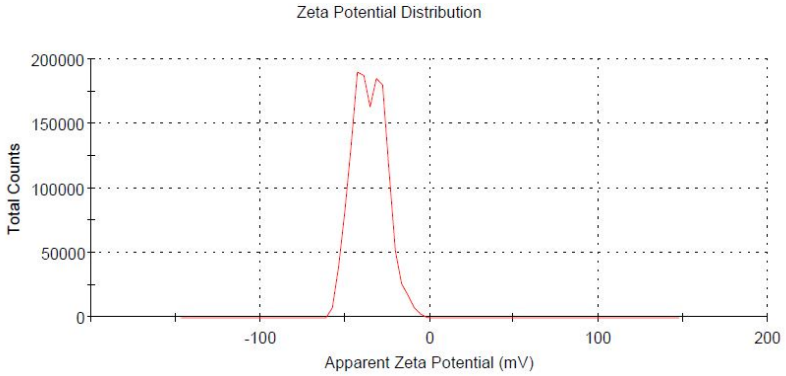

(b) Zeta potential- PFD 50

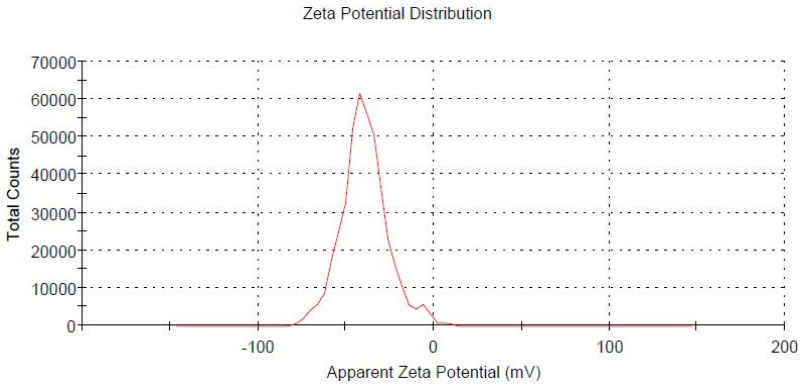

(c) Zeta potential- PFD 70

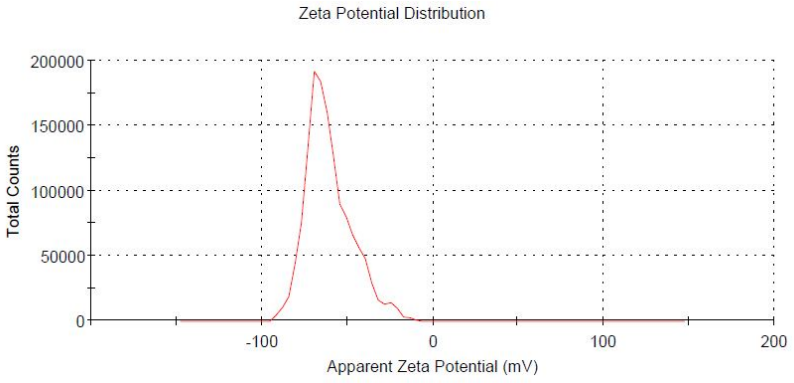

(d) Zeta potential- PFD 90

Figure 4.9: Determination of surface charge of perfluorodecalin emulsions

4.3.7 Variation in the surface charge of perfluorodecalin emulsions

The surface charge of the perfluorodecalin emulsions (PFD 30, PFD 50, PFD 70 and PFD 90) is determined using zeta potential apparatus. Figure 4.9 shows the zeta potential of PFD emulsions. It is found that the zeta potential measurement of PFD 30 emulsion after its preparation is determined to be -37.6 ± 1.6 mV. The zeta value suggests that a negative charge exists in the perfluorodecalin emulsion droplets in spite of the presence of a non ionic surfactant like Span 20. It has been already reported that in the presence of non ionic surfactants in the emulsions there might be an absorption of hydroxyl ions at the oil/water interface that results in a negative charge [146]. These hydroxyl ions are released by the dissocation or association of the water molecules adsorbed at the oil/water interface [147]. Therefore, the slight negative charge in the PFD 30 emulsion is well understood. When the concentration of perfluorodecalin is increased to 50% (w/v), in this case, only the non polar phase of emulsion is enhanced. Hence, there is a very marginal change in the zeta potential measurement to $-38.7 \pm 4.6\ mV$. Further increment to perfluordecalin to 70% (w/v) and PFD 90% also shows a similar trend; the zeta potential for PFD 70 and PFD 90 emulsions are determined to be $-40 \pm 2.2\ mV$ and $-39.4 \pm 1.2\ mV$. The results of all perfluorodecalin emulsions (i.e. PFD 30, PFD 50, PFD 70 and PFD 90) demonstrate an interesting similarity of a slightly negative zeta potential. This can be attributed to the absorption of hydroxyl ions as mentioned earlier. In accordance with the study reported by Riddick [142], a zeta potential measurement closer to $-40\ mV$ that is found in these perfluorodecalin emulsions suggests reasonable colloidal stability.

4.3.8 Analysis of thermophysical properties of perfluorodecalin emulsions

In this study, the thermophysical properties are estimated for freshly prepared PFD emulsions. Further, the thermal conductivity values of the perflurodecalin emulsions (i.e. PFD 30, 50, 70 and 90) are estimated using Maxwell equation [143]. Table 4.6 shows the theoretically obtained thermal conductivity measurements of all PFD emulsions. The thermal conductivity of perfluorodecalin (the dispersed phase) i.e., k_p is 0.057 W/mK and the thermal conductivity of water (other component) i.e. k_o is 0.6 W/m.K. The volume fraction of the dispersed phase (ϕ) is calculated and found to be 0.135, 0.206, 0.266 and 0.319 (i.e. 30% (w/v), 50% (w/v), 70% (w/v) and 90% (w/v)). Using the values of thermal conductivity of perfluorodecalin, water and volume fraction, the calculation of theoretical $k_{effective}$ is carried out. PFD 30 emulsions possess a thermal conductivity of 0.50 W/m.K. Further, for PFD 50 emulsion, with addition of more perfluodecalin phase in emulsion, the thermal conductivity lessens to 0.452 W/m.K. A similar trend of decrease is evident with more increase in perfluorodecalin to 70% (w/v) and 90% (w/v) in the emulsion, the thermal conductivity

Table 4.6: Theoretical determination of thermal conductivity for perfluorodecalin emulsions

Sample	Thermal conductivity (W/mK)
PFD 30	0.50
PFD 50	0.45
PFD 70	0.41
PFD 90	0.38

is determined to be 0.414 W/m.K and 0.38 W/m.K. Thus, in all perfluorodecalin emulsions (PFD 30, PFD 50, PFD 70 and PFD 90 emulsions), these thermal conductivity measurements reveal a decrease with the increase in concentration of perfluorodecalin concentration in the emulsions. This is understood as with the increment in the perfluorodecalin concentration, the volume fraction of low thermal conductivity perfluorodecalin phase increases in the emulsions, thereby lessening its thermal conductivity. The basis of calculation of average density of the mixture is the volume fraction of each phase at room temperature. The values of average density of PFD 30, PFD 50, PFD 70 and PFD 90 emulsions are 1.22 g/cm^3, 1.36 g/cm^3, 1.59 g/cm^3 and 1.778 g/cm^3 respectively.

The determination of specific heat is carried out by C_p ratio method (using DSC, Proteus software, Netszch, Germany) and the values of specific heat should obtained in this study are in the sensible heat change region where there is no phase change (i.e. 0^oC to 37^oC). During phase change there is lack of thermodynamic equilibrium in the system and hence specific heat should not be determined during the phase change as the values are unrealistic. Further, for practical use in cryosurgery, the emulsion would be used as an insulation at the body core temperature of 37^oC. Therefore, the specific heat of PFD 30, PFD 50, PFD 70 and PFD 90 emulsions is measured by differential scanning calorimetry at 37^oC and found to be 3.04 $J/g.K$, 2.88 $J/g.K$, 2.41 $J/g.K$ and 2.004 $J/g.K$ respectively.

The results indicate that the value of specific heat decreases with the addition of perfluorodecalin in the emulsions. Figure 4.10 depicts the variation of specific heat with temperature for perfluorodecalin emulsions. It is seen that the emulsion with higher amount of perfluorodecalin, i.e. PFD 90 has a lower specific heat when compared to PFD 70, PFD 50 and PFD 30 emulsions. Thus, suggesting the usefulness of the concentrated perfluorodecalin emulsions in being used as the solution layer around the tumour interface during cryosurgery. Using the values of thermal conductivity (experimentally obtained using KD2 Pro system), average density and specific heat (using DSC), thermal diffusivity is evaluated at 37^oC (Table 4.5). There is a decrease in the thermal diffusivity of emulsions with the increase in perfluorodecalin concentration to 90% (w/v). In the same context, it is observed that the thermal diffusivity of PFD 30 emulsion is found to be 1.48×10^{-7} m^2/s whereas PFD 90 emulsion possesses a thermal diffusivity of 8.13×10^{-8} m^2/s. Lower thermal conductivity

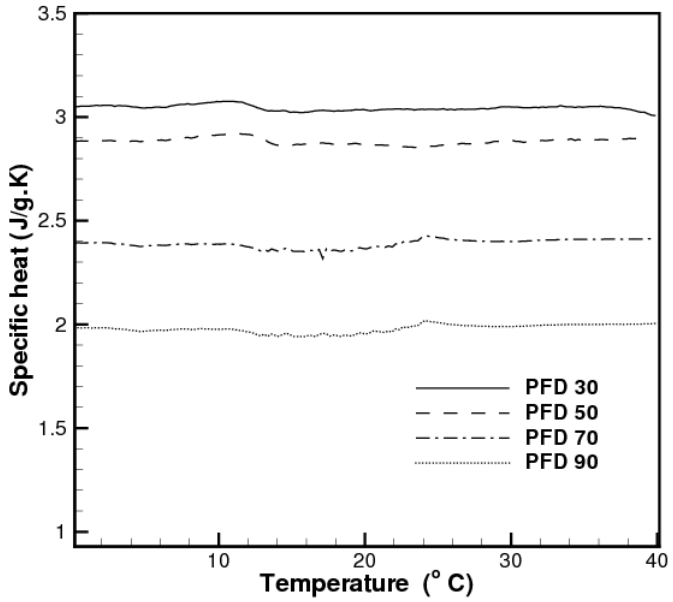

Figure 4.10: Determination of specific heat with the help of differential scanning calorimetry

and thermal diffusivity of the PFD 90 emulsion makes it a potential material for insulation around the tumour interface during cryosurgery. Thus, this study presents emulsions of low thermal conductivity that finds potential application in the field of cryosurgery.

4.3.9 Application of perfluorodecalin emulsions during cryosurgery

It can be seen that in the presence of emulsion layer of perfluorodecalin (90% (w/v)) freezing front is unable to penetrate the gel-perfluorocarbon interface. After cryosurgery of gel phantom in the absence of perfluorodecalin emulsion layer, the temperature is determined to be -4^oC at the 10 mm axially placed thermocouple from the probe, while with the use of this emulsion layer, the temperature at the same location is found to be 11^oC (Figure 4.11(a) and Figure 4.11(b)). Thus, proving that this emulsion layer does not allow the freezing front to cross the thermocouple placed at a position of 10 mm axial location. After cooling the tissue mimicking gel phantom for 10 minutes, the ice ball shape and size is determined qualitatively. The images of ice ball obtained after cryosurgery in presence and absence of the emulsion layer is shown in Figure 4.12. From this figure, it is clearly seen that the ice ball formed in presence of emulsion layer as a barrier has an axial depth which is lesser by 1 mm as compared to the normal agarose gel ice ball. This further corroborates the fact that this emulsion acts as a barrier to heat transfer during cryosurgery process.

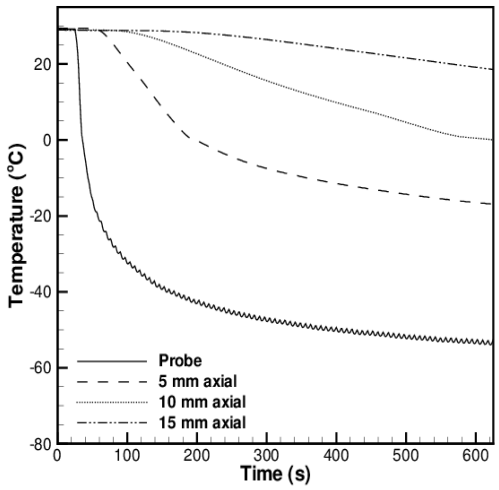

(a) Axial gel cooling without emulsion layer

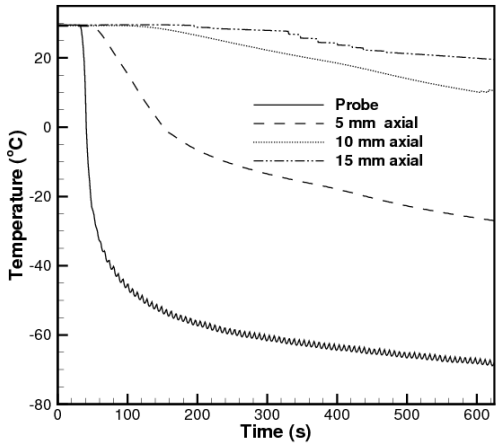

(b) Axial gel cooling in presence of emulsion layer

Figure 4.11: Comparison of axial freezing of agarose gel phantom during cryosurgery in absence and presence of emulsion layer at gel interface

4.4 Summary

In the earlier part of this chapter, efforts are made to optimise the most suitable perfluorohexane emulsion that could be used for cryosurgical application as an insulating layer. The z-average diameter of PFH emulsions and PFHL emulsions are similar but since perfluorohexane emulsions with Span 20 possess lower thermal conductivity, further studies are carried out for these emulsions. In the same context, it can be concluded that the value of thermal conductivity for the emulsions prepared with Span 20 for highest concentration of perfluorohexane (PFH 90) is found to be 0.30 $\pm$ 0.01 W/m.K respectively. Even the theoretical estimation yields a similar value of thermal conductivity. Zeta potential studies for these emulsion also indicates a stable suspension.

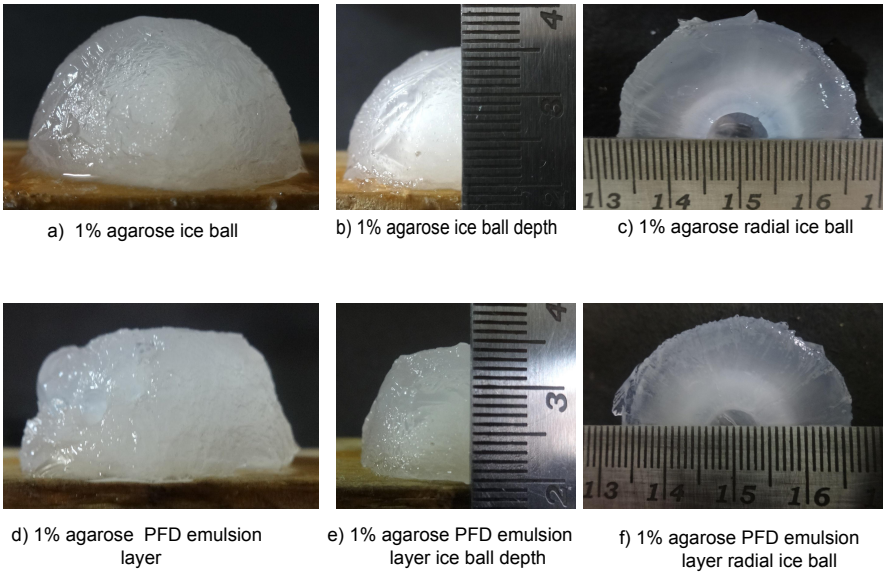

Figure 4.12: Ice ball formation during cryosurgery with and without perfluorodecalin emulsion layer (image obtained through a digital camera (SONY, WX80))

The second half of this chapter demonstrates the formation of monodisperse and homogenous emulsions of another perfluorocarbon, perfluorodecalin. It is found that perfluorodecalin emulsions (i.e. PFD 30, PFD 50, PFD 70 and PFD 90) possess a z-average diameter of 170.5 $\pm$ 10.69 nm, 191.7 $\pm$ 3.98 nm, 199.1 $\pm$ 4.01 nm and 206.1 $\pm$ 5.1 nm respectively. The value of suspension stability for all PFD emulsions represented by the Zeta potential measurements indicate a value between -38 to -40 mV that suggests moderate colloidal stability. It is observed that Span 20 based perfluorocarbon emulsions produces better heat insulation than other two surfactants (Pluronic F-68 and L-phosphatidylamine) as the emulsions formed are moderately stable with span and aging is relatively slower. In the other cases, due to lesser stability, the perfluorocarbon phase separates out, thereby, lowering the thermal conductivity of the bulk solution. The evaluation of thermal conductivity theoretically and experimentally suggests that with the increase in perfluorodecalin phase, the thermal conductivity decreases. The results of specific heat determined through differential scanning calorimetry study reveals that the addition in perfluorodecalin phase results in the decrement of specific heat. Furthermore, PFD 90 emulsion present a lower thermal diffusivity ($8.13 \times 10^{-8}\ m^2/s$) when compared to PFD 30 emulsion (1.48×10^{-7} m^2/s). It can be seen that in presence of low thermal conductivity perfluorodecalin emulsion (90% w/v), it is observed that the freezing front is not able to penetrate the gel. Normally, in the absence of perfluorodecalin emulsion layer, the temperature is -4^oC at the 10 mm axially placed thermocouple, while in presence of this emulsion layer, the temperature at the same location is found to be 11^oC. Even the images of ice ball obtained after cryosurgery in presence of the emulsion layer suggest that these highly concentrated emulsions can be used effectively as an insulating material. Hence, the preparation of such optimised emulsions of low thermal conductivity and thermal diffusivity will aid in the increasing of the efficacy

of cryosurgery process, thereby, improving the therapeutic outcome of the cryosurgical technique immensely.

Chapter 5

New strategies for improving cryosurgical outcome in gel phantoms

5.1 Introduction

Cancer cases have drastically risen over the last few decades. Therefore, surgeons are now looking for other treatment methods like cryosurgery that uses a low temperature in the order of -196^oC to ablate the tumour. Many in-vivo and in-vitro experiments have been carried out to improve the effectiveness of the cryosurgical protocol. In another in vivo study, researchers have observed that a higher concentration phosphate buffered saline solution of antifreeze proteins (10 mg/ml) causes spicular ice formation during cooling [128]. This ruptures cell membrane resulting in cell death, thus, acting as an adjuvant. Several chemotherapy adjuvants such as adriamycin and peplomycin have been used in a combinative manner with cryosurgery and have shown improved clinical outcome [129, 148]. Further, from the study of Wang et al. [149]; it is evident that the addition of glycine results in enhancement of destruction in MCF-7 breast cancer cells. Further, the study of Wang et al. also suggests that glycine causes a depression in freezing point. Hence, its addition would lead to a shift or lowering of the end temperature achieved during cryosurgical freezing. However, these studies have been limited to cell suspensions. Therefore, further work needs to be carried out on solid tissues and gel phantoms.

There are numerous studies as seen earlier in the section of literature review that suggest improvement in the efficacy of cryosurgery process. However, there are drawbacks that need to be addressed. To address these issues, the current study proposes a method of increasing the freezing inside the gel mimicking tissue phantoms during cryosurgery by using an amino acid such as glycine. Till date, studies have not been carried out to investigate the role of glycine in lowering the end temperature during cryosurgery of gel phantoms. Hence, glycine concentration is increased in the agarose gel phantoms and subsequently, the gels are cooled using the cryosurgery system.

Secondly, since there is increased freezing due to glycine, it would be highly beneficial if the ice front could be limited to the desired location in the gel phantom. In the same

context, this study proposes a novel strategy that advocates the use of a perfluorocarbon (liquid) layer of low thermal conductivity at the gel interface. This layer can be made by perfluorohexane, a perfluorocarbon that has a low thermal conductivity of 0.093 W/m.K (experimentally determined using KD2 probe thermal analyser). Therefore, in the current chapter, experiments are carried out to evaluate the increased freezing in gel phantoms due to the addition of glycine. Further, a study has also been performed to visualise the role of a perfluorohexane solution layer as insulation to the glycine consisting gel phantom during cryosurgical cooling. In a real time scenario, this perfluorohexane layer can be applied in biological systems using the approach suggested by researchers in a numerical study carried out recently [134]. Further, this study also suggests that perfluorocarbon molecules can be attached to the tumour. The surface antigen of the tumour can be targeted by its specific monoclonal antibody [135]. Biotinylated monoclonal antibodies can be used to conjugate with avidin. With high specificity to biotin, the antibody-avidin conjugate would attach to biotinylated perfluorocarbon [136], thus, providing a new approach for the maintenance of perfluorohexane layer around the tumour interface. On the other hand, glycine can be injected directly to the tumour site through hypodermal needles.

Till date, alumina emulsions have not been used for increasing the thermal conductivity of gel phantoms for the betterment of cryosurgical outcome. Hence, this study proposes to enhance the freezing inside the agarose gels by using alumina as an adjuvant. The concentration of alumina in the emulsions is varied to obtain the optimal emulsion that has a higher thermal conductivity. There is an urgent need for a combinative treatment modality where the freezing in increased in a localised region but does not affect the region immediately neighbouring it. Therefore, the ability of perfluorohexane layer (i.e perfluorocarbon liquid layer) to insulate the alumina containing gel phantoms is studied exhaustively. A parametric study is also carried out to visualise the effect of change in the insertion depth on the cooling of these alumina containing gels. In addition, experiments have also been performed to verify the effectiveness of perfluorohexane layer as an insulation with the increase in insertion depth of the cryoprobe. Also, cooling studies have been carried out to see the effect of addition of glycine to the alumina containing gel phantoms. The presence of glycine in alumina containing gel phantom results in a two fold effect: a) the alumina particles result in a higher thermal conductivity of the gel phantom thereby causing a faster diffusion of heat and a lower temperature owing to a higher thermal gradient, and b) during cryosurgery, the addition of glycine in alumina containing gel phantoms causes eutectic freezing lowering the temperature even more further. Similar to the previous case, this approach can be implemented by directly injecting the alumina emulsions at a particular location and susbeuently cooling it using cryosurgery.

Prior to cryosurgery, the tissues can be injected with a defined concentration of adjuvants (alumina and glycine). For the sake of homogenous distribution of adjuvants multiple injections can be given so that there is a uniform distribution of adjuvants. Subsequently,

cryosurgery can be performed for 10-20 minutes. Since this strategy focuses on injecting solid tumours with adjuvants and the tissue is frozen immediately due to cryosurgery, the blood flow inside the tumour will be minimal or absent. In the gel phantoms, for maintaining a uniform composition of adjuvants and for ease of thermal history measurements during the cryo-freezing process, the gel phantom was made by adding adjuvants prior to gel solidification instead of injecting the gel with adjuvants. The biocompatibility of alumina is well known in vivo and it is used as a scaffold for seeding cells in vivo for tissue engineering applications. Glycine, on the other hand, is and amino acid and naturally available in the human physiological system. Therefore, the approach proposed in the current study is practical and quite useful for improving the cryosurgery process.

5.2 Materials and methods

5.2.1 Materials

In the first half of this chapter, glycine (HIMEDIA Chemicals) is used as an adjuvant. Agarose (Low EEO, HIMEDIA Chemicals) is dissolved in water for making tissue-mimicking gel phantoms. Perfluorohexane (SIGMA ALDRICH), a perfluorocarbon, is used for making the insulating layer. Acrylic sheets of a thickness of 5 mm are procured from a local supplier. The cooling of gel phantoms is carried out by cryosurgery system KCH 450 A (SMT Praha, Czech Republic). For thermal history measurement, K-type thermocouples are used and the acquisition of the temperature signals is done through a data acquisition system, USB 9213 (National Instruments, USA). For the placement of thermocouples, wooden planks are used to make fixtures as shown in Figure 5.1 and a digital camera (Sony WX80, Japan) is used to acquire ice ball images after cryosurgery of phantoms.

In the second half of this chapter aluminium oxide (Al_2O_3, HIMEDIA Chemicals) is used as the primary phase for the preparation of the emulsions. For the preparation of an emulsion, a surfactant is needed and in this study, Span 20 (sorbitan monolaurate, Loba Chemie) is utilised as the surfactant for the formation of alumina emulsions. Deionized double-distilled water is the other phase required for the preparation of these emulsions. In this study, glycine (NH_2CH_2COOH, HIMEDIA Chemicals) is used as an adjuvant in combination with aluminium oxide. Agarose (Low EEO, HIMEDIA Chemicals) is dissolved in water for making gel phantoms. The cooling of gel phantoms is also carried out by the same cryosurgery system KCH 450 A (SMT Praha, Czech Republic). For thermal history measurement, K-Type thermocouples are connnected to a data acquisition system USB 9213 (National Instruments, USA) which is further connected to a computer as mentioned earlier. Wooden planks used for fabricating thermocouple fixtures are purchased from local carpentary units. Perfluorohexane (SIGMA ALDRICH, 95% pure) is used for making the insulating layer. For thermocouple placement, wooden planks are used to make fixtures

(Figure 5.1) and immediately after cryosurgery ice ball images are captured using a digital camera (Sony WX80, Japan) for all studied cases.

5.2.2 Methods

Gel phantom with glycine as adjuvant

1% (w/v) agarose is used for the preparation of the gel phantoms and the concentration of agarose is kept constant in the entire study. For the formation of gel phantom containing adjuvants, the weighed agarose in a concentration of 1% (w/v) is added to 650 ml of water consisting appropriate amount of glycine (i.e. 0.2% (w/v), 1% (w/v) and 5% (w/v)). Subsequently, the solution is heated for two minutes (900 W) in a microwave oven. Then the adjuvant (glycine) gel mixture is cooled and poured into the acrylic container of a definite size (12 cm$\times$12 cm$\times$6 cm). The acrylic container is fabricated using mechanical operations like cutting, filing and polishing. The thermocouple fixtures that are used are customised and designed through basic mechanical operations (Figure 5.1). Once the thermocouple fixture is placed on the acrylic container, the gel consisting of glycine is poured into the container and allowed for solidification. After gel solidification, freezing is carried out using the cryosurgery system for 10 minutes. The thermocouples are connected to a data acquisition system (connected to a computer) for the measurement of temperature distribution during cryosurgery. LabVIEW 2013 (software by National Instruments, US) is utilised to record and visualise the temperature signals in the computer. Further, the accuracy of thermocouples is verified by dipping the thermocouple in liquid nitrogen and recording the temperature by using LabVIEW 2013. The temperature obtained through the thermocouples after dipping it in liquid nitrogen for a minute is $-194°C$. Hence, the error in the temperature measurement using these thermocouples is in the order of $\pm 2^oC$. It should also be noted that the thermal conductivity values mentioned in the study are obtained using KD2 probe thermal analyser (Decagon Devices, US). For confirming its accuracy, the thermal conductivity of known substance like water has been measured accurately and found to be in close agreement with the reported literature value of 0.596 W/m.K (at a temperature of $37°C$).

Cooling of glycine containing gel in presence of perfluorohexane layer

In presence of perfluorohexane (perfluorocarbon) liquid layer as insulation to the gel with glycine, there are two parts in the thermocouple fixture (marked as 1 and 2 in the Top view, Figure 5.1). The first part of the thermocouple fixture contains all radial thermocouples and a 5 mm axially placed thermocouple. After placing the first thermocouple fixture in the acrylic container, an acrylic fixture of a fixed size 9 cm$\times$1 cm$\times$12 cm is mounted over the container. Subsequently, the prepared gel consisting glycine is poured in the acrylic container. Once the solidification occurs, the acrylic fixture is carefully removed without

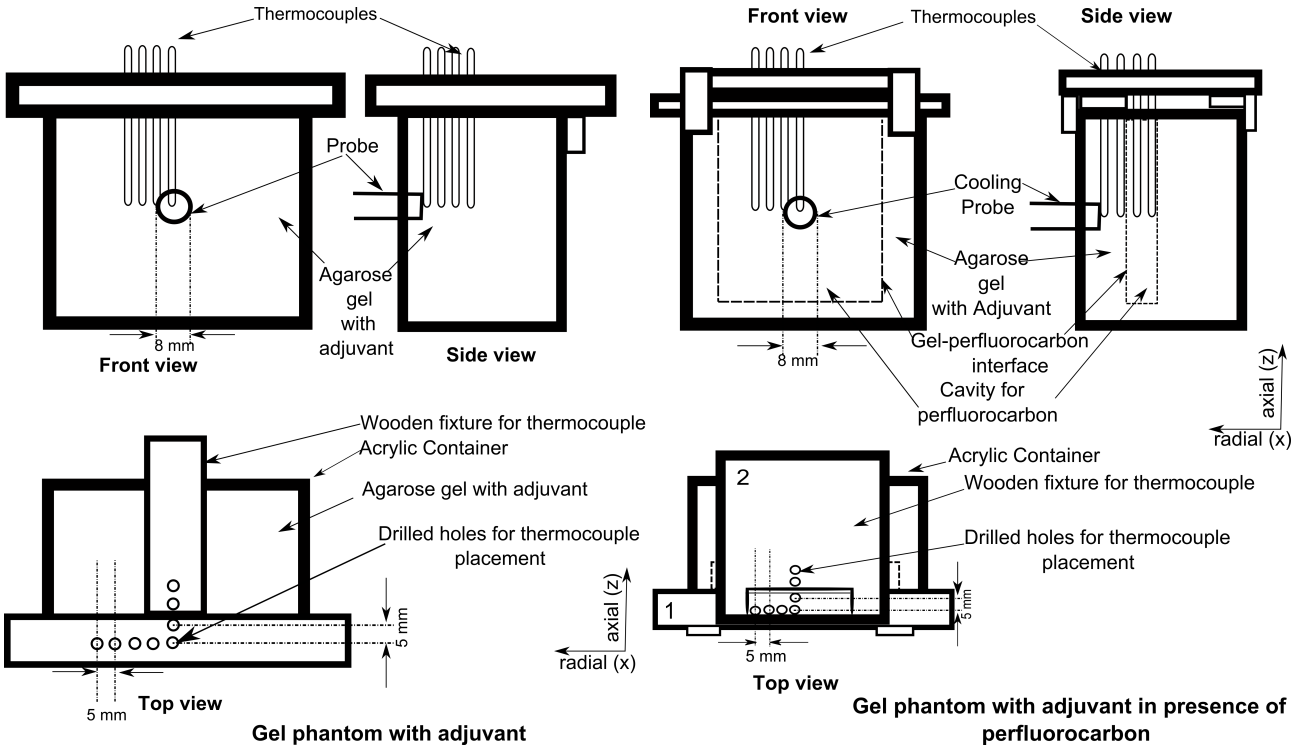

(a) Adjuvant gel cooling (b) Adjuvant gel cooling in presence of perfluorocarbon

(c) Experimental set up

Figure 5.1: Schematic diagram of the adjuvant gel cooling in absence or presence of perfluorocarbon and experimental design for cryosurgery

disturbing the earlier placed thermocouples. The cuboidal cavity, thus formed is used for filling the perfluorohexane solution. Then, the second thermocouple fixture (marked as 2 in Figure 5.1) having 10 mm and 15 mm axially located thermocouples is mounted over the acrylic container. It should be noted that the thermocouples placed at 10 mm and 15 mm axial locations are placed inside the perfluorohexane layer while rest of the radial and axial thermocouples are inside the glycine containing gel. Followed by the thermocouple placement, cryosurgery is performed for 10 minutes and its thermal history is recorded as mentioned earlier.

Repeatability of freezing during cryosurgery of gel phantoms

The repeatability of temperature measurements during cryosurgery is very crucial and to ascertain the same, a number of freezing experiments of 1% (w/v) agarose gels are carried out. It is found that two thermal measurements of freezing are nearly similar. The mean temperature is plotted with respect to time and standard deviation from mean is calculated to verify the closeness of the obtained values at each thermocouple location (Figure 5.2). The measurements suggest that the temperature is nearly the same at each thermocouple location in the two freezing trials. Also, the error bars again clearly point out that the standard deviation from mean is marginal and therefore, reliable and reproducible temperature measurements can be achieved using this experimental design.

Preparation of emulsion

The preparation of alumina emulsions (i.e. 0.2% (w/v), 1% (w/v), 2% (w/v) and glycine-alumina emulsions (i.e. 1% (w/v) glycine - 1% (w/v) alumina and 5% (w/v) glycine - 1% (w/v) alumina) is carried out by using probe sonication (Vibrionics Ultrasonic processor, India). The surfactant used is Span 20 and its concentration in the emulsions is 5% (w/v). The other phase utilised for emulsion preparation is water. Prior to sonication, alumina, Span 20 and water are added in a beaker to form a mixture and stirred using a magnetic stirrer for 10 minutes. Subsequently, the preparation of all alumina emulsions require a single cycle of probe sonication for 20 minutes. The operating frequency of probe sonicator for emulsion preparation is 20 kHz. It should be noted that in case of glycine-alumina emulsions, glycine is first dissolved in water, then alumina and Span 20 are added before for emulsion preparation using sonication as mentioned earlier. Table 5.1 summarises the composition of the emulsions and the images of the prepared alumina emulsions are shown in Figure 5.3.

Measurement of thermal conductivity

The experimental determination of thermal conductivity is carried out by using the KD2 Pro thermal analyser at room temperature (Decagon Devices Inc, US). This probe utilises the principle of line source method for estimation of thermal conductivity of the emulsion

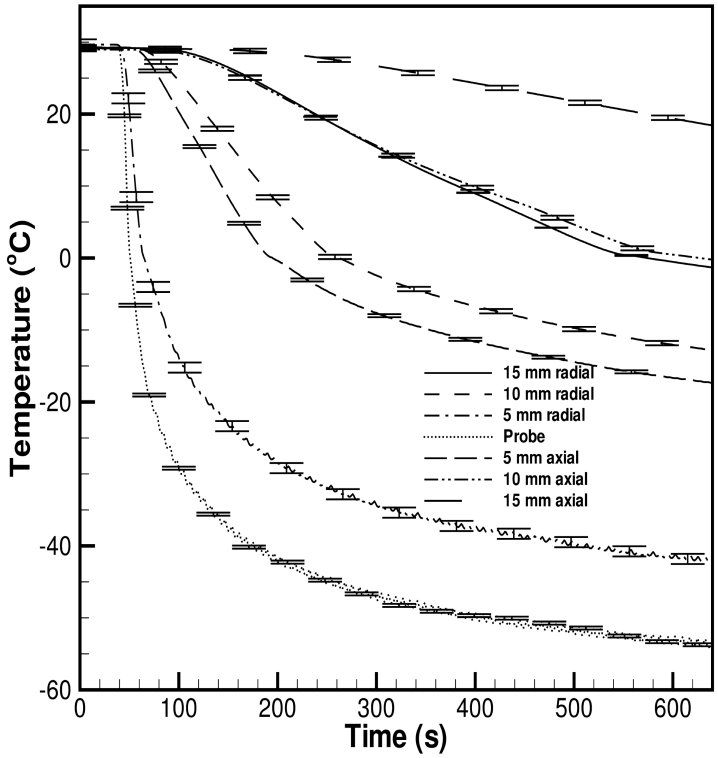

Figure 5.2: Repeatability in freezing to verify the accuracy in thermal history measurement

Table 5.1: Composition of the alumina emulsions

Emulsion	Weight (adjuvant) (g)	Surfactant(5%)	Weight (surfactant)(g)	Volume of water used(ml)
0.2% (w/v) Alumina	1.3	Span 20	32.5	650
1% (w/v) Alumina	6.5	Span 20	32.5	650
2% (w/v) Alumina	13	Span 20	32.5	650
1% (w/v) Glycine 1% (w/v) Alumina	Glycine- 6.5 Alumina- 6.5	Span 20	32.5	650
5% (w/v) Glycine 1% (w/v) Alumina	Glycine- 32.5 Alumina- 6.5	Span 20	32.5	650

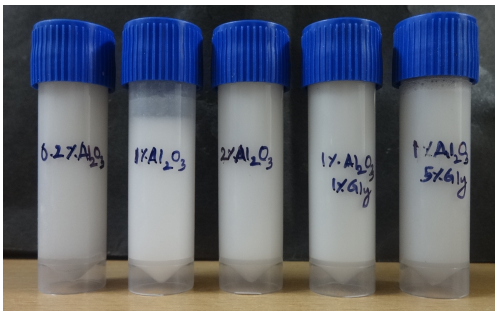

Figure 5.3: Images of alumina emulsions used as adjuvant during cryosurgery obtained by a digital camera (Sony,WX80)

samples. The thermal conductivity measurements are determined out in triplicates using the thermal analyser. Followed by that, the mean and standard deviation are calculated, based on that the uncertainty in thermal conductivity is determined and the values obtained are mentioned along with the mean thermal conductivity value in the results section.

Preparation and experimental design for cryosurgery of alumina containing gel phantoms

The concentration of agarose in all gel phantoms is 1% (w/v) and is kept constant in the entire study. For making the gel phantom containing adjuvants, agarose is weighed in a concentration of 1% (w/v) and added to the prepared alumina emulsions. It is subsequently heated for two minutes (900 W) in a microwave oven. The solution is then cooled and poured into a container of 12 cm$\times 12$ cm$\times 6$ cm that is fabricated from the acryclic sheets. The thermocouple fixtures that are fabricated and used in this study are illustrated in Figure 5.1(a) and 5.1(b). Once the thermocouple fixture is placed on the acrylic container (Figure5.1(a)), the adjuvant consisting gel solution is poured into the container and allowed for solidification. The gel is solidified and freezing is carried out using the crysourgery system for 10 minutes. The thermal history measurements are made using thermocouples connected to a data acquisition system (connected to a computer). LabVIEW 2013 (a software by National Instruments, US) is utilised to record and visualise the temperature signals in the computer. Further, the accuracy of thermocouples is verified by dipping the thermocouple in liquid nitrogen and recording the temperature by using LabVIEW 2013. The temperature thus obtained in the thermocouples after a minute is -194^oC. Hence, the error in the temperature measurement using these thermocouples is $\pm 2^oC$.

In case of perfluorohexane layer as an insulation to the gel phantom containing alumina (Figure 5.1(b)), there are two parts in the thermocouple fixture (marked in Figure 5.1(b) as 1 and 2 in the Top view). The first part of the thermocouple fixture contains all radial thermocouples and a 5 mm axially placed thermocouple. After placing the first part of the thermocouple fixture in the acrylic container, an acrylic fixture of 9 cm$\times 9$ cm$\times 1$ cm is mounted over the container. Subsequently, the prepared gel with adjuvants is poured

in the container. Once the solidification occurs, the acrylic fixture is slowly and carefully removed without disturbing the earlier placed thermocouples. The cuboidal cavity, thus formed is used for filling the perfluorohexane layer that acts as an insulation. Then, the second part of the thermocouple fixture having 10 mm and 15 mm axially located thermocouples is mounted over the gel phantom in such a way that these thermocouples are placed in the perfluorohexane liquid layer while rest of the radial and axial thermocouples are inside the adjuvant (alumina) containing gel phantom. Followed by the placement of the thermocouples, the cryosurgery of gel phantom is performed for 10 minutes and the temperature profile is recorded as mentioned earlier. The cryosurgical device along with the experimental set up is shown in Figure 5.1(c).

5.3 Results and discussion

5.3.1 Agarose gel phantom cooling using cryosurgery

In the current study, 1% (w/v) agarose gel is used as tissue mimicking gel phantom as it has a thermal conductivity of 0.541 $\pm$ 0.017 W/m.K (measured experimentally through KD2 Pro thermal analyser, value mentioned along with standard deviation). This is in close agreement to the thermal conductivity of biological tissue [137]. The insertion depth of the cryoprobe is 1 cm and the cryosurgery of gel phantoms is carried out for a freezing cycle of 10 minutes. It should be noted down that the end temperature values reported in this study are the temperature measurements obtained after the completion of a single freezing cycle of 10 minutes (Figure 5.4). From the results, it is evident that the probe experiences a temperature of -53.1^oC after 10 minutes of freezing as it is in direct contact with liquid nitrogen. The transient temperature values obtained at a thermocouple location during freezing indicate that the corresponding temperature isotherm has reached the particular location. Further, from the temperature measurements it is seen that after 49 s, the ice front (0^oC isotherm) travels a radial distance of 5 mm (Figure 5.4(a)). Also, the temperature at this thermocouple location reduces to -41.16^oC after a complete freezing cycle of 10 minutes. With advancement in time, the ice front (0^oC) reaches the thermocouple placed at a radial location of 10 mm and 15 mm in 251 s and 561 s respectively. Also, the end temperature achieved at a radial location of 10 mm and 15 mm after 10 minutes of cryosurgery is -12.61^oC and -1.27^oC. It is interesting to note that till a distance of 5 mm the cooling propagates swiftly and a lethal temperature (40^oC) is achieved at the end of a freezing cycle. Further, the axial temperature at 15 mm, 10 mm and 5 mm is found to be 18.54^oC, 0.03^oC and -16.94^oC respectively (Figure 5.4(b)). When a comparison is made between the radial and axial temperature measurements, the graph reveals that radial temperature values are substantially lower than the axial ones at the same thermocouple location (Figure 5.4(a) and Figure 5.4(b)). This is indicative of the fact that the cooling propagates more in the radial direction owing to the

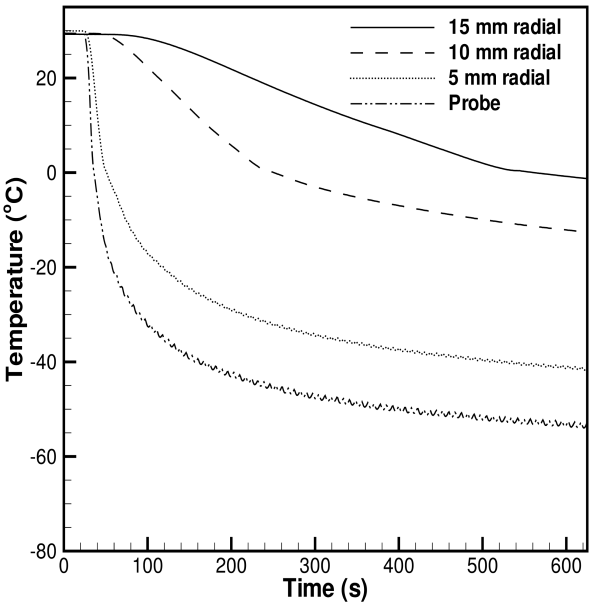

(a) Radial temperature profile

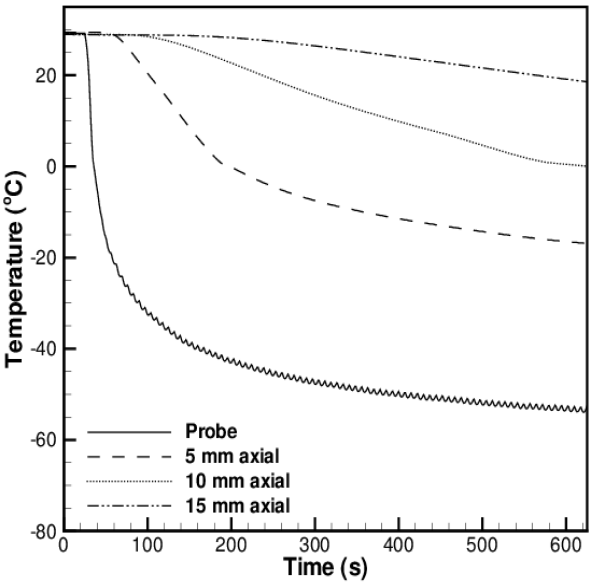

(b) Axial temperature profile

Figure 5.4: Temperature distribution radially and axially in agarose gel phantom during cryosurgery

larger surface area of the cryoprobe radially.

5.3.2 Decreased end temperature due to glycine

The effect of glycine is evaluated by adding it to the agarose solution before gel solidification. After cooling the 1% (w/v) agarose gel containing 0.2% (w/v) glycine using the cryosurgery system, the end temperature is found to be -1.15^oC, -16.14^oC, -46.18^oC and -65.4^oC at the radial locations of 15 mm, 10 mm, 5 mm and probe respectively. When a comparison is drawn between the radial temperature obtained in the present case and 1% (w/v) agarose gel without any adjuvant like glycine, it is observed that there is a substantial decrease in temperature (from -53.1^oC to -65.4^oC, i.e. around 12.3^oC) at probe (Figure 5.5(a) and Figure 5.4(a)). Further, for the thermocouple placed at 5 mm radial location this temperature decrease is 5^oC (Figure 5.5(a) and Figure 5.4(a)). This comparison of temperature distribution also suggests that as the distance increases to 10 mm radially, the temperature difference at the same location in agarose gel and gel with glycine as adjuvant is marginal (around 3.54^oC). This is due to meager temperature gradient as one proceeds farther away from the cryoprobe. Also, the temperature at the axial locations of 15 mm, 10 mm and 5 mm is determined to be 14.19^oC, -4.28^oC and -21.34^oC respectively (Figure 5.5(b)). A similar trend which was obtained earlier in case of agarose gels is evident here and it is seen that at the same thermocouple location radial temperature is considerably lesser than the axial temperature (Figure 5.5(a) and Figure 5.5(b)). As seen earlier, this higher cooling is due to the cylindrical probe that provides more surface area for cooling in the radial direction as compared to the axial one.

The axial temperature plot demonstrates a slight decrease in temperature due to addition of 0.2% (w/v) glycine and this is obvious as glycine is an adjuvant that lowers the freezing temperature and causes eutectic freezing. The results reveal a noteworthy trend of higher temperature decrease with an increase in glycine concentration to 5% (w/v) in the gel (Figure 5.5(c) and Figure 5.5(d)). Figure 5.5(c) shows the radial temperature distribution during cooling of 5% (w/v) glycine containing gel phantom. The graph demonstrates that the ice front (0^oC isotherm) reaches the radial position of 5 mm in merely 38 s. However, in the case of agarose gel phantoms, the ice front reached the same location in 49 s. Therefore, with addition of glycine to 5% (w/v), ice front moves quickly. A similar trend of faster ice front movement is also visible when the front advances to a radial distance of 10 mm; it propagates and reaches this location at 114 s while in agarose gel phantom similar distance is travelled in 250 s. Hence, the temperature measurements reveal that glycine addition presents swifter movement of the ice front in the gel phantoms.

When the radial temperature profile of glycine (5% (w/v)) containing gel phantom is observed, the graph indicates an end temperature of -7.37^oC, -27.68^oC, -52.21^oC and -71.72^oC with thermocouples located at 15 mm , 10 mm and 5 mm and probe respectively

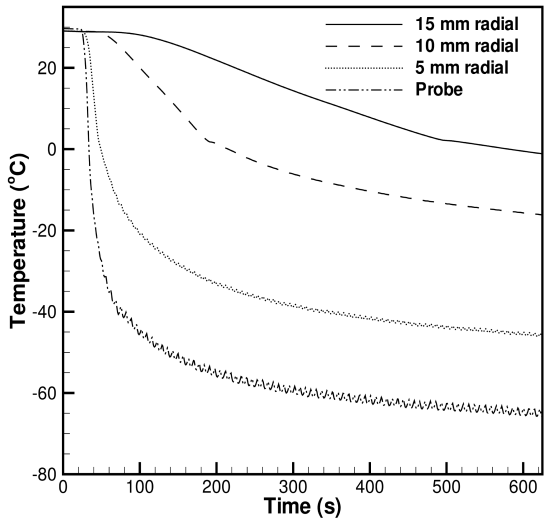

(a) 0.2% glycine radial temperature profile

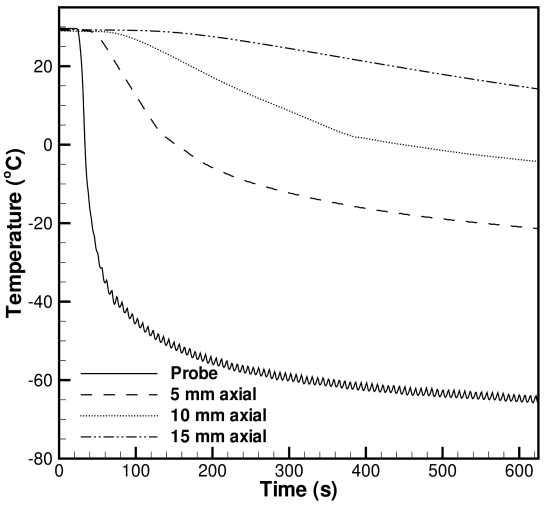

(b) 0.2% glycine axial temperature profile

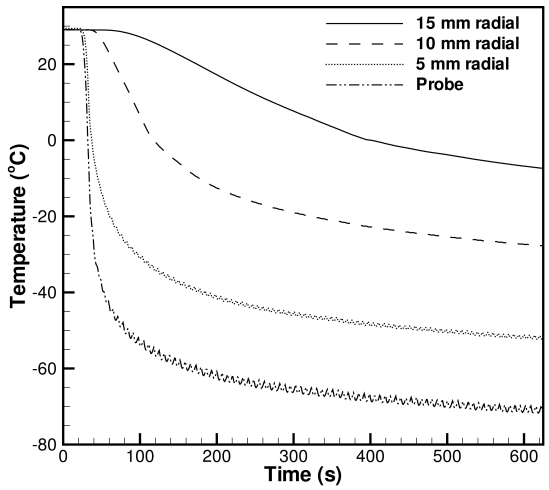

(c) 5% glycine radial temperature profile

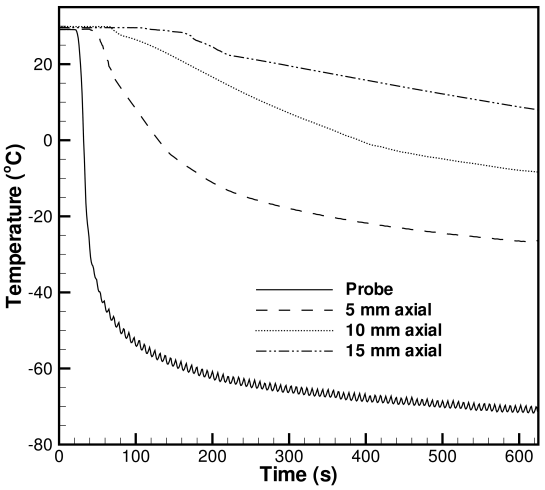

(d) 5% glycine axial temperature profile

Figure 5.5: Effect of glycine concentration on enhancing the freezing of gels during cryosurgery

(Figure 5.5(c)). These temperature measurements are lower than the ones achieved while cooling of 0.2% (w/v) glycine containing gel phantoms at the same thermocouple location. When temperature distribution attained during 5% (w/v) glycine gel cooling is compared to 0.2% (w/v) gel cooling, it is observed that there is a significant reduction in end temperature (from -65.4^oC to -71.72^oC, i.e. 6.3^oC) at probe (Figure 5.5(a) and Figure 5.5(c)). Further, at a radial location of 5 mm and 10 mm, the thermocouple experiences a temperature drop of 6.03^oC and 11.54^oC when compared to the previous case of 0.2% (w/v) glycine gel cooling. After cryosurgery of 5% (w/v) glycine consisting gel phantoms, the temperature measured at an axial location of 15 mm, 10 mm and 5 mm is -26.14^oC, -8.38^oC and 7.99^oC respectively (Figure 5.5(d)). These values are lesser than the axial temperature readings obtained in 0.2% (w/v) revealing that in all cases, both radially and axially, the addition of glycine results in a reduction in the end temperature achieved after cryosurgery.

5.3.3 Effect of perfluorohexane layer on glycine consisting gel phantoms

For studying the role of perfluorohexane as insulation, 1% (w/v) agarose with 5% (w/v) glycine is cooled in its presence using cryosurgery. The cryosurgery of glycine gel with perfluorohexane solution layer results in a temperature of $-7.85°C$, -28.15^oC, -55.64^oC and -71.06^oC at the radial location of 15 mm, 10 mm, 5 mm and probe respectively (Figure 5.6(a)). These radial temperature measurements are marginally lower than those obtained in glycine gel without the insulating layer of perfluorohexane. Furthermore, axial measurement indicates a temperature of 23.83^oC, 23.77^oC and -26.84^oC at a position of 15 mm, 10 mm and 5 mm respectively (Figure 5.6(a)). A comparison between the axial end temperature of glycine containing gel with and without perfluorohexane suggests that the two thermocouples placed at 10 mm and 15 mm in the cuboidal cavity containing perfluorohexane solution have a higher temperature of 23.77^oC and 23.83^oC respectively (Figure 5.6(a) and Figure 5.5(d)). On the other hand, in 5% (w/v) glycine gel, the axial end temperature of thermocouples placed inside the gel at 10 mm and 15 mm is -8.38^oC and 7.88^oC (Figure 5.5(d)). Since perfluorohexane possesses low thermal conductivity (k = 0.093 W/m.K) it is clearly noticeable that the freezing front is unable to cross the gel-perfluorohexane interface.

The images of the ice ball captured immediately after cryosurgery reveal an interesting observation; when perfluorohexane is insulating the gel interface, the ice ball formed has a depth of 13 mm whereas, in the absence of this insulating layer (1% (w/v) agarose with 5% (w/v) glycine), the ice ball depth is 16 mm (Figure 5.6(b)). Thus, there is a difference of 3 mm in the ice ball depth owing to the insulating ability of perfluorohexane, which is also noticed from the shape of the ice ball. Further, the ice ball obtained in the case of agarose gel cooling also suggests a depth of 16 mm. In both cases, the cryosurgery of 1% (w/v) agarose

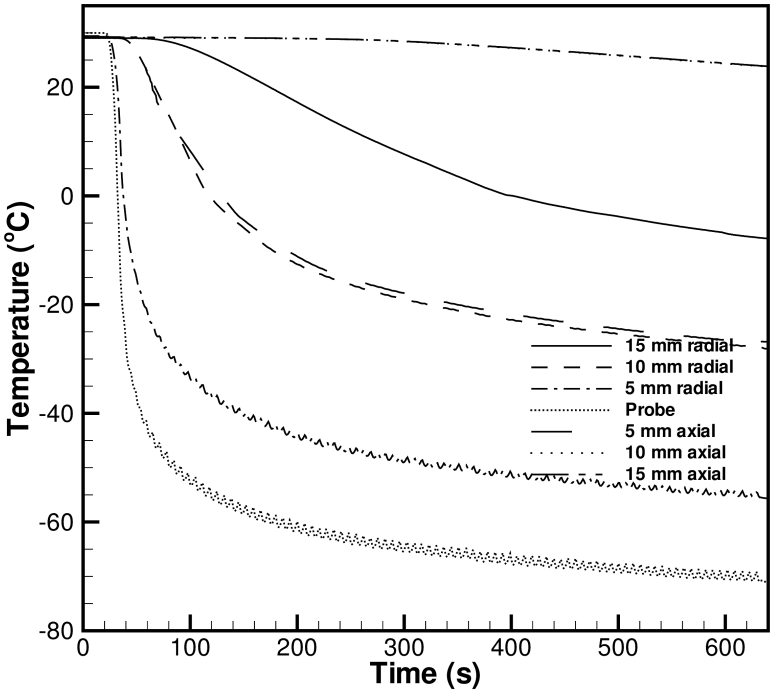

(a) 5% Glycine gel phantom with perfluorohexane layer

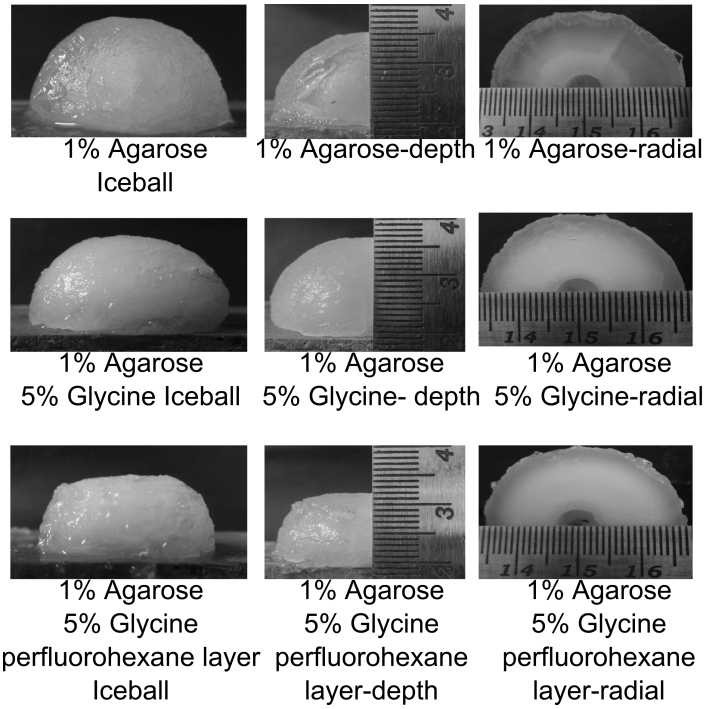

(b) Comparison of ice ball

Figure 5.6: Temperature distribution of glycine gel phantom with perfluorohexane layer as barrier during cryosurgery and ice ball comparison after cryosurgery of agarose gel phantom, 5% (w/v) glycine containing gel phantom in absence and presence of perfluorohexane layer (ice ball images captured through a digital camera (SONY, WX80))

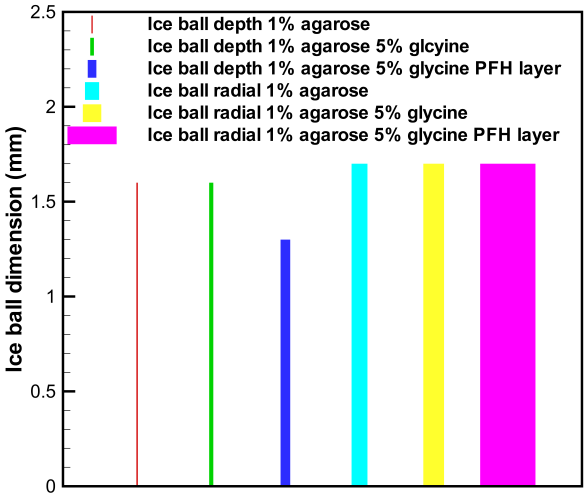

Figure 5.7: Images of alumina ice ball obtained after cryosurgery obtained by a digital camera (Sony,WX80)

gel and 1% (w/v) agarose gel with 5% (w/v) glycine reveals the same ice ball depth of 16 mm (Figure 5.6(b)). However, in the presence of glycine it is fascinating to observe that there is a considerable reduction in the end temperature obtained after cryosurgery. Therefore, this indicates that although addition of glycine does not have any effect on the ice ball depth but it results in substantial decrease in end temperature. The significance of this approach is that it presents two-fold benefits: a) glycine induces a lower temperature at each thermocouple location in the gel phantom as compared to the agarose gel and b) even with the lower temperature experienced in the glycine gel phantom, perfluorohexane layer insulates the gel phantom. Hence, this study provides a new strategy that aims at maximising freezing inside a desired location while minimising its spread to its immediate surrounding region. For the sake of better clarity, ice ball images are also represented in the form of bar graph (Figure 5.7).

5.3.4 The use of alumina as an adjuvant with multiple strategies to improve cryosurgery process

In the second half of this study, the amount of alumina (i.e. 0.2% (w/v), 1% (w/v), 2% (w/v)) is varied in presence of surfactant (5% (w/v)) to formulate gel phantoms that have optimal thermal conductivity. A higher value of thermal conductivity would result in a faster propagation of heat inside the gel phantom, thereby, lowering the end temperature obtained after the cryosurgical freezing. Therefore, after the formulation of alumina emulsions, 1% (w/v) agarose is added to form alumina consisting gel phantoms. A detailed study is also carried out to investigate the dependence of increase in alumina concentration on the end

Table 5.2: Thermal conductivity of alumina gel phantoms

Gel phantom	Thermal conductivity (W/mK)
0.2% alumina	0.69 ± 0.06
1% alumina	0.73 ± 0.04
2% alumina	0.64 ± 0.09

temperature obtained after cryosurgery in these alumina containing gel phantoms. The thermal conductivity values of the gel phantom reveals that 1% (w/v) alumina containing gel phantoms have a marginally higher thermal conductivity than the other gel phantoms. Hence, for further studies, 1% (w/v) alumina containing gel phantoms are used. A parametric study of cryosurgical freezing of the gel phantoms is carried out by increasing the insertion depth of the cryoprobe (from 1 cm to 1.25 cm and subsequently to 1.5 cm). It is important to limit the freezing injury to a desired region during cryosurgery. Therefore, the effect of a low thermal conductivity layer of perfluorohexane as a barrier to adjuvant (alumina) gel cooling is evaluated with increase in the insertion depth of the cryoprobe. Since the primary objective of cryosurgery process is to increase the freezing for inducing damage, a new method is proposed in this chapter that results in rapid freezing due to the combined effect of adjuvants like alumina and glycine. Glycine is added in a concentration of 1% (w/v) and 5% (w/v) keeping the amount of alumina and agarose constant (i.e. 1% (w/v)) during the preparation of the gel phantom. Till date, adjuvants used in cryosurgery either result in faster diffusion of heat or lower the end temperature, however, in this study, the freezing of gel phantoms that contain glycine-alumina present a novel class of adjuvants that show better outcome with regard to swifter freezing and attainment of lower end temperature, thus, improving the outcome of the cryosurgery process.

5.3.5 Effect of alumina concentration on the freezing of gel phantom during cryosurgery

The concentration of alumina in the emulsion plays a critical role in deciding the thermal conductivity of the emulsions. Generally, emulsion preparation requires a surfactant molecule that creates a steric hindrance between the two phases [150]. In this study, the preparation of alumina emulsions (at 0.2% (w/v), 1% (w/v) and 2% (w/v)) is carried out using probe sonication in presence of Span 20 (5% (w/v)) as the surfactant. Subsequently, after the emulsion preparation, agarose is added to the alumina emulsion for the formation of alumina containing gel phantoms. The thermal conductivity of alumina consisting gel phantoms is measured using the KD2 probe thermal analyser (Table 5.2). It is observed that the thermal conductivity value of 1% (w/v) alumina containing gel phantom is marginally

higher than the other alumina consisting gels and found to be 0.73 ± 0.04 (W/mK) (Table 5.2). Also, in case of 2% (w/v) alumina emulsion, the surfactant volume (5% (w/v)) is not sufficient enough to form emulsions and there is a settlement of pure alumina particles at the bottom of the beaker as visible through naked eyes after the emulsion preparation. Therefore, the thermal conductivity of the phase with higher concentration of alumina (i.e. more than 1% (w/v)) is marginally lower. For 1% (w/v) alumina emulsion, the alumina particles do not sediment at the bottom of the beaker after emulsion preparation. Therefore, the emulsion formation is homogenous leading to a better thermal conductivity. Therefore, 1% (w/v) alumina consisting gel phantoms are used for further studies that deal with insertion depth and adjuvant gel cooling in the presence of the perfluorohexane layer.

After freezing the gel phantoms containing alumina as adjuvant, the results of thermal history indicate a same trend as seen from the values of thermal conductivity; the freezing of gel phantoms consisting 1% (w/v) alumina reveals a lower end temperature in comparison to 0.2% (w/v) and 2% (w/v) alumina gel phantoms after 10 minutes of cryosurgery (Figure 5.8). It should be noted that in all figures the caption probe represents the thermocouple placed near the probe at a distance of nearly 1 mm and all other thermocouple distances are relative to this thermocouple. Figure 5.8(a) depicts the comparison of cooling for 1% (w/v) agarose gel phantom, 0.2% (w/v) alumina, 1% alumina (w/v) and 2% (w/v) alumina containing gel phantom for the thermocouple placed near the probe. From Figure 5.8(a), it is evident that after cryosurgery, the end temperature achieved in the alumina consisting gel phantom is lesser than the agarose gel phantom. It is also observed that the end tempearature is decreased from -52.56^oC in the case of agarose gel phantoms to -60.72^oC, -62.34^oC and -61.34^oC for 0.2%, 1% and 2% (w/v) alumina containing gels. There is a very minor tempearature decrease and this clearly suggests that with the addition of alumina to 1% (w/v), there is a decrease in the end temperature. However, if the alumina concentration in the gel phantom is enhanced to 2% (w/v), the end temperature does not decrease further. Thus, indicating that 1% (w/v) alumina concentration is optimal for carrying out further studies.

A comparison of end temperature at 5 mm radially placed thermocouple in all cases reveals a similar trend. The end temperature is found to be -41.16^oC for agarose gel phantoms. With the addition of alumina to the gel phantom there is a better diffusion of cooling as visible from the temperature measurements. The temperature for 0.2% (w/v), 1% (w/v) and 2% (w/v) alumina containing gel phantoms at this location is found to be -45.96^oC, -49.06^oC and -46.37^oC respectively. It is clearly seen that there is a reduction of around 4.8^oC, 7.9^oC and 5.2^oC in comparison to the end temperature obtained after cooling of agarose gel phantoms which substantiates the fact that alumina addition aids in better diffusion of heat across the phantom (Figure 5.8(b)). Similar results are observed when the end temperature is measured for the 10 mm radially placed thermocouple for these gel phantoms (i.e. 1% (w/v) agarose, 0.2% (w/v), 1% (w/v) and 2%(w/v) alumina containing gels). The temperature values are found to be -12.61^oC, -22.64^oC, -25.98^oC

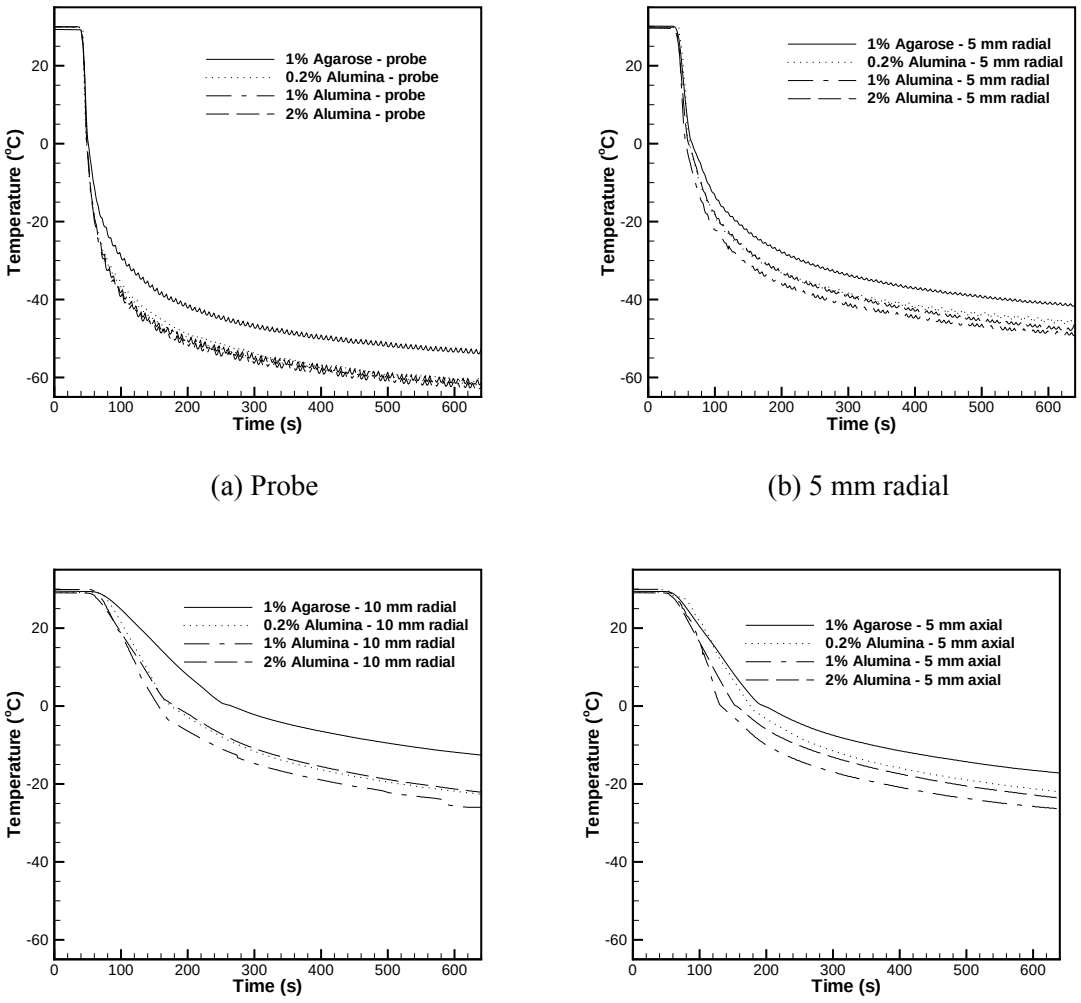

(a) Probe (b) 5 mm radial

(c) 10 mm radial (d) 5 mm axial

Figure 5.8: Comparison of freezing of agarose and alumina consisting gel phantoms during cryosurgery

and -21.97^oC respectively. Figure 5.8(c) shows that there is a decrease of 10^oC in the end temperature when a comparison is made between the agarose gel phantom and the 0.2% (w/v) alumina containing gel phantom. This decrease is also observed when the alumina concentration is increased to 1% (w/v) and 2% (w/v) in the gel phantoms with the maximum end temperature decrease in the 1% (w/v) alumina containing gel phantoms. All these radial measurements have a commonality; there is a visible decrease in the end temperature at both 5 mm and 10 mm radially placed thermcouples. Furthermore, it is interesting to note that 5 mm axially placed thermocouple also shows a marked decrease in the end temperature measurement after cryosurgery. From figure 5.8(d), it is observed that agarose gel phantom experiences an end temperature of -17.21^oC while the alumina containing gels (0.2% (w/v), 1% (w/v) and 2% (w/v)) attain an end temperature of -22.01^oC, -26.45^oC and -23.78^oC respectively. In comparison to the agarose gel phantoms, at this particular location, the maximum end temperature decrease of around 9.24^oC is observed in case of 1% (w/v) alumina containing gel phantoms.

When a comparison of thermal history is made between 0.2% (w/v), 1% (w/v) and 1% (w/v) alumina containing gel phantom (Figure 5.8(a)-(d)), the temperature profile obtained after cryosurgery for 1% alumina containing gel phantom at each thermocouple is marginally lower than the 0.2% (w/v) and 2% (w/v) alumina containing gel phantom. The reason for this is the marginlly higher thermal conductivity of the 1% alumina gel phantom in comparison to the 0.2% (w/v) and 2% (w/v) alumina conisting gel phantoms (Table 5.2). Therefore, from this section of the study, it is clear that the introduction of alumina in the gel phantoms results in rapid freezing leading to proper diffusion of cooling to farther locations during crysourgery freezing in comparison to the agarose gel phantoms. It is also observed that 1% (w/v) alumina containing gel phantom has a better thermal conductivity and attains lower end temperature after cryosurgery, therefore, for further parametric studies carried out in this study, this alumina concentration is utilsed during gel phantom preparation.

5.3.6 Variation of insertion depth (id) during cryosurgery of alumina containing gel phantoms

Earlier, in the case of variation of alumina in gel phantoms, the insertion depth (id) of the cryoprobe used was 1 cm (Figure 5.8). Further, the results also revealed that 1% (w/v) alumina gels experience a higher temperature drop as compared to 0.2% (w/v) and 2% (w/v) alumina gels. However, for studying the role of insertion depth of the cryoprobe, it is varied from 1 to 1.25 cm and subsequently to 1.5 cm, keeping the alumina concentration constant at 1% (w/v). Figure 5.9(a) represents the temperature distribution at probe in case of 1% (w/v) alumina gel with variation depth from 1 cm to 1.5 cm.

From these results, it is interesting to observe that the end temperature at the probe reduces by 22.6% as the insertion depth is increased from 1 cm to 1.25 cm. Further, a similar

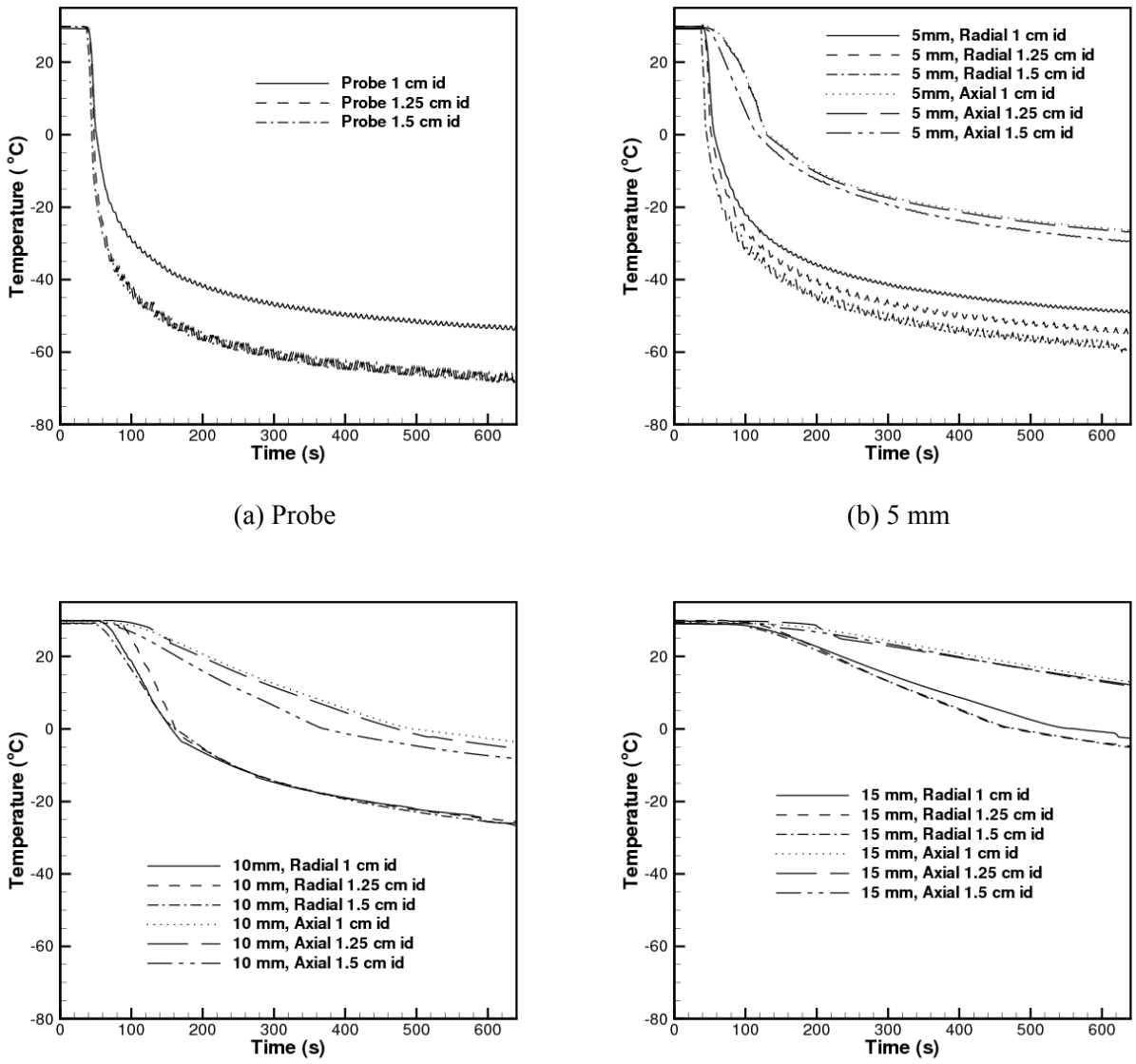

(a) Probe

(b) 5 mm

(c) 10 mm

(d) 15 mm

Figure 5.9: Variation of freezing due to change in insertion depth in agarose-alumina containing gels during cryosurgery

kind of reduction in the end temperature (in the order of 21.2%) is seen when the insertion depth is varied from 1 cm to 1.5 cm. As one moves farther away from the probe radially, it is noticed that in comparison to the insertion depth of 1 cm, the end temperature in these alumina gel phantoms after cryosurgery decreases by 9.4% and 16.6% when the insertion depth is 1.25 cm and 1.5 cm respectively (Figure 5.9(b)). The reason for the significant temperature reduction at the probe and 5 mm radially placed thermocouple is the presence of a higher thermal gradient. Since the probe is cylindrical, the a higher radial surface presents a larger thermal gradient in the radial direction as compared to the axial one. This lesser axial cooling can be verified if one keenly observes the axial thermal history. Even if there is an increase in the insertion depth to 1.25 cm and 1.5 cm, the temperature decrease is found to be 1.8% and 10.5% respectively. This clearly states that as the insertion depth is increased from 1 cm to 1.5 cm, there is a reduction in the end temperature. However, the radial temperature decrease is higher in comparison to the axial one owing to the higher surface area of cooling as stated earlier.

It is natural for this freezing process to achieve steady state after few minutes of cooling as liquid nitrogen is providing a constant cooling at temperature of -196^oC (i.e. probe). For a fixed cooling power, any biological material that has a finite thermal conductivity like this gel phantom allows a particular amount of heat to flow or diffuse inside the gel. Therefore, after a particular distance in the gel phantom heat does not diffuse and there is very meager difference in the thermal history measurements at different thermocouples. In this case, it is evident that the thermocouples at 10 mm, 15 mm radial and axial locations show a marginal decrease in temperature even with the increase in the insertion depth unlike the regions (probe and 5 mm) that receive a higher gradient as discussed earlier. For example, in case of 10 mm and 15 mm radially placed thermocouple, for an insertion depth of 1 cm, the end temperature obtained is found to be -25.98^oC and -2.5^oC. Even with the increase in insertion depth to 1.5 cm, the temperature values at 10 mm and 15 mm thermocouples are determined to be -27.32^oC and -4.98^oC respectively (Figure 5.9(c)-(d)) indicating a mild decrement in temperature.

The ice ball images clearly suggest the effect of the increase in insertion depth (Figure 5.10). Since the probe is inserted deeper into the gel phantom, the ice ball formed in case of a higher insertion depth is larger axially. Figure 5.10(a) and (b) show that the axial depth of the ice ball obtained after freezing 1% alumina gel phantom with an insertion depth of 1 cm is found to be 16 mm and its radial spread is also 16 mm. It is observed that as the insertion depth is increased to 1.25 cm, there is an increment in the ice ball axial depth and it is determined to be 19 mm. This is understandable from the fact that there is an increment of 0.25 cm (2.5 mm) axial penetration with the increase in depth of the cryoprobe which results in the larger axial ice ball (3 mm larger), changing its shape from a hemispherical profile to a slightly elliptical one. Thus, showing that this approach is beneficial in cases where more axial penetration is required while keeping the concentration of alumina same

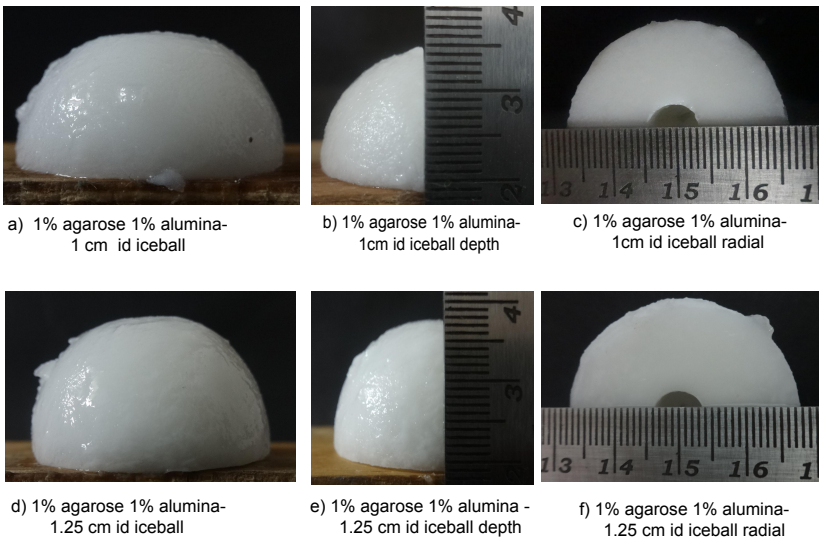

(a) Images obtained through a digital camera (SONY, WX80)

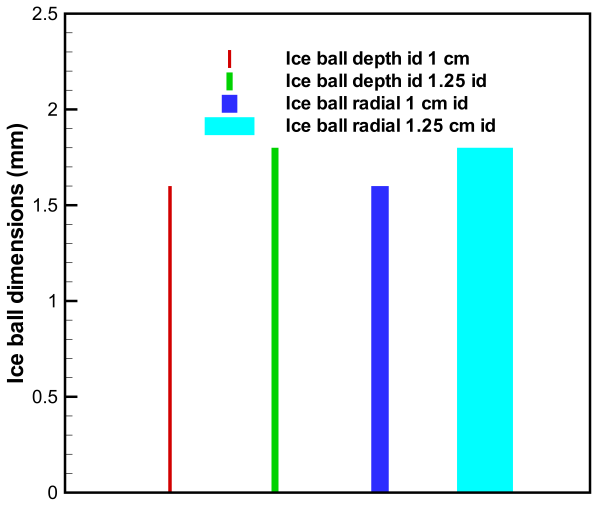

(b) Bar graph showing the dimensions of the ice ball

Figure 5.10: Changes in ice ball shape due to insertion depth

in the gel phantom.

5.3.7 Combinative approach using alumina as adjuvant and perfluorohexane layer as barrier

The major drawback during cryosurgery is the destruction to the healthy tissue surrounding the tumour. To improve the efficacy of this technique, limiting the ice formation to the desired region while increasing the rate of ablation inside the tumour is necessary. In the same context, this study proposes a combinative approach that involves the increment in freezing inside the gel phantoms while minimising the gel freezing by using an insulating layer of perfluorohexane (perfluorocarbon) solution at the gel boundary. This strategy has two benefits: a) the alumina in the gel phantoms results in increased freezing, and b) the perfluorohexane layer at the gel interface insulates and acts as a barrier to freezing during cryosurgery. To verify the effectiveness of the perfluorohexane solution layer (0.091 W/mK) in insulating the gel, cooling of alumina gels is carried out by varying the insertion depth of the cryoprobe in presence of perfluorohexane layer. Immediately after the 5 mm axially placed thermocouple, a cuboidal cavity is present in the gel. Within this cuboidal cavity, perfluorohexane (liquid) is filled and the 10 mm and 15 mm axial thermocouples are placed. When cryosurgery is performed on 1% (w/v) alumina consisting gels in presence of the perfluorohexane layer as a barrier at an insertion depth of 1 cm, it is fascinating to note that the 10 mm and 15 mm axially located thermocouples that lie in the perfluorohexane layer show an end temperature of 24.82^oC and 26.22^oC respectively (Figure 5.11(a)). This clearly points out the role that perfluorohexane layer plays in acting as a barrier to gel cooling. Also, the thermocouple located axially at 5 mm that lies in the gel phantom experiences an end temperature of -25.48^oC. This temperature measurement is similar to the one obtained while freezing 1% (w/v) alumina containing gels (Figure 5.8(c)), thus, suggesting the enhanced freezing in the gel phantom as seen earlier.

Similar results are obtained with further increase in insertion depth to 1.25 cm during cryosurgery in the presence of perfluorohexane layer at the gel interface. The axial temperature measurements demonstrate a significant trend; even with the increment in insertion depth to 1.25 cm, the axial thermocouples placed at a location 10 mm and 15 mm attain a temperature of 24.51^oC and 25.83^oC respectively. Without the layer, temperature at the same 10 mm and 15 mm axial location is found to be -5.47^oC and 12.18^oC respectively (Figure 5.9(c)-(d)). This again reiterates the fact that perfluorohexane solution is able to insulate the gel. Similar inference can also be drawn for gel cooling results with insertion depth of 1.5 cm in presence of the perfluorohexane layer (Figure 5.11(c)). Hence, this particular section of the study advocates that even with alumina as an adjuvant that results in enhanced freezing, insulation to the gel interface can be achieved during cryosurgery by the use of perfluorohexane layer as a barrier, thus, providing a new approach which

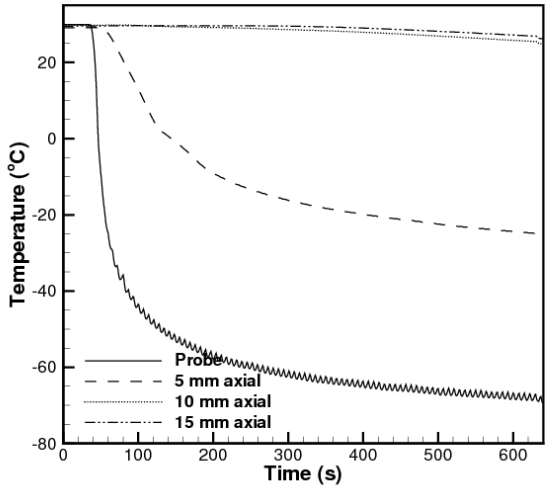

(a) Perfluorohexane layer with 1 cm id

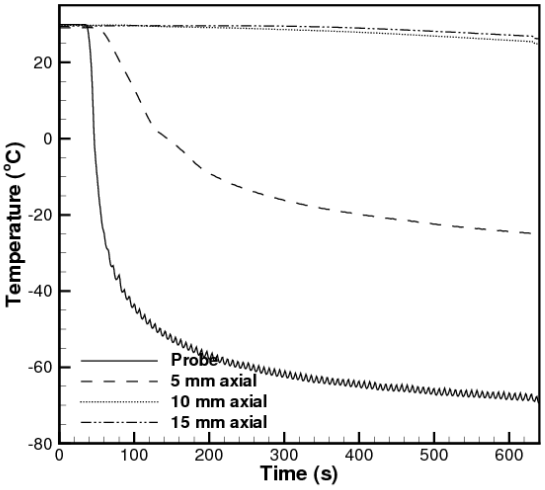

(b) Perfluorohexane layer with 1.25 cm id

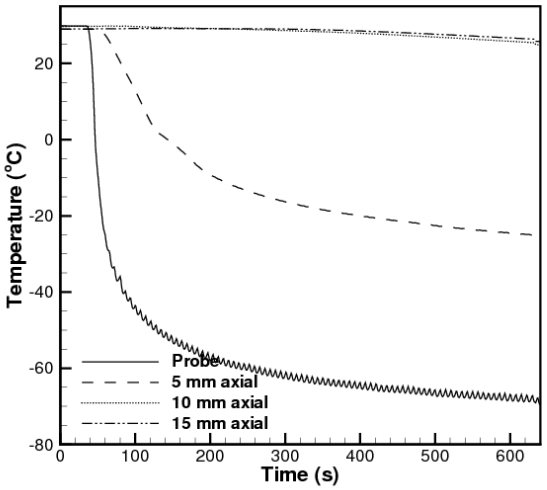

(c) Perfluorohexane layer with 1.5 cm id

Figure 5.11: Effect of perfluorohexane insulation layer with variation in insertion depth during cryosurgery

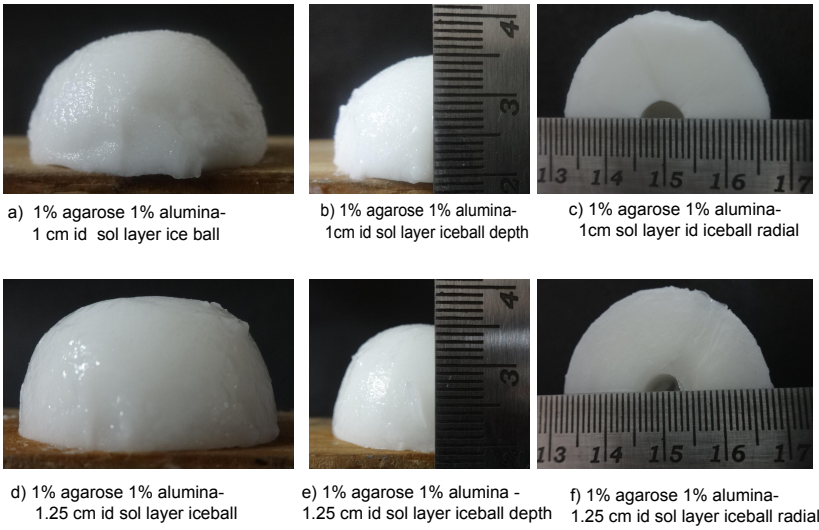

(a) Images captured through a digital camera (SONY, WX80)

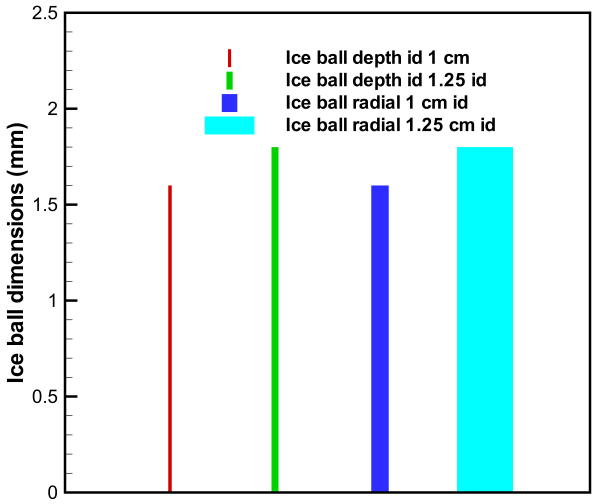

(b) Bar graph showing the dimensions of the ice ball

Figure 5.12: Change in ice ball shape in presence of perfluorohexane layer and increasing insertion depth

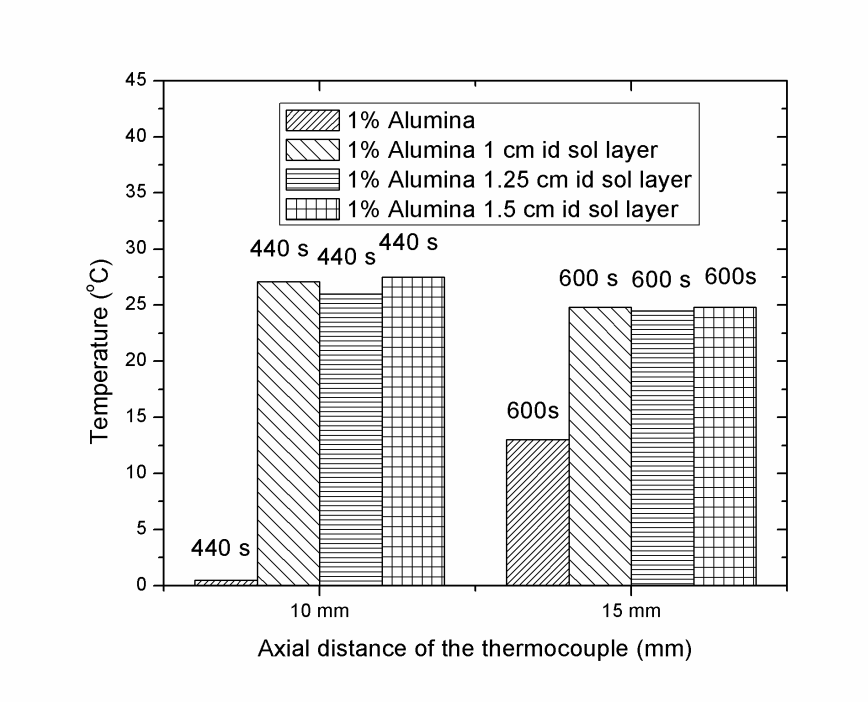

Figure 5.13: Distance travelled and time taken by the fronts with and without perfluorohexane layer

improves the efficacy of cryosurgery immensely. The comparison of the ice ball images with an insertion depth of 1 cm and 1.25 cm in presence of perfluorohexane layer presents an interesting observation which indicates that the axial depth of ice ball is similar in both cases (i.e 15 mm) in spite of the increase in depth of the cryoprobe (Figure 5.12(a) and (b)). In the previous section, it was observed that the ice ball had an axial depth of 16 mm and 19 mm for an insertion depth of 1 cm and 1.25 cm respectively. This is obvious as the low thermal conductivity perfluorohexane layer limits the ice to the desired region as seen earlier from the temperature profile. In conclusion, it is interesting to note that the visual observation of ice shape and size corroborates with the temperature distribution of the alumina containing gel phantoms while being cooled in presence of the this layer.

A deeper analysis of thermal history helps in understanding the distance covered by various fronts at different time intervals. In the same context, figure 5.13 illustrates the difference in distance covered by the isotherms in the alumina containing gels in absence and presence of perfluorohexane solution layer. It can be seen that in case of alumina gels, the freezing front (0^oC isotherm) reaches the axial thermocouple at 10 mm in 440 s while in case of perfluorohexane layer at the same location and time point, the temperature is found to be between $25^oC - 26^oC$. After 600 s of cryosurgery, the temperature in the alumina gels is 13^oC while it is interesting to note that the thermocouples in the perfluorohexane solution experience a temperature of 25^oC. Thus, suggesting that perfluorohexane can be used to inhibit ice formation and limit freezing to a specific location which of great practical significance inside the biological systems.

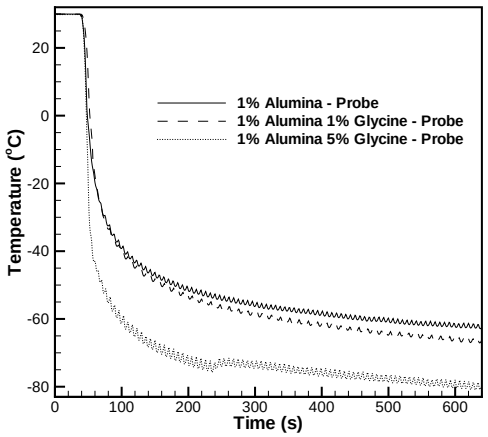

(a) Probe

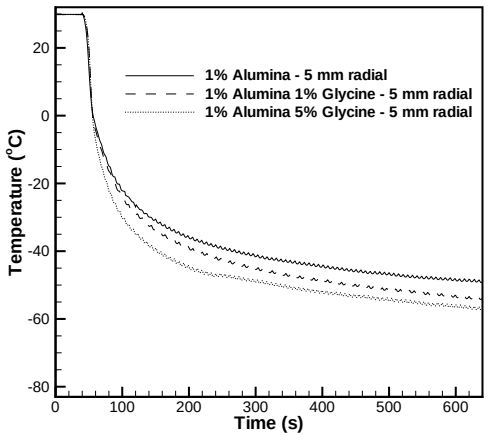

(b) 5 mm radial

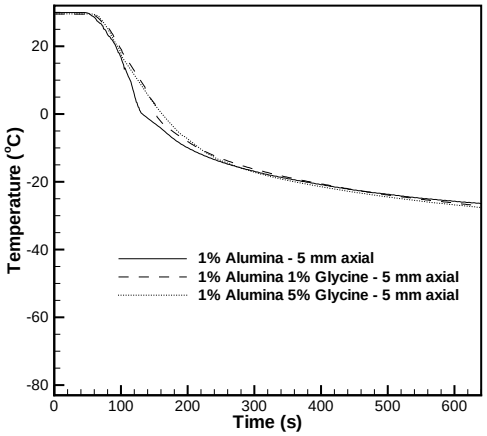

(d) 5 mm axial

Figure 5.14: Role of glycine in increasing the freezing of alumina gels during cryosurgery

5.3.8 Glycine-Alumina adjuvant strategy for improving the effectiveness of cryosurgery

Till date, adjuvants that have been formulated that are either thermophysical or eutectic. However, the synthesis of glycine-alumina emulsions results in the formation of gel phantoms that lead to faster diffusion of cooling due to alumina and the presence of eutectic glycine reduces the end temperature even further during cryosurgery. In earlier section of this study, it has been reported that the addition of alumina increases the rate of cooling inside the gel phantoms. This study further reports that eutectic adjuvant glycine in presence of alumina decreases the end temperature even more drastically when compared to alumina containing gel phantoms, thereby, improving the effectiveness of the cryosurgery process significantly.

After adding 1% (w/v) agarose to the glycine alumina emulsion, glycine- alumina

containing gel phantoms are formed. When a comparison is carried out between the temperature distribution of 1%(w/v) alumina, 1% (w/v) glycine 1% (w/v) alumina and 1% (w/v) alumina 5% (w/v) glycine containing gel phantoms, it is observed that after cryosurgery, the end temperature obtained at the thermocouple placed near the probe reveals a value of -62.34^oC, -66.12^oC, -79.39^oC respectively (Figure 5.14(a)). With increase in amount of glycine to 1% (w/v), as observed from the thermal history there is a marginal decrease in temperature. Further, the addition of glycine to 5% (w/v) in the gel phantoms decreases the temperature by 17.05^oC (from -62.34^oC in the alumina containing gel phantom to -79.39^oC in the 1% (w/v) alumina 5%(w/v) glycine containing gel phantom), thus, showing that the rate of decrease is substantial and causes a sharp decrement in the end temperature attained after cryosurgery.

It is also observed that the thermocouple placed at a distances of 5 mm from the probe in the radial direction shows a decrease in the end temperature of gel phantoms after cryosurgery. When a comparison is made between the thermal history of 1%(w/v) alumina, 1% (w/v) glycine 1% (w/v) alumina and 1% (w/v) alumina 5% (w/v) glycine containing gel phantoms, it is seen that the value of end temperature is found to be -49.06^oC, -53.76^oC and -56.96^oC respectively at this particlular location (Figure 5.14(b)). This shows that even at this thermocouple position, glycine influences the end temperature and decreases the temperature by 7.9^oC (from -49.06^oC to -56.96^oC). It is interesting to note the thermal history of these gel phantoms in the thermocouple placed in the 5 mm axial direction suggests a very miniscule reduction in the end temperature after cryosurgery and there is a very marginal decrease of around 1^oC after the addition of glycine (Figure 5.14(c)). The glycine incorporated gel phantoms have miniscule decrease in the end temperature in the axial direction than the alumina gel phantoms. Since the probe is cylindrical, the radial surface available for cooling is more. Thus, radially the temperature gradient is more and the effect of freezing is more pronounced than the axial one. Also, alumina results in a faster diffusion of cooling and therefore in comparison to the agarose gel phantoms there is better diffusion of cooling leading to a lower end temperature. However, in a combinative system where both alumina and glycine are present in the gel phantom, like the present case, there is a faster diffsion of cooling but the presence of glycine leads to lowering of end temperature in regions where there is a higher cooling rate like thermocouples placed near the probe and 5 mm radial position. There is no or miminal effect seen in the thermcocouples placed farther away from the probe. For glycine to play an important as an eutectic adjuvant, lower temperature is needed and in this particular case, therefore, it is observed that the effect of glycine in lowering the temperature is predominant at a location near the probe. From the results of this study, it can be concluded that higher concentration of glycine in the alumina gel phantoms can cause rapid freezing in a defined region, thus, providing a better outcome during cryosurgery.

Table 5.3: Transient temperature readings obtained during cryosurgery of different gel phantoms at various thermocouple locations

Gel Phantom	Time (s)	T_{Probe} (^oC)	ΔT_{Probe} (^oC)	T_{5mm} (^oC)	ΔT_{5mm} (^oC)
1% (w/v) agarose	0	29.13	58.18	29.95	43.55
	60	-29.05	9.25	-13.6	10.34
	120	-38.3	4.98	-23.94	5.37
	180	-43.28	3.29	-29.31	3.78
	240	-46.57	1.3	-33.09	2.11
	300	-47.87	1.27	-35.02	1.69
	360	-49.14	1.12	-36.89	1.21
1% (w/v) alumina	0	29.47	68.64	29.47	51.49
	60	-39.17	9.42	-22.02	10.46
	120	-48.59	3.56	-32.48	4.54
	180	-52.15	3.11	-37.02	3.7
	240	-55.26	2.1	-40.72	2.23
	300	-57.36	1.09	-42.95	1.42
	360	-58.45	2.01	-44.37	1.87
1% (w/v) alumina 5% (w/v) glycine	0	29.73	90.86	29.82	58.96
	60	-61.13	8.96	-29.14	11.58
	120	-70.09	3.07	-40.72	4.9
	180	-73.16	0.03	-45.62	2.95
	240	-73.19	2.38	-48.57	1.76
	300	-75.57	0.14	-50.33	1.29
	360	-76.61	0.96	-51.62	0.47

5.3.9 Comparison of temperature distribution in agarose gel phantoms, alumina containing gel and alumina-glycine consisting gel phantoms

The comparison of thermal history of agarose gel phantoms, alumina consisting gels and glycine-alumina consisting gels for the first 6 minutes of cooling using cryosurgery helps in a better understanding of the role played by adjuvants in increased freezing (after 6 minutes of freezing, there is no drastic change in the thermal gradient with respect to time as seen from the temperature profile of these gel phantoms experimentally). For simplicity and ease of explanation, the temperature measurements of probe and 5 mm radially placed thermocouples are only taken into consideration. Table 5.3 shows the temperature values

obtained during cryosurgery for 6 minutes. In table 5.3, T_{probe} represents the temperature at the probe and $\triangle T_{probe}$ indicates the difference between the consecutive temperature measurements at the probe. Similarly, T_{5mm} presents the temperature measurement at a radial distance of 5 mm and $\triangle T_{5mm}$ suggest the temperature gradient at the same distance. For 1% agarose gel phantoms (Table 5.3) after 60 s, a steep temperature gradient ($\triangle T_{probe}$ and $\triangle T_{5mm}$) of 58.18^oC and 29.95^oC is observed at the probe and a radial location of 5 mm. Further, this temperature gradient reduces to 1.12^oC and 1.21^oC after 360 s at the previously mentioned thermocouple positions. With the incorporation of alumina (1% (w/v) alumina) in the agarose gel phantom, a substantial temperature gradient is observed from the temperature measurements (Table 5.3).

The temperature gradient evident at the probe and a radial location of 5 mm is 68.64^oC and 51.49^oC respectively. This again reiterates that incorporation of alumina results in increased freezing of gel phantom. The increment in freezing can also be seen when a comparison is made between temperature measurements for agarose and alumina gel phantoms after 360 s of freezing (Table 5.3). The addition of glycine to the alumina gel phantoms results in the eutectic freezing in cryosurgery and also points out the usefulness of combined thermal-eutectic adjuvants in lowering the temperature. In the presence of glycine, after 60 s, a drastic temperature gradient ($\triangle T_{probe}$ and $\triangle T_{5mm}$) of 90.86^oC and 58.96^oC is found at the probe and a radial thermocouple position of 5 mm. Also, the temperature readings after 360 s of freezing indicate a value of -76.61^oC and -51.62^oC. When compared to both alumina and agarose gel phantoms, glycine added gel phantoms show an enhanced freezing as clearly seen from the lower temperature values obtained after cryosurgery (Table 5.3). Therefore, the results from this part of the study suggest that the adjuvants added in the gel phantoms lower the temperature substantially, thus, enhancing the freezing during cryosurgery.

After cryosurgery, a noteworthy observation can be made, it is very important to note that the ice ball size is different in gel phantoms for various cases studied above. In order to have a qualitative understanding of the shape and size of ice ball formed, immediately after cryosurgery for 10 minutes, the ice ball is carefully removed from the gel phantom. The ice ball is then imaged with a digital camera to calculate the depth (z axis, axially) and radial spread (x axis). Figure 5.15 shows the ice ball obtained after cryosurgery for various cases ((a)-(c) Ice ball of 1% (w/v) agarose (insertion depth of 1 cm), (d)-(f) 1% (w/v) alumina (insertion depth 1 cm), (g)-(i) 1% (w/v) alumina with insertion depth of 1.5 cm, (j)-(l) 1% (w/v) alumina insertion depth of 1.5 cm with perfluorohexane layer, (m)-(o) 1% (w/v) alumina- 5% (w/v) glycine (insertion depth 1 cm)).

Further, the ice ball weight and the dimensional measurements are carried out with the help of a weighing balance and steel ruler (Table 5.4). Figure 5.15(a) represents the complete shape of the ice ball, (b) depth of the ice ball and (c) the radial spread of the ice ball after cryosurgery. The ice ball obtained for 1% (w/v) agarose gel phantom has a radial and axial

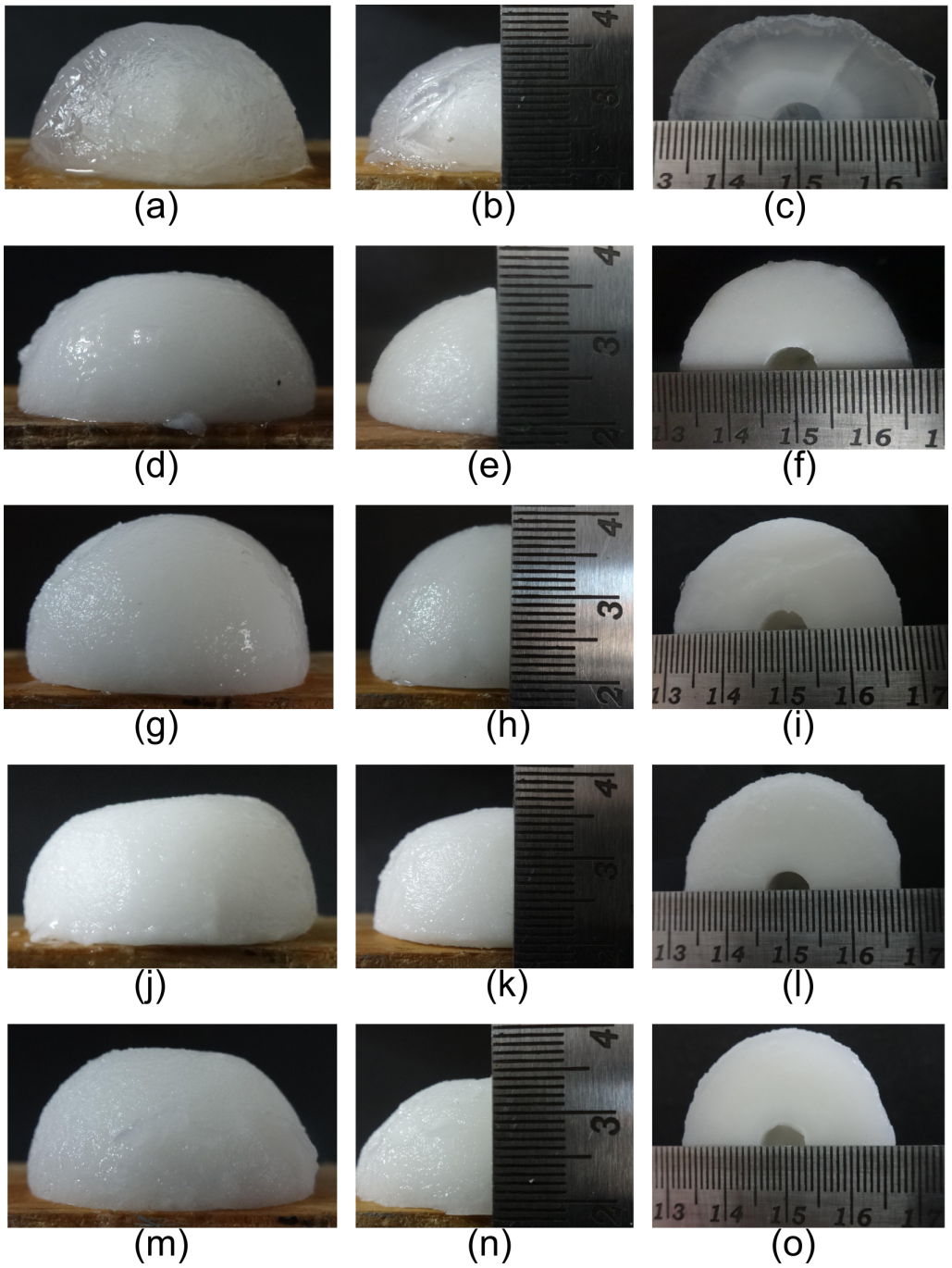

Figure 5.15: Comparison of ice ball images after cryosurgery of gel phantoms for various cases (obtained through a digital camera (SONY WX 80))

spread of 1.7 cm and 1.6 cm respectively (Figure 5.15(a)-(c)) and the weight of the ice ball is found to be 9.80 g (Table 5.4). When the adjuvant gel phantom consisting of alumina is frozen using cryosurgery, the freezing results in radial and axial spread of 1.7 cm and 1.6 cm respectively. The addition of alumina makes the ice ball look white in appearance while the ice ball obtained in the previous case is translucent (Figure 5.15(d)-(f)). It is seen that with the addition of alumina, the weight of the ice ball is 11.50 g. This is understood as the gel phantom which was earlier devoid of alumina as an adjuvant now has alumina particles in

Table 5.4: Measurement of dimensions and determination of weight of ice ball obtained after cryosurgery

Iceball	Depth (r_z, in cm)	Radial (r_x, in cm)	Weight (g)
1% (w/v) agarose	1.6	1.7	9.8
1% (w/v) alumina	1.6	1.7	11.5
1% (w/v) alumina 1.5 cm id	2.0	1.8	16.9
1% (w/v) alumina 1.5 cm id perfluorocarbon layer	1.5	1.7	13.3
1% (w/v) alumina 5% (w/v) glycine	1.6	1.7	12.8

its matrix.

A key inference can be drawn with the increase in insertion depth to 1.5 cm; it is observed that the ice ball has a axial spread of 2.0 cm while the radial length is 1.8 cm (Figure 5.15(g)-(i)). It is quite clear as stated earlier that increase in insertion depth amounts to higher surface area of cooling by the cryoprobe. Therefore, the ice ball is larger in size and this can also be seen in terms of weight of the ice ball as it weighs 16.90 g (Table 5.4). The ice ball in case of insertion depth of 1.5 cm with perfluorohexane solution as a barrier to gel cooling reveals a very significant observation; it is seen that the ice ball formed is smaller in size in comparison to the previous case (Figure 5.15(j)-(l) and Figure 5.15(g)-(i)). The ice ball has a radial and axial length of 1.7 cm and 1.5 cm respectively (Figure 5.15(j)-(l)). The axial length with insertion depth and perfluorohexane layer is lesser than the ice ball axial measurement (i.e 2.0 cm) obtained in case of insertion depth without perfluorohexane layer. It is quite interesting to observe that the ice ball axial length in presence of perfluorohexane solution is 0.5 cm (or 5 mm) lesser in comparison to the case where perfluorohexane layer is absent. Also, since the perfluorohexane layer is present after an axial distance of 5 mm from the probe, radially, all thermocouples are inside the gel, therefore, the ice ball obtained has a similar length in the radial direction (1.7 cm). These results corroborate with the findings of temperature distribution of gel phantoms and clearly indicate that perfluorohexane layer is able to insulate the gel phantom.

Another important objective of this study is to suggest the use of combined glycine-alumina adjuvant as that leads to increased freezing in the gel phantoms. It can be seen that the ice ball obtained in glycine alumina gel phantom (5% (w/v) glycine 1% (w/v) alumina) has a radial and axial length of 1.7 cm and 1.6 cm respectively (Figure 5.15(m)-(o)). This is similar to the measurements of ice ball found in alumina gel phantoms and agarose gel phantoms (Figure 5.15(a)-(c) and Figure 5.15(d)-(f)). Hence, this study provides the images of ice ball that indicate its shape, size and appearance in various cases of cryosurgical

cooling. Therefore, this work would enable the surgeons with a better idea of the zone of freezing after cryosurgery and would also suggest different methods that can be utilised for the improvement of cryosurgery process.

5.4 Summary

In conclusion, the results obtained in the study reveal that the addition of glycine in a higher concentration (5% (w/v)) results in considerable temperature decrease at various thermocouple locations in the gel phantoms. This study also suggests that perfluorohexane solution layer insulates the glycine gel effectively during cryosurgical cooling. Due to this insulation, the ice ball formed has a depth of 13 mm, i.e. 3 mm lesser than the normal ice ball observed after cryosurgery of glycine consisting gel phantom. It can also be concluded that 1% (w/v) alumina gel phantoms possess superior thermophysical properties that makes it useful as an adjuvant that enhances the freezing inside the gel phantoms. Therefore, heat diffuses in a better way in these gel phantoms leading to achievement of lower end temperature after cryosurgery. It is fascinating to observe that with the increase in insertion depth of the cryoprobe in the alumina gel phantoms (from 1 cm to 1.25 cm and further to 1.5 cm), there is a decrease in temperature at each thermocouple location in the gel phantom. This is understood from the fact that higher surface area of the probe results in more cooling. This study also proposes a novel concept that suggests cooling of 1% (w/v) alumina gel phantom in presence of perfluorohexane layer as a barrier. It is quite clearly evident that in presence of a barrier of perfluorhexane solution, the axial temperature measurement at the thermocouple placed at 10 mm indicates a value of 25^oC while in its absence (alumina gel phantom without layer) at the same location the temperature is found to be -5.47^oC (Figure 5.9(c)). It is interesting to note that the axial depth of ice ball is also reduced from 2 cm to 1.5 cm owing to the perfluorohexane insulation at the gel interface (Figure5.15(g)-(i) and Figure 5.15(j)-(l)). In this chapter, another new strategy has been proposed that advocates the use of a combined thermo-eutectic adjuvant (glycine-alumina gel phantom) in lowering the end temperature after cryosurgery. Alumina helps in faster diffusion of cooling and glycine induces eutectic freezing lowering the end temperature further. After cryosurgery of glycine-alumina containing gel phantoms (5% (w/v) glycine 1% (w/v) alumina), it is noticed that a substantial temperature decrease is visible at the probe and thermocouple located at a radial and axial position of 5 mm. In conclusion, this study demonstrates the use of new methods to improve the cryosurgery in tissue mimicking gel phantoms (gel phantoms that mimick the thermophysical property of tissue). In near future, these studies can be extended into in-vivo animal models so that the proposed approaches become a routine clinical practice in cryosurgical tumour ablation. Hence, this study presents a novel combinative approach that focuses on maximising freezing inside the gel phantom using glycine and alumina and limits the freezing to a desired region by using an insulating perfluorohexane layer at the gel

interface, thereby, improving the efficacy of cryosurgery significantly.

Chapter 6

Conclusion

One of the major drawbacks faced by the surgeons while performing cryosurgery is the inability to monitor freezing which leads to destruction of the healthy tissue surrounding the tumour. This problem can be solved if the cooling can be restricted to a particular region. In the same context, this thesis presents new approaches through which the cooling can be enhanced and at the same time be restricted to a particular region. In this thesis, a numerical study is carried out to study the freezing process during cryosurgery of tumour in presence of a perfluorocarbon (liquid) layer. During the presence of this perfluorocarbon layer, the time taken to achieve lethal temperature is lesser and lethal front reaches the tumour boundary quickly. However, in the absence of this layer, the time taken for ablation is more and the chances of destruction to the healthy tissue neigbouring the tumour is higher. For a particular configuration, there exists an offset that provides uniform cooling to the entire volume of tissue, this offset which is termed as optimal offset decreases linearly with an increase in the active length for a given radius of the tumour. For every 2.5 mm increase in the tumour radius with same active length of the cryoprobe, the time taken for complete ablation by the larger tumour is nearly 2.7 times the time taken by the smaller one. It is also observed that the most suitable substance required for making this insulating layer is perfluorohexane and the optimal thickness of this layer is found to be 1 mm. Emulsion systems of perfluorocarbon (perfluorohexane and perfluorodecalin) have been synthesised and perfluorodecalin emulsions made with Span 20 seem to possess lower thermal conductivity and are found suitable for application in cryosurgery. It is also observed that in presence of a low thermal conductivity emulsion (90% (w/v)), the freezing front is not able to penetrate the gel-emulsion interface. Normally, in the absence of emulsion layer, the temperature is found to be -4^oC at a 10 mm axially placed thermocouple (from probe), while with the use of this emulsion, the temperature at the same location is found to be 11^oC. From this part of the study, it can be concluded that highly concentrated perfluorocarbon emulsion can be used as an insulating layer during cryosurgery of gel phantoms.

This thesis also suggests the use of adjuvants to enhance the freezing in a particular region and the use of perfluorocarbon layer to confine the cooling to a defined region during cryosurgery of gel phantoms. From the results, it can be concluded that the addition

of glycine in a higher concentration (5% (w/v)) to the gel phantoms causes considerable temperature decrease at all thermocouple locations. In addition, this study indicates that perfluorohexane layer insulates the glycine containing gel phantom effectively during cryosurgery. Due to this insulation, the ice ball formed has a depth that is lesser than the normal ice ball. It can also be concluded that 1% (w/v) alumina gel phantoms possess superior thermophysical properties. This makes it useful for being used as an adjuvant that enhances the freezing inside the gel phantoms. It is fascinating to observe that with the increase in insertion depth of the cryoprobe in the alumina containing gel phantoms, there is a decrease in temperature at each thermocouple. To verify the effectiveness of perfluorohexane as an insulating layer, 1% (w/v) alumina gel phantom is cooled using cryosurgery. It is quite clearly evident that in presence of perfluorohexane (perfluorocarbon) layer, the axial temperature measurement at the thermocouple placed at 10 mm indicates a value of 25^oC, while in its absence (alumina gel phantom without layer) at the same location the temperature is found to be -5.47^oC. The axial depth of ice ball is also reduced by 5 mm due to this insulating layer. Furthermore, after cryosurgery of glycine-alumina containing gel phantoms (5% (w/v) glycine 1% (w/v) alumina), it is noticed that a substantial temperature decrease is visible at the probe and thermocouple located at a radial and axial position of 5 mm. In conclusion, this thesis demonstrates the use of new approaches to improve the cryosurgery process by enhancing the freezing and confining it to particular region through the use of various strategies mentioned above, thus, providing ways to improve the cryosurgical outcome.

Scope for Further Research

In near future, these studies can be extended into in-vivo animal models so that the proposed concept of perfluorohexane (perfluorocarbon) layer of low thermal conductivity can be used along the tumour boundary. This would eventually lead to cryosurgery becoming a routine clinical practice for tumour ablation. The maintenance of the perfluorohexane layer along the tumour boundary is a challenge. Therefore, studies have to be carried out for developing methods for maintaining the layer at the tumour boundary using specific reactions in mice models so that this study can move on to its next phase, i.e. experimental human trials culminating in clinical practice.

References

[1] B. Rubinsky, Cryosurgery, Annual Review of Bioemdical Engineering 02 (2000) 157–187.

[2] E.G. Kuflik, A.A.Gage, Cryosurgical Treatment for Skin Cancer, IGAKU-SHOIN Medical Publishers, New York, 1990.

[3] B.A. Mascarenhas, T.S. Ravikumar, Experimental basis for hepatic cryotherapy, Seminars in Surgical Oncology 14 (2) (1998) 110–115.

[4] A. Zhang, L.X. Xu, G.A. Sandison, J. Zhang, A microscale model for prediction of breast cancer cell damage during cryosurgery, Cryobiology 47 (2) (2003) 143–154.

[5] J. Zhang, G. Sandison, A. George, J.Y. Murthy, L.X. Xu, Numerical simulation for heat transfer in prostate cancer cryosurgery, Journal of Biomechanical Engineering, ASME 127 (2) (2005) 279–294.

[6] J. Baust, A.A. Gage, H. Ma, C.M. Zhang, Minimally invasive cryosurgery-technical advances, Cryobiology 34 (4) (1997) 373–384.

[7] T.E. Cooper, W.K. Petrovic, An experimental investigation of the temperature field produced by a cryosurgical cannula, Journal of Heat Transfer 96 (3) (1974) 415–420.

[8] A. Sguazzi, D. Bracco, A historical account of the technical means used in cryotherapy, Minerva Medica 65 (70) (1974) 3718–3722.

[9] D.C Schechter, I.A. Sarot, Historical accounts of injuries due to cold, Surgery 63 (3) (1968) 527–535.

[10] J.B. Arnott, On treatment of cancer by the regulated application of an anaesthetic temperature, Churchill, 1851.

[11] R.F. Barron, Cryogenic Systems, Oxford University Press, New York, 1985.

[12] C.A. White, Liquid air: Its application in medicine and surgery, Medication Reconciliation 56 (1899) 109–112.

[13] H. Irvine, D. Turnacliff, Liquid oxygen in dermatology, Arch. Dermatol. Syphilol 19 (2) (1929) 270–280.

[14] H. Allington, Liquid nitrogen in the treatment of skin diseases, California Medicine 72 (3) (1950) 153–155.

[15] I.S. Cooper, A. Lee, Cryostatic congelation: a system for producing a limited controlled region of cooling or freezing of biological tissues, The Journal of Nervous and Mental Disease 133 (1961) 259–263.

[16] R.W. Rand, A.M. Dashe, D.E. Paglia, L.W. Conway, D.H. Solomon, Stereotactic cryo-hypophysectomy, The Journal of the American Medical Association 189 (1964) 255–259.

[17] R. Marcover, T. Miller, The treatment of primary and metastatic bone tumors by cryosurgery, The Surgical Clinics of North America 49 (2) (1969) 421–430.

[18] D. Torre, Cutaneous cryosurgery, New York State Journal of Medicine 70 (1970) 2551–2554.

[19] S. Zacarian, M. Adham, Cryotherapy of cutaneous malignancy, Cryobiology 2 (4) (1966) 212–218.

[20] W. Cahan, Cryosurgery of the uterus: description of techniques and potential applications, American Journal of Obstetrics & Gynecology 88 (1964) 410–414.

[21] S.A. Zacarian, Cryo Corner: Is Lateral Spread of Freeze a Valid Guide to Depth of Freeze?, The Journal of Dermatologic Surgery & Oncology 4 (1978) 561–563.

[22] P.J.L. Pivert, P. Binder, T. Ougier, Measurement of intratissue bioelectrical low frequency impedance: a new method to predict per-operatively the destructive effect of cryosurgery, Cryobiology 14 (2) (1977) 245–250.

[23] R.B. Pappenfmort, Semicircular thermocouple needle depth gauge for cryoprocedure, Cutis 27 (6) (1981) 605–608.

[24] G.M. Onik, J.K. Cohen, G.D. Reyes, B.Rubinsky, Z. Chang, J. Baust, Transrectal ultrasound-guided percutaneous radical cryosurgical ablation of the prostate, Cancer 72 (4) (1993) 1291–9.

[25] B. Rubinsky, J.C. Gilbert , G.M. Onik, M.S. Roos, S.T. Wong, K.M. Brennan, Monitoring cryosurgery in the brain and in the prostate with proton nmr, Cryobiology 30 (2) (1993) 191–199.

[26] G.M. Onik, C. Cooper, H.I. Goldberg, A.A. Moss, B. Rubinsky, M. Christianson, Ultrasonic chracteristics of frozen liver, Cryobiology 21 (3) (1984) 321–328.

[27] P.R. Morrison, S.G. Silverman, K. Tuncali, S. Tatli, Mri guided cryotherapy, Journal of Magnetic Resonance Imaging 27 (2) (2008) 410–420.

[28] R.P. Usatine, D.L. Stulberg, G.B. Colver, Cutaneous Cryosurgery, CRC Press, New York, 2005.

[29] S. Zacarian, M. Adham, Cryogenic temperature studies of human skin: Temperature recordings at 2 mm human skin depth following application with liquid nitrogen, Journal of Invasive Dermatology 48 (1) (1967) 7–10.

[30] H. Whitehouse, Liquid air in dermatology: its indications and limitations, JAMA 49 (5) (1907) 371–377.

[31] S. Zacarian, Cryosurgery of Skin Cancer, Charles C. Thomas, Springfield, IL, 1969.

[32] G. Onik, Cryosurgery, Critical Reviews in Oncology/Hematology 23 (1996) 1–24.

[33] A.A. Gage, Current issues in cryosurgery, Cryobiology 19 (3) (1982) 219–222.

[34] A.A. Gage, J. Baust, Mechanism of tissue injury in cryosurgery, Cryobiology 37 (3) (1998) 171–186.

[35] R. Chambers, H.P. Hale, The formation of ice in protoplasm, Proceedings of the Royal Society of London. Series B, Biological Sciences 110 (1932) 336–352.

[36] C.H Koonz, J.M. Ramsbottom, Influence of freezing on color of bones and adjacent tissues, Food Research 12 (5) (1939) 393–409.

[37] J.S. Hong, B. Rubinsky, Patterns of ice formation in normal and malignant breast tissue, Cryobiology 31 (2) (1994) 109–120.

[38] J.C. Bischof, K. Christov, B. Rubinsky, A morphological study of cooling rate response in normal and neoplastic human liver tissue: cryosurgical implications, Cryobiology 30 (5) (1993) 482–492.

[39] P. Mazur, Physical factors implicated in the death of micro-organisms at subzero temperatures, Annals New York Academy of Sciences 85 (2) (1960) 610–628.

[40] P. Mazur, Cryobiology: The freezing of biological systems, Science 168 (3934) (1970) 939–949.

[41] P. Mazur, Freezing of living cells: mechanisms and implications, American Journal of Physiology 247 (3) (1984) C125–C142.

[42] P. Mazur, S.P. Leibo, E.H.Y Chu, A two-factor hypothesis of freezing injury, Experimental Cell Research 71 (2) (1972) 345–355.

[43] P. Mazur, U. Schneider, Osmotic responses of preimplantation mouse and bovine embryos and their cryobiological implications, Cell Biophysics 8 (4) (1986) 259–285.

[44] P. Mazur, The role of intracellular freezing in the death of cells cooled at supraoptimal rates, Cryobiology 14 (3) (1977) 251–272.

[45] P. Mazur, Principles of Cryobiology, CRC Press, New York, 2004.

[46] B. Rubinsky, C.Y. Lee, The mechanism of freezing in biological tissue: the liver, Cryo-Letters 8 (1987) 370–381.

[47] J.C. Bischof, K. Christov, B. Rubinsky, A morphological study of cooling rate response in normal and neoplastic human liver tissue: cryosurgical implications, Cryobiology 30 (5) (1993) 482–492.

[48] N.E. Hoffmann, J.C. Bischof, The cryobiology of cryosurgical injury, Urology 60 (2) (2002) 40–49.

[49] C. Bernard, Lecons sur la chaleur animale, Bailliere, Paris, 1876.

[50] W. Berger, B. Uhrik, Freeze-induced shrinkage of individual cells and cell-to-cell propagation of intracellular ice in cell chains from salivary glands, Experientia. 52 (9) (1996) 843–850.

[51] R.M. Love, The Freezing of Animal Tissue, Academic Press, London and New York, 1966.

[52] J.C. Bischof, B. Rubinsky, Large crystals in the nucleus of rapidly frozen liver cells, Cryobiology 30 (6) (1993) 597–603.

[53] J.C. Bischof, D. Smith, P.V. Pazhayannur, C. J. Hulbert , K.P. Roberts, Cryosurgery of dunning AT-1 rat prostate tumor: thermal, biophysical and viability response at the cellular and tissue level, Cryobiology 34 (1) (1997) 42–69.

[54] A. Gagge, C.A. Winslow, L.P. Herrington, The influence of clothing on the physiological reactions of the human body to varying environmental temperatures, American Journal of Physiology 124 (1938) 30–50.

[55] J.D. Hardy, E.F. Dubois, Basal metabolism, rediation, convection and vaporization at temperatures of 22 to 35 degree celsius, The Journal of Nutrition 15 (5) (1938) 477–497.

[56] H.C. Bazett, B. McGlone, Temperature gradients in the tissues in man, American Journal of Physiology 82 (1927) 415–451.

[57] E.S. Mendelson, Measurement of the superfacial temperature gradient in man, American Journal of Physiology 114 (1936) 642–647.

[58] H.H Pennes, Analysis of tissue and arterial blood temperatures in the resting human forearm, Journal of Applied Physiology 1 (2) (1948) 93–122.

[59] S.T. Clegg, R.B. Roemer, T.C. Cetas, Estimation of complete temperature fields from measured transient temperatures, International Journal of Hyperthermia 1 (3) (1985) 265–286.

[60] C.K. Charny, M.J. Hagmann, R.L. Levin, A whole body thermal model of man during hyperthermia, IEEE Transactions on Biomedical Engineering 34 (5) (1987) 375–387.

[61] A. Shitzer, J.C. Chato, Analytical solutions to the problem of transient heat transfer in living tissue, Journal of Biomechanical Engineering, ASME 100 (4) (1978) 202–210.

[62] C.E Huckaba, H.S. Tam, R.C. Darling, J.A. Downey, Prediction of dynamic temperature distributions in the human body, AIChE Journal 21 (5) (1975) 1006–1012.

[63] C.K. Charny, Mathematical models of bioheat transfer, Advances in Heat Transfer Series 22 (1992) 19–155.

[64] R. Plank, Theories concerning the changes taking place in the cell membranes and animal flesh during refrigeration, Ice and cold storage 28 (1925) 234.

[65] T. Moran, The frozen state in mammalian muscle, Proceedings of the Royal Society B, Biological Sciences 118 (1930) 182–187.

[66] H.W. Rothenborg, Cutaneous circulation in rabbits and human before, during, and after cryosurgical procedures measured by xenon-133 clearance, Cryobiology 6 (6) (1970) 507–514.

[67] R.J. Ablin, An appreciation and realization of the concept of cryoimmunology, in Percutaneous Prostate Cryoablation, Quality Medical Publishing, Inc., St. Louis, 1995.

[68] J. Cohnheim, ”Lectures on General Pathology.” A Handbook for Practitioners and Students, The New Sydenham Society, London, 1877.

[69] G. Comini, S.D. Giudice, Thermal aspects of cryosurgery, Journal of Heat Transfer 98 (4) (1976) 543–549.

[70] H. Budman, A. Shitzer, S.D. Giudice, Investigation of temperature fields around embedded cryoprobes, Journal of Biomechanical Engineering, ASME 108 (1) (1986) 42–48.

[71] J.S. Hong, S. Wong, G. Pease, B. Rubinsky, MR imaging assisted temperature calculations during cryosurgery, Magnetic Resonance Imaging 12 (7) (1994) 1021–1031.

[72] Y. Rabin, A. Shitzer, Numerical solution of the multidimensional freezing problem during cryosurgery, Journal of Biomechanical Engineering, ASME 120 (1) (1998) 32–37.

[73] J.C. Rewcastle, G.A.Sandisonand K.Muldrew, J.C. Saliken, B.J.Donnelly, A model for the time dependent three-dimensional thermal distribution within iceballs surrounding multiple cryoprobes, Medical Physics 28 (6) (2001) 1125–1137.

[74] Z. Liu, K. Muldrew, R. Wan, J.C. Rewcastle, A finite element model for ice ball evolution in a multi-probe cryosurgery, Computer Methods in Biomechanics and Biomedical Engineering 6 (3) (2003) 197–208.

[75] A. Weill, A. Shitzer, P.B. Yoseph, Finite element analysis of the temperature field around two adjacent cryo-probes, Journal of Biomechanics 115 (4A) (1993) 374–379.

[76] D.J. Smith, R.V. Devireddy, J.C. Bischof, Prediction of thermal history and interface propagation during freezing in biological systems - latent heat and temperature-dependent property effects, Proceedings of 5th ASME/JSME Joint Thermal Engineering Conference, San Diego, California.

[77] G.A. Sandison, M.P. Loye, J.C. Rewcastle, L.J. Hahn, J.C. Saliken, J.G. Mckinnon, B. J. Donnelly, X-ray CT monitoring of iceball growth and thermal distribution during cryosurgery, Physics in Medicine and Biology 43 (11) (1998) 3309–3324.

[78] J.C. Saliken, J.G. Mckinnon, R. Gray, Computer tomography for cryotherapy monitoring, American Journal of Roentgenology 166 (1996) 853–855.

[79] G.R. Pease, B. Rubinsky, S.T. Wong, M.S. Roos, J. C. Gilbert, A. Arav, An integrated probe for magnetic resonance imaging monitored skin cryosurgery, Journal of Biomechanical Engineering, ASME 117 (1) (1995) 59–63.

[80] B.L. Daniel, K. Butts, W.F. Block, Magnetic resonance imaging for frozen tissues:temperature-dependent MR signal characteristics and relevance for MR monitoring of cryosurgery, Magnetic resonance in medicine 41 (3) (1999) 627–630.

[81] T.E. Cooper, G.K. Trezek, Rate of lesion growth around spherical and cylindrical cryoprobes, Cryobiology 7 (4-6) (1971) 183–190.

[82] Z.S. Deng, J. Liu, Numerical simulation of selective freezing of target biological tissues following injection of solutions with specific thermal properties, Cryobiology 50 (2) (2005) 183–192.

[83] M.R. Rossi, K. Shimada, D. Tanaka, Y. Rabin, Computerised planning of prostate cryosurgery using variable cryoprobe, Cryobiology 60 (1) (2010) 71–79.

[84] C. Thaokar, Y Rabin, Temperature field reconstruction for minimally invasive cryosurgery with application to wireless implantable temperature sensors and/or medical imaging, Cryobiology 65 (3) (2012) 270–277.

[85] A. Sehrawat, K. Shimada, Y. Rabin, Generating prostate models by means of geometric deformation with application to computerized training of cryosurgery, International journal of computer assisted radiology and surgery 8 (2) (2013) 301–312.

[86] C.Thaokar, M Rossi, Y Rabin, A new method for temperature-field reconstruction during ultrasound-monitored cryosurgery using potential-field analogy, Cryobiology 72 (1) (2015) 69–77.

[87] A. Sehrawat, R. Keelan, K. Shimada, D.M. Wilfong, R.N. James, J.T.McCormick, Y Rabin, Simulation-based cryosurgery intelligent tutoring system prototype, Technology in cancer research and treatment 15 (2) (2015) 396–407.

[88] Z. Chang, J.J. Finkelstein, H. Ma, J. Baust, Development of a high-performance multiprobe cryosurgical device, Biomedical Instrumentation and Technology 28 (5) (1994) 383–390.

[89] J.J. Smith, J. Fraser, An estimation of tissue damage and thermal history in the cryolesion, Cryobiology 11 (2) (1974) 139–147.

[90] M.L. Rivoire, E.J. Voiglio, P. Kaemmerlenand G.Molina, I. Treilleux, J. Finzy, E. Delay, F.Gory, Hepatic cryosurgery precision: evaluation of ultrasonography, thermometry, and impedancemetry in a pig model, Journal of Surgical Oncology 61 (4) (1996) 242–248.

[91] J.H. LeFebvre, L.E. Folke, Effects of subzero temperatures on the microcirculation in the oral mucous membrane, Microvascular Research 10 (3) (1975) 360–372.

[92] A.A.Gage, J.A. Caruana, M. Montes, Critical temperature for skin necrosis in experimental cryosurgery, Cryobiology 19 (3) (1982) 273–282.

[93] S. Yamada, S. Tsubouchi, Rapid cell death and cell population recovery in mouse skin epidermis after freezing, Cryobiology 13 (3) (1976) 317–327.

[94] A.A. Gage, Experimental cryogenic injury of the palate: observations pertinent to cryosurgical destruction of tumors, Cryobiology 15 (4) (1978) 415–425.

[95] H.B. Neel, A.S. Ketcham, W.G. Hammond, Requisites for successful cryogenic surgery of cancer, Archives of Surgery 102 (1) (1971) 45–48.

[96] E.D. Staren, M. S. Sabel, L. M. Gianakakis, G.A. Wiener, V. M. Hart, M. Gorski, K. Dowlatshahi, B. F. Corning, M. F. Haklin, G. Koukoulis, Cryosurgery of breast cancer, Archives of Surgery 132 (1) (1997) 28–33.

[97] A.A.Gage, G.W. Greene, M.E. Neiders, F.G. Emmings, Freezing bone without excision. an experimental study of bone-cell destruction and manner of regrowth in dogs., Journal of American Medical Association 196 (9) (1966) 770–774.

[98] G. Jacob, M.N. Kurzer, B.J. Fuller, An assessment of tumor cell viability after in vitro freezing, Cryobiology 22 (5) (1985) 417–426.

[99] K. Tatsutani, B. Rubinsky, G. Onik, R. Dahiya, Effect of thermal variables on frozen human primary prostatic adenocarcinoma cells, Journal of Urology 48 (3) (1996) 441–447.

[100] D.J. Smith, W.M. Fahssi, D.J. Swanland, J.C. Bischof, A parametric study of freezing injury in AT-1 rat prostate tumour cells, Cryobiology 39 (1) (1999) 13–28.

[101] H.B. Neel, A.S. Ketcham, W.G. Hammond, Cryonecrosis of normal and tumor-bearing rat liver potentiated by inflow occlusion, Cancer 28 (5) (1971) 1211–1218.

[102] D. Whittaker, Electron microscopy of the ice crystals formed during cryosurgery: relationship to duration of freeze, Cryobiology 15 (5) (1978) 603–607.

[103] H.D. Meryman, Mechanics of freezing in living cells and tissues, Science 124 (3221) (1956) 512–521.

[104] D. Whittaker, Ice crystals formed in tissue during cryosurgery. ii. electron microscopy, Cryobiology 11 (3) (1974) 202–217.

[105] D. Whittaker, Mechanism of tissue destruction following cryosurgery, Ann. R. Col. Surg. England 66 (5) (1984) 313–318.

[106] K.J. Chua, S.K. Chou, On the study of the freeze-thaw thermal process of a biological system, Applied Thermal Engineering 29 (17-18) (2009) 3696–3709.

[107] S.D Augustynovvicz, A.A. Gage, Temperature and cooling rate variations during cryosurgical probe testing, International Journal of Refrigeration 8 (4) (1985) 198–208.

[108] J.P. Homasson, J.P. Thiery, M. Angebault, L. Ovtracht, O.J. Maiwand, The operation and efficacy of cryosurgical, nitrous oxide-driven cryoprobe, Cryobiology 31 (3) (1994) 290–304.

[109] C.M. Lam, S.M. Shimi, A. Cuschieri, Thermal characteristics of a hepatic cryolesion formed in vitro by a 3-mm implantable cryoprobe, Cryobiology 36 (2) (1998) 156–164.

[110] M.H. Yang, H.H. Peng, H.C. Chang, An in vitro monitoring system for simulated thermal process in cryosurgery, Cryobiology 40 (2) (2000) 159–170.

[111] V.S. Chernyshev, M. Skliar, Surface tension of water in the presence of perfluorocarbon vapors, Soft Matter 10 (12) (2014) 1937–1943.

[112] A.M.A. Dias, R.P. Bonifácio, I.M. Marrucho, A.A.H. Pádua, M.F. Costa Gomes, Solubility of oxygen in n-hexane and in n-perfluorohexane: Experimental determination and prediction by numerical simulation, Physical Chemistry Chemical Physics 5 (2003) 543–549.

[113] A.M.A. Dias, M. Freire, J.A.P. Coutinho, I.M. Marrucho, Solubility of liquid oxygen in perfluorocarbons, Fluid phase equilibria 25 (2004) 222–223.

[114] G.M. Lanza, 1H/19F magnetic resonance molecular imaging with perfluorocarbon nanoparticles, Curr. Top. Dev. Biol. 70 (2005) 57–76.

[115] S.K. Patel, J. Williams, J.M. Janjic, Cell labelling for 19 F MRI: New and improved approach to perfluorocarbon nanoemulsion design, Biosensors 3 (3) (2013) 341–359.

[116] L.C. Clark, F. Gollan, Survival of mammals breathing organic liquids equilibrated with oxygen at atmospheric pressure, Science 152 (3730) (1966) 1755–1756.

[117] C.A. Fraker, A.J. Mendez, L. Inverardi, C. Ricordi, C.L. Stabler, Optimization of perfluoro nano-scale emulsions: The importance of particle sizefor enhanced oxygen transfer in biomedical applications, Colloids and Surfaces B: Biointerfaces 98 (2012) 26–35.

[118] P.K. Bae, B.H. Chung, Multiplexed detection of various breast cancer cells by perfluorocarbon/quantum dot nanoemulsions conjugated with antibodies, Nano Convergence 1 (23) (2014) 1–8.

[119] P.K. Bae, J. Jung, B.H. Chung, Highly enhanced optical properties of indocyanine green/perfluorocarbon nanoemulsions for efficient lymph node mapping using near infrared and magnetic resonance imaging, Nano Convergence 1 (6) (2014) 1–10.

[120] Y.T. Lim, Y.W. Noh, J.N. Kwon, B.H. Chung, Multifunctional perfluorocarbon nanoemulsions for 19F-based magnetic resonance and near-infrared optical imaging of dendritic cells, Chemical Communications (2009) 6952–6954.

[121] M.G. Freire, A.M.A. Dias, M.A.Z. Coelho, J.A.P. Coutinho, I. M. Marrucho, Aging mechanisms of perfluorocarbon emulsions using image analysis, Journal of Colloid and Interface Science 286 (1) (2005) 224–232.

[122] C. Wagner, Theorie der Alterung von Niederschlagen durch Umlasen (Ostwald-Reifung), Z. Elektrochemie 65 (1961) 581–591.

[123] B. P. Binks, W-G. Cho, P.D.I. Fletcher, D.N. Petsev, Stability of Oil-in-Water Emulsions in a Low Interfacial Tension System, Langmuir 16 (3) (2000) 1025–1034.

[124] B.P. Barnett, J. Ruiz-Cabello, P. Hota, R. Ouwerkerke, M.J. Shamblott, C. Lauzon, P. Walczak, W. D. Gilsona, V. P. Chacko, D. L. Kraitchman, A. Arepally, J. W. M. Bulte, Use of perfluorocarbon nanoparticles for non-invasive multimodal cell tracking of human pancreatic islets, Contrast Media and Molecular Imaging 6 (4) (2011) 251–259.

[125] H.Y. Lee, M.J. McCarthy, S.R. Dungana, Experimental Characterization of Emulsion Formation and Coalescence by Nuclear Magnetic Resonance Restricted Diffusion Techniques, Journal of American Oil Chemists Society 75 (4) (1998) 463–475.

[126] T.S. Ravikumar, G. Steele Jr., R. Kane, V. King, Experimental and clinical observations on hepatic cryosurgery for colorectal metastases, Cancer Research 51 (23) (1991) 6323–6327.

[127] C.C. Rupp, N.E. Hoffmann, F.R. Schimdlin, D.J. Swanlund, J.C. Bischof, J.E. Coad, Cryosurgical changes in the porcine kidney:histologic analysis with thermal history correlation, Cryobiology 45 (2) (2002) 167–182.

[128] L. Pham, R. Dahiya, B. Rubinsky, An in vivo study of antifreeze protein adjuvant cryosurgery, Cryobiology 38 (2) (1999) 169–175.

[129] S. Ikekawa, K. Ishihara, S. Tanaka, S. Ikeda, Basic studies of cryochemotherapy in a murine tumour system, Cryobiology 22 (5) (1985) 477–483.

[130] B. Han, J.C. Bischof, Direct cell injury associated with eutectic crystallization during freezing, Cryobiology 48 (1) (2004) 8–21.

[131] T.H. Yu, J. Liu, Y.X. Zhou, Selective freezing of target biological tissues after injection of solutions with specific thermal properties, Cryobiology 50 (2) (2005) 174–182.

[132] J. Jiang, R. Goel, S. Schmechel, G. Vercellotti, J. Bischof, Pre-conditioning cryosurgery:Cellular and molecular mechanisms and dynamics of TNF-alpha enhanced cryotherapy in an in vivo prostate cancer model system, Cryobiology 61 (3) (2010) 280–288.

[133] Y. Rabin, T.F. Stahovich, Cryoheater as a means of cryosurgery control, Physics in Medicine and Biology 48 (5) (2003) 619–632.

[134] K.K. Ramajayam, A. Kumar, A novel approach to improve the efficacy of tumour ablation during cryosurgery, Cryobiology 67 (2) (2013) 201–213.

[135] E.O. Olapade Olaopa, D.K. Moscatello, E.H.Mackay, T. Horsburgh, D.P.S. Sandhur, T.R. Terry, A.J. Wong, F.K. Habib, Evidence for the differential expression of a variant EGF receptor protein in human prostate cancer, British Journal of Cancer 82 (1) (2000) 186–194.

[136] G.M. Lanza, K.D. Wallace, M.J. Scott, W.P. Cacheris, D.R. Abendschein, D.H. Christy, A.M. Sharkey, J.G. Miller, P.J. Gaffney, S.A. Wickline, A Novel Site-Targeted Ultrasonic Contrast Agent With Broad Biomedical Application, Circulation 94 (12) (1996) 3334–3340.

[137] K.J. Chua, S.K. Chou, J.C. Ho, An analytical study on the thermal effects of cryosurgery on selective cell destruction, Journal of Biomechanics 40 (1) (2007) 100–116.

[138] Y. Rabin, A. Shitzer, Exact solution to the one-dimensional inverse stefan problem in non ideal biological tissue, Journal of Heat Transfer 117 (2) (1995) 425–431.

[139] V.R. Voller, C. Prakash, A fixed grid numerical modelling methodology for convection-diffusion mushy-region phase change problems, International Journal of Heat and Mass Transfer 30 (8) (1987) 1709–1719.

[140] H. J. Ferziger, M. Peric, Computational Methods for Fluid Dynamics, Springer, 2002.

[141] J.C. Rewcastle, G.A. Sandison, K. Muldrew, J.C. Saliken, B.J. Donnelly, A model for time dependent three-dimensional thermal distribution within iceballs surrounding multiple cryoprobes, Med.Phys. 28 (6) (2001) 1125–1137.

[142] T. Riddick, Control of colloid stability through zeta potential with a closing chapter to cardiovascular disease, Livingston publishing company, Pennsylvania, 1968.

[143] J.C. Maxwell, A Treatise on Electricity and Magnetism, 3rd Edition, Vol. 1, Dover, New York, 1954.

[144] S.C. Cheng, R.L. Vachon, A technique for predicting the thermal conductivity of suspensions, emulsions and porous materials, International Journal of Heat and Mass Transfer 13 (3) (1970) 537–546.

[145] M.J. O'Neill, Measurement of Specific Heat Functions by Differential Scanning Calorimetry, Analytical Chemistry 38 (10) (1966) 1331–1336.

[146] A.A. Al-Shamrani, A. James, H. Xiao, Destabilisation of oil-water emulsions and separation by dissolved air floatation, Water Research 36 (6) (2002) 1503–1512.

[147] K. G. Marinova, R. G. Alargova, N. D. Denkov, O. D. Velev, D. N. Petsev, I. B. Ivanov, R. P. Borwankar, Charging of oil-water interfaces due to spontaneous adsorption of hydroxyl ions, Langmuir 12 (8) (1996) 2045–2051.

[148] D.M. Clarke, J.M. Baust, R.G. Van Buskirk, Chemo-Cryo Combination Therapy:An Adjunctive Model for the Treatment of Prostate Cancer, Cryobiology 42 (4) (2001) 274–285.

[149] C.L. Wang, K.Y. Teo, B. Han, An amino acidic adjuvant to augment cryoinjury of MCF-7 breast cancer cells, Cryobiology 57 (1) (2008) 52–59.

[150] R. Pichot, Stability and characterisation of emulsions in the presence of colloidal particles and surfactants, Graduate thesis, Department of Chemical Engineering, School of Engineering, University of Birmingham (Nov. 2010).

Dissemination

Articles published [1] (*Web of Science, SCI, Scopus, etc.*)[1]

1. K.K. Ramajayam, A. Kumar, A novel approach to improve the efficacy of tumour ablation during cryosurgery, Cryobiology, 67 (2013), 201-213

2. K.K. Ramajayam, A. Kumar, S.K. Sarangi, A.Thirugnanam, A novel adjuvant-solution layer strategy for improving the efficacy of cryosurgery, Cryoletters, 37 (2016), 346-356

3. K.K. Ramajayam, A. Kumar, S.K. Sarangi, A.Thirugnanam, A numerical study on optimising the cryosurgical process for effective tumour necrosis, Heat and Mass transfer, 53(5), 1685-1695

Conferences [1]

1. K.K. Ramajayam, A. Kumar, C. Kumari, S.K. Sarangi and A.Thirugnanam, A new approach to improve the efficacy of cryosurgery in gel phantoms, CRYO 2017, 21^{st}-24^{th} July 2017, Fengda International Hotel, Hefei, China (Organised by Society for Cryobiology, UK)

2. K.K. Ramajayam, A. Kumar, S.K. Sarangi, A.Thirugnanam, A novel strategy to enhance the cryosurgical outcome in gel phantoms, CRYO 2016, 24^{th}-27^{th} July, 2016, Fairmount Chateau Laurier, Ottawa, Canada (Organised by Society for Cryobiology, UK)

3. K.K. Ramajayam, A. Kumar, S.K. Sarangi, A.Thirugnanam, Perfluorocarbons as a promising material for increasing efficacy of cryosurgery, International conference on modeling and simulation of diffusive processes and applications, 29^{th}-31^{st} October 2014, IIT, BHU, Varanasi, India

4. K.K. Ramajayam, A. Kumar, A novel method to calculate defect and need of an optimal solution layer thickness during cryosurgery, 11^{th} ASME and 22^{nd}

[1] Articles already published, in press, or formally accepted for publication.

ISHMT-Heat and Mass Transfer Conference, 27^{th}-31^{st} December, 2013, IIT Kharagpur, India

5. K.K. Ramajayam, K.A. Lokesh, A. Kumar, An analysis of heat transfer characteristics during Cryoablation, International conference on modeling and simulation of diffusive processes and applications, 9^{th}-12^{th}, October 2012, IIT, BHU,Varanasi, India

6. K.K. Ramajayam, S.Yadav, A. Kumar, A novel method to determine the thermal conductivity of Tissue-Mimicking Gels, International conference in tissue engineering and regenerative medicine, 15^{th}-17^{th} November, 2013, NIT Rourkela, Odisha, India

Article under review [2]

1. K.K. Ramajayam, A. Kumar, S.K. Sarangi, A.Thirugnanam, A novel combinative thermophysical adjuvant-solution layer approach for improving the effectiveness of tumour ablation during cryosurgery, (Under revision in International of Thermal Sciences, Elsevier)

Articles to be communicated [3]

1. K.K. Ramajayam, A. Kumar, S.K. Sarangi, A.Thirugnanam, Designing low thermal conductivity perfluorodecalin emulsions for improving the efficacy of cryosurgery.

[2] Articles under review
[3] Articles to be communicated

Index

Krishna Kumar Ramajayam

Personal Data

Date of Birth:	20^{th} February 1989
Address:	326, 1B First Floor, Chameli Building, Near Tank no. 4, Dum Dum Park, Kolkata- 700055, West Bengal, India
Phone:	+91 9439734986
email:	krishnakumar.ramajayam@yahoo.com

Career Objective

Looking to use my research abilities to solve problems of industry, academia and people

Synopsis

- A Bachelors degree in Engineering (Industrial Biotechnology)
- Five years of research experience as a research fellow during doctoral degree (PhD)
- Good managerial abilities and real time problem solving skills acquired during doctoral programme
- Nice presentation and oratory skills
- Good experience and knowledge of softwares like MS-Office™, MS-Excel™, MS-Powerpoint™, Latex, LabVIEW, Image J, Origin and Inkscape

Major Equipments handled

- Bright field and fluorescence microscopy
- Data Acquisition system for temperature measurement
- Particle size analyser and Zetasizer
- Probe sonicator
- Cryosurgery system
- Controlled rate freezer
- Differential scanning calorimeter
- Thermal Analyser (KD2 probe system), Differential Scanning calorimeter
- Basic cell culture and assays

Education and Training

PhD

Research Scholar, National Institute of Technology Rourkela, Institute fellow through GATE fellowship

- General Interests: Pursued active research in the broad field of bioheat transfer, cryobiology during the doctoral degree (PhD, Biomedical Engineering)
- Specific interests: Novel strategies for improving the efficacy of cryosurgery on gel phantoms and tissues, a study of thermal properties of emulsions for low-temperature applications, synthesis of emulsions
- Membership: Society for cryobiology, UK: Student member
- Awards: Travel award to attend CRYO 2017 at Hefei, China from Society for Cryobiology, UK, Travel award to attend CRYO 2016 at Ottawa, Canada from Society for Cryobiology, UK and CICS, Govt. of India.

B.Tech

B. Tech Industrial Biotechnology from SASTRA University, Thanjavur, Tamilnadu (July 2007 to June 2011)

- CGPA: 8.57 (On a scale of 10), Pursued active research for undergraduate thesis on “Studies on the role of zinc in Cr(VI) induced apoptosis of lymphocytes and the role of metallothioneins in regulating it”, under guidance of Dr. Rama Rajaram, Biochemistry division CLRI (CSIR), Chennai, India

CBSE

Science stream

- AISSCE- 2007 (Class XII), Percentage of Marks: 80.2
- AISSE- 2005 (CLASS X), Percentage of Marks: 92.5

Other Achievements

- Summer research Fellow at IIT Kharagpur (2010), Indian Academy of Sciences
- Summer research Fellow at IISc Banagalore (2011), Indian Academy of Sciences

Publications

- K.K. Ramajayam, A. Kumar, A novel approach to improve the efficacy of tumour ablation during cryosurgery, Cryobiology, 67 (2013), 201-213
- K.K. Ramajayam, A. Kumar, S.K. Sarangi, A.Thirugnanam, A novel adjuvant-solution layer strategy for improving the efficacy of cryosurgery, Cryoletters, 37 (2016), 346-356
- K.K. Ramajayam, A. Kumar, S.K. Sarangi, A.Thirugnanam , A numerical study on optimising the cryosurgical process for effective tumour necrosis, Heat and Mass transfer 53(5), 1685-1695
- S.Sankar, K.K. Ramajayam, A.Thirugnanam, A Novel Method to Fabricate Porous Tri-calcium phosphate Composite Scaffolds for Bone Tissue Engineering Applications, Materials Technology: Advanced Performance Materials,37(2016), 595-692

Conferences

- K.K. Ramajayam, K.A. Lokesh, A. Kumar, An analysis of heat transfer characteristics during Cryoablation, International conference on modeling and simulation of diffusive processes and application, $9^{th} - 12^{th}$, October 2012, IIT, BHU, Varanasi, India
- K.K. Ramajayam, S.Yadav, A. Kumar, A novel method to determine the thermal conductivity of Tissue-Mimicking Gels, International conference in tissue engineering and regenerative medicine,$15^{th} - 17^{th}$ November, 2013, NIT Rourkela
- K.K. Ramajayam, A. Kumar, A novel method to calculate defect and need of an optimal solution layer thickness during cryosurgery, 11^{th} ASME and 22^{nd} ISHMT-Heat and Mass Transfer Conference, $27^{th} - 31^{st}$ December, 2013, IIT Kharagpur, India
- K.K. Ramajayam, A. Kumar, S.K. Sarangi, A.Thirugnanam, Perfluorocarbons as a promising material for increasing efficacy of cryosurgery, International conference on modeling and simulation of diffusive processes and applications, $29^{th} - 31^{st}$ October 2014, IIT, BHU, Varanasi, India
- K.K. Ramajayam, A. Kumar, S.K. Sarangi, A.Thirugnanam, A novel strategy to enhance the cryosurgical outcome in gel phantoms, CRYO 2016, $24^{th} - 27^{th}$ July, 2016, Fairmount Chateau Laurier, Ottawa, Canada (Organised by Society for Cryobiology, UK)
- K.K. Ramajayam, A. Kumar, S.K. Sarangi, A.Thirugnanam, A new approach to improve the efficacy of cryosurgery in gel phantoms, CRYO 2017, $21^{st} - 24^{th}$ July 2017, Fengda International Hotel, Hefei, China (Organised by Society for Cryobiology, UK)
- D.Devismita, K.K. Ramajayam, A. Kumar, Cryopreservation of Human Sperm: Effect of Cooling Rate on Intracellular Ice Formation, International conference in emerging trends, March, 2012, NIT Durgapur, India

Languages

Tamil:	Mother tongue
English:	Fluent
Hindi:	Fluent
Bengali	Basic User

Computer Skills

- Basic Knowledge: Various computational softwares- Origin, LabView, Image J, Tecplot, Inkscape, Lyx, programming Linux, fedora, LaTeX

Invited workshops and events

- Invited for idea presentation competition (BEST 2012 organised by ABLE, Department of Biotechnology, India), among the top 20 teams of the country , entrenpreneurship workshop and idea presentation event
- Invited for attending the Science communication workshop organised in November 2014 by DBT-Wellcome trust UK at Hyderabad